

NBSIR 85-3163

Development of A Model for the Heat Release Rate of Wood - A Status Report

William J. Parker

**U.S. DEPARTMENT OF COMMERCE
National Bureau of Standards
National Engineering Laboratory
Center for Fire Research
Gaithersburg, MD 20899**

May 1985

**Sponsored in part by:
Federal Emergency Management Agency**

NBSIR 85-3163

**DEVELOPMENT OF A MODEL FOR THE
HEAT RELEASE RATE OF WOOD -
A STATUS REPORT**

William J. Parker

U.S. DEPARTMENT OF COMMERCE
National Bureau of Standards
National Engineering Laboratory
Center for Fire Research
Gaithersburg, MD 20899

May 1985

Sponsored in part by:
Federal Emergency Management Agency



U.S. DEPARTMENT OF COMMERCE, Malcolm Baldrige, *Secretary*
NATIONAL BUREAU OF STANDARDS, Ernest Ambler, *Director*

REPORT DOCUMENTATION PAGE		READ INSTRUCTIONS BEFORE COMPLETING FORM
1. REPORT NUMBER	2. GOVT ACCESSION NO.	3. RECIPIENT'S CATALOG NUMBER
4. TITLE (and Subtitle) DEVELOPMENT OF A MODEL FOR THE HEAT RELEASE RATE OF WOOD - A STATUS REPORT		5. TYPE OF REPORT & PERIOD COVERED Final
7. AUTHOR(s) William J. Parker		6. PERFORMING ORG. REPORT NUMBER NBSIR 85-3163
9. PERFORMING ORGANIZATION NAME AND ADDRESS Center for Fire Research U.S. National Bureau of Standards Gaithersburg, MD 20899		8. CONTRACT OR GRANT NUMBER(s) EMW-E-1239
11. CONTROLLING OFFICE NAME AND ADDRESS Federal Emergency Management Agency Washington, D.C. 20472		10. PROGRAM ELEMENT, PROJECT, TASK AREA & WORK UNIT NUMBERS 2531 G
14. MONITORING AGENCY NAME & ADDRESS (if different from Controlling Office)		12. REPORT DATE May 1985
		13. NUMBER OF PAGES 106
		15. SECURITY CLASS. (of this report) Unclassified
		15a. DECLASSIFICATION/DOWNGRADING SCHEDULE
16. DISTRIBUTION STATEMENT (of this Report) Approved for public release: Distribution Unlimited		
17. DISTRIBUTION STATEMENT (of the abstract entered in Block 20, if different from Report) Approved for public release: Distribution Unlimited		
18. SUPPLEMENTARY NOTES		
19. KEY WORDS (Continue on reverse side if necessary and identify by block number) heat release rate, wood, pyrolysis, heat of combustion, thermal conductivity, computer models		
20. ABSTRACT (Continue on reverse side if necessary and identify by block number) This report describes the status of the development of a method for predicting the heat release rate of wood for different thicknesses, moisture contents, and exposure conditions. A computer program has been set up on a microcomputer. Experimental techniques have been devised to obtain the input data required by the model. These include (1) the thermal conductivity as a function of temperature and percent loss, (2) the kinetic constants needed to describe the mass		

(Block 20)

loss rate, (3) the heat of combustion of the volatile pyrolysis products, and (4) the contraction factors due to charring. Sufficient data on these parameters were taken to exercise the model. Heat release rates and effective heats of combustion were measured as a function of external radiant flux on 12.5 mm thick dry vertical specimens of Douglas fir particle board. The calculated and measured peak heat release rate curves are similar in shape and amplitude but differ significantly in time scale. This may be due to the lack of thermal conductivity data on the char in the high temperature range. There is very good agreement between the calculated and measured effective heats of combustion. The initial results with the model are promising.

TABLE OF CONTENTS

	<u>Page</u>
LIST OF FIGURES	v
LIST OF TABLES	viii
NOMENCLATURE	ix
Abstract	1
1. INTRODUCTION	1
2. HEAT RELEASE RATE MODEL	5
3. THERMOCHEMICAL PROPERTIES	15
3.1 Pyrolyzer	15
3.2 Heat of Combustion of Pyrolysis Vapor	17
3.3 Calculation of Kinetic Constants from Mass Loss Data at Constant Temperature	18
3.4 Contraction Factors	20
3.5 Heat of Pyrolysis	20
3.6 Parameters Dealing with Moisture	21
4. THERMOPHYSICAL PROPERTIES	21
4.1 Heat Capacity	21
4.2 Thermal Conductivity Data from Literature	22
4.3 Thermal Conductivity Measurements	24
5. CALCULATIONS OF HEAT RELEASE RATE USING THE MODEL	28
6. HEAT RELEASE RATE MEASUREMENTS IN THE CONE CALORIMETER	30
7. DISCUSSION	32
8. SUMMARY	40
9. FUTURE PLANS	41
10. ACKNOWLEDGEMENTS	42
11. REFERENCES	43
APPENDIX A. CALCULATION OF THE DENSITY OF THE GAS IN THE EXHAUST DUCT ..	52
APPENDIX B. CALCULATION OF THE FLOW OF NITROGEN THROUGH THE EXHAUST DUCT	55
APPENDIX C. CALCULATION OF THE CARBON, HYDROGEN, AND OXYGEN RELEASE RATES FROM BURNING WOOD	57

LIST OF FIGURES

	<u>Page</u>
Figure 1. Boundary Conditions and Subdivision of Burning Vertical Slab	65
Figure 2. Flow Chart for Computer Program	66
Figure 3. Pyrolyzer	67
Figure 4. Closure Slide	68
Figure 5. Heat of Combustion of Pyrolysis Vapor for Douglas Fir Particle Board	69
Figure 6. Arrhenius Plot for Douglas Fir Particle Board	70
Figure 7. Contraction Factors for Southern Pine	71
Figure 8. Contraction Factors for Douglas Fir Particle Board	72
Figure 9. Experimental Setup for Determining Thermal Conductivity	73
Figure 10. Thermal Conductivity as a Function of Temperature for Charred and Uncharred Specimens of Southern Pine	74
Figure 11. Thermal Conductivity as a Function of Temperature for Charred and Uncharred Specimens of Douglas Fir Particle Board	75
Figure 12. Calculated Front and Rear Surface Temperatures for Dry 12.7 mm Specimen of Douglas Fir Particle Board Exposed at an External Radiant Flux of 50 kW/m ²	76
Figure 13. Calculated Char Depth for Dry 12.7 mm Specimen of Douglas Fir Particle Board Exposed at an External Radiant Flux of 50 kW/m ²	77
Figure 14. Calculated Mass Loss Rate for Dry 12.7 mm Specimen of Douglas Fir Particle Board Exposed at an External Radiant Flux of 50 kW/m ²	78
Figure 15. Calculated Heat Release Rate for Dry 12.7 mm Specimen of Douglas Fir Particle Board Exposed at an External Radiant Flux of 50 kW/m ²	79
Figure 16. Calculated Effective Heat of Combustion for Dry 12.7 mm Specimen of Douglas Fir Particle Board Exposed at an External Radiant Flux of 50 kW/m ²	80
Figure 17. Calculated Heat Release Rate for Dry 12.7 mm Specimen of Douglas Fir Particle Board with an Assumed Heat of Pyrolysis of 400 kJ/kg Exposed at an External Radiant Flux of 50 kW/m ²	81

List of Figures (continued)

	<u>Page</u>
Figure 18. Calculated Heat Release Rate for 7% Moisture Content 12.7 mm Specimen of Douglas Fir Particle Board Exposed at an External Radiant Flux of 50 kW/m ²	82
Figure 19. Calculated Heat Release Rate for Dry 6 mm Specimen of Douglas Fir Particle Board Exposed at an External Radiant Flux of 50 kW/m ²	83
Figure 20. Calculated Heat Release Rate for Dry 12.7 mm Specimen of Douglas Fir Particle Board Exposed at an External Radiant Flux of 25 kW/m ²	84
Figure 21. Calculated Heat Release Rate for Dry 12.7 mm Specimen of Douglas Fir Particle Board Exposed at an External Radiant Flux of 75 kW/m ²	85
Figure 22. Calculated Heat Release Rate for Dry 12.7 mm Specimen of Douglas Fir Particle Board Exposed at an External Radiant Flux of 100 kW/m ²	86
Figure 23. Measured Heat Release Rate for Dry 12.7 mm Specimen of Douglas Fir Particle Board Exposed at an External Radiant Flux of 25 kW/m ²	87
Figure 24. Measured Heat Release Rate for Dry 12.7 mm Specimen of Douglas Fir Particle Board Exposed at an External Radiant Flux of 50 kW/m ²	88
Figure 25. Measured Heat Release Rate for Dry 12.7 mm Specimen of Douglas Fir Particle Board Exposed at an External Radiant Flux of 75 kW/m ²	89
Figure 26. Measured Heat Release Rate for Dry 12.7 mm Specimen of Douglas Fir Particle Board Exposed at an External Radiant Flux of 100 kW/m ²	90
Figure 27. Measured Effective Heat of Combustion for Dry 12.7 mm Specimen of Douglas Fir Particle Board Exposed at an External Radiant Flux of 25 kW/m ²	91
Figure 28. Measured Effective Heat of Combustion for Dry 12.7 mm Specimen of Douglas Fir Particle Board Exposed at an External Radiant Flux of 50 kW/m ²	92
Figure 29. Measured Effective Heat of Combustion for Dry 12.7 mm Specimen of Douglas Fir Particle Board Exposed at an External Radiant Flux of 75 kW/m ²	93

List of Figures (continued)

	<u>Page</u>
Figure 30. Measured Effective Heat of Combustion for Dry 12.7 mm Specimen of Douglas Fir Particle Board Exposed at External Radiant Flux of 100 kW/2	94
Figure 31. Measured Heat Release Rate Determined by the Three Analyzer Method for Dry 12.7 mm Specimen of Douglas Fir Particle Board Exposed at an External Radiant Flux of 50 kW/m2	95
Figure 32. Measured Effective Heat of Combustion Determined by the Three Analyzer Method for Dry 12.7 mm Specimen of Douglas Fir Particle Board Exposed at an External Radiant Flux of 50 kW/m2	96

LIST OF TABLES

	<u>Page</u>
1. Thermal Conductivity Data on Fiberboard and Particle Board from the Literature.....	45
2. Thermal Conductivity of Oven Dry Southern Pine as a Function of Temperature.....	46
3. Thermal Conductivity of Charred Southern Pine as a Function of Temperature.....	47
4. Thermal Conductivity of Oven Dry Douglas Fir Particle Board as a Function of Temperature.....	48
5. Thermal Conductivity of Charred Douglas Fir Particle Board as a Function of Temperature.....	49
6. Input Data for Running the Model for Douglas Fir Particle Board	50

NOMENCLATURE

A	frequency factor (s^{-1})
B	mass transfer number
C	heat capacity (kJ/kgK)
E	activation energy (kJ/mol)
F	heat of combustion of volatiles (kJ/kg) (positive when heat is evolved)
h	convective heat transfer coefficient (kW/m^2K)
h_p	heat of pyrolysis (kJ/kg) (positive when heat is absorbed)
K	thermal conductivity ($kW/m \cdot K$)
ℓ	contraction factor
L	effective heat of gasification (kJ/kg) (positive)
L_v	latent heat of vaporization of water (kJ/kg) (positive)
m	mass (kg)
M	% moisture content
n	number of components
N	number of subdivisions of the specimen
\dot{n}	molar flow (mol/s)
P	grouping defined by equation (2-14)
q	heat (kJ) (positive)
\dot{q}_e	external radiant flux (kW/m^2)
\dot{q}_{rel}	rate of heat release (kW)
R	gas constant (8.314 kJ/mol \cdot K)
t	time (s)
T	temperature ($^{\circ}C$)
\hat{V}	volume flow (m^3/s)
x	distance up from bottom of specimen (m)

X volume fraction
 Z mass retention fraction
 α radiative absorptivity and emissivity
 ΔH heat of combustion (kJ/kg) (positive when heat is evolved)
 Δp pressure drop across orifice plate (P_a)
 Δt time step (s)
 ΔX thickness of each slice (m)
 ω defined by equation (2-20)
 ρ density (kg/m^3)
 σ Stefan-Boltzmann constant ($5.67 \times 10^{-11} \text{ kW/m}^2 \cdot \text{K}^4$)

Subscripts

c convection
 C carbon
 D thickness of specimen (m)
 e external or exhaust
 f flame
 g gas
 H hydrogen
 i designates a particular slice
 k designates a particular wood component
 N designates the slice bounded by the rear surface
 o ambient or original
 O oxygen
 R radiation
 rel release
 S front surface of specimen
 vol volatiles

w water
x normal to surface
y parallel to surface normal to grain
z parallel to surface along grain

Superscripts

A analyzer
A' analyzer with CO₂ trapped out of it
S exhaust duct
· per unit time
" per unit area

DEVELOPMENT OF A MODEL FOR THE HEAT RELEASE RATE OF WOOD - A STATUS REPORT

William J. Parker

Abstract

This report describes the status of the development of a method for predicting the heat release rate of wood for different thicknesses, moisture contents, and exposure conditions. A computer model has been set up on a microcomputer. Experimental techniques have been devised to obtain the input data required by the model. These include (1) the thermal conductivity as a function of temperature and percent mass loss, (2) the kinetic constants needed to describe the mass loss rate, (3) the heat of combustion of the volatile pyrolysis products, and (4) the contraction factors due to charring. Sufficient data on these parameters were taken to exercise the model. Heat release rates and effective heats of combustion were calculated and measured as a function of external radiant flux on 12.5 mm thick dry vertical specimens of Douglas fir particle board. The initial results with the model are promising.

Key words: heat release rate, wood, pyrolysis, heat of combustion, thermal conductivity.

1. INTRODUCTION

The heat release rate is one of the most important fire properties of a material. Whether a room fire will attain flashover depends on the total heat release rate of all the materials in the room as well as its ventilation and surface heat losses [1,2]. The rate of flame spread in the direction of air

flow is strongly dependent on the rate of heat release. In order to model the fire growth in a room it is essential to have data on the heat release rate of all of the materials involved as a function of the net heat transfer through their front surface.

A number of calorimeters have been developed to measure the heat release rate per unit area as a function of the external radiant flux [3,7]. The corresponding net heat transfer through the flaming surface as required by room fire growth models is not measured in any of these calorimeters. The heat release rate curves as a function of time at a particular external radiant flux are in general different for different calorimeters because of the different conditions under which the data are obtained. The variables include orientation, specimen size, heat transfer conditions at the rear face, piloting arrangements, etc.

An approach which has been used with apparent success for determining the heat release rate of polymethylmethacrylate (PMMA) is to define an effective heat of gasification as

$$L = \dot{q}''_{\text{net}} / \dot{m}'' \quad (1-1)$$

where \dot{q}''_{net} is the net heat transfer through the surface and \dot{m}'' is the outward mass flux. The mass loss rate used in equation (1-1) is measured under non-flaming conditions thus avoiding the uncertainties in measuring the flame heat transfer. The net heat transfer to the specimen is equal to the absorbed external radiant flux minus the reradiation and convective heat losses from the front face. Tewarson [8] has cataloged values of L and the effective heat of combustion, $(\Delta H)_{\text{eff}}$, for many materials.

A room fire growth model can calculate the net heat transfer rate through the surface and use equation (1-1) along with the experimentally measured value of L to determine the mass loss rate. The calculated heat release rate is simply equal to

$$\dot{q}_{rel} = \dot{m}'' (\Delta H)_{eff}. \quad (1-2)$$

Unfortunately both $(\Delta H)_{eff}$ and L vary throughout the burning period for char forming materials.

When L reaches a steady value it is an order of magnitude greater than the heat of pyrolysis of cellulose [9], which is the major component of wood. This suggests that L in this case is dominated by heat transfer and thus depends on density, thickness, etc. Therefore, the effective heat of gasification is not a useful concept for wood.

A better approach for char forming materials is to develop a model which predicts the mass loss rate as a function of time based on their thermochemical and thermophysical properties. Two general types of mass loss rate models have been developed. Kanury [10] and others have used a pyrolysis temperature model which can be solved analytically. It is assumed that a thin pyrolysis front moves through the material. Virgin wood exists at all temperatures below the pyrolysis temperature and the final char exists above it. This is satisfactory for high heat fluxes and long times.

However, for fire buildup in rooms we have to deal with the whole range of fluxes and are particularly interested in early times. This requires the

use of kinetic models such as that originated by Kung [11] and improved upon by Tamanini [12] and Atreya [13]. The kinetic models allow for pyrolysis to occur at any temperature at a rate determined by an appropriate Arrhenius expression. Again there are a number of other models but it is the one refined by Atreya which will be built upon in this report.

It is also important to allow for moisture evaporation. The temperature at any point in the solid is determined by solving the energy equation numerically.

Even the kinetic mass loss rate models are not without problems. Wood decomposes along two principal pathways. In one case all of the gasified material escapes; it will generally decompose into a variety of products before it passes through the surface. It will have an overall heat of combustion similar to that determined with an oxygen bomb calorimeter. Along the other pathway, char is formed with the release of water and other volatiles having low heats of combustion. The effective heat of combustion, $(\Delta H)_{\text{eff}}$, will be determined by the ratio of the quantities following these two routes. This ratio changes during the course of the test. The mass loss rate model cannot accurately predict the heat release rate unless the change in effective heat of combustion during the burning period is known.

In this report a model is presented which calculates the heat release rate directly. Methods of providing the thermochemical and thermophysical properties required as input data for the model are described. Some of these data are presented for Douglas fir particle board and the calculated and measured heat release rates are compared. Douglas fir particle board was

chosen because of its use in a number of other fire research projects. The material used was supplied by the Weyerhaeuser Company. It has an oven dry density of 709 kg/m^3 . It is 12.7 mm thick and uses urea formaldehyde (6% of the mass of the original wood) as the adhesive. In addition there is 1/4% add-on each of urea and a paraffin-type wax. While the binder may have some effect on the chemical and physical properties of the particle board, these resultant properties are measured on the project.

2. HEAT RELEASE RATE MODEL

The heat release rate model described in this report (1) breaks the specimen down into thin slices of equal thickness parallel to the surface as seen in figure 1, (2) calculates the temperature of each slice using the energy equation, (3) calculates the mass loss rate for each wood component (cellulose, lignin, and hemicellulose) in each slice using the rate equations, (4) multiplies these rates by the local heat of combustion of the volatiles generated by each component, and (5) sums these contributions over the depth of the specimen to obtain the total heat release rate assuming complete combustion of the volatiles leaving the front surface. The flow chart for the computer program written to implement these calculations is shown in figure 2. The boundaries of each slice move as the specimen shrinks during the burning period so that no solid material crosses a boundary. All of the volatiles pass through the front surface. The transit time of the volatiles from their generation site to the surface is neglected. However, the internal surface convective heat transfer coefficient is assumed to be so large that the volatiles are maintained in thermal equilibrium with the char through which they pass. Secondary chemical reactions with the char layer are

neglected. The rate of mass generation for each component is expressed as a function of the temperature and the mass retention fraction of that component for each slice using an Arrhenius type expression. The mass retention fraction is the ratio of the mass at any time to the original mass. It is assumed that the instantaneous heat of combustion of the volatiles generated by each component depends only on the mass retention fraction for that component. This implies that the chemical composition of each component is a unique function of its mass. The temperature profile as a function of time is calculated from the energy equation using finite differences. The rate of change of enthalpy, heat conduction, internal heat generation or absorption and convective cooling by the flow of volatiles is taken into account. The thermal properties are assumed to be a function of the temperature and the total mass retention fraction for each slice. Then the instantaneous mass retention fraction profile is determined by accounting for the cumulative loss of volatiles. An adiabatic boundary condition is assumed at the rear surface while the front face is exposed to a constant external radiant flux. Both of these conditions can be made more general later if desired. The front surface also loses heat by reradiation. Up to the time of ignition it also loses heat by laminar free convection. This is justified for small surfaces such as those in the heat release rate calorimeters. For wall fires it will be necessary to take turbulence into account. After ignition the convective heat transfer from the flame to the surface is taken into account along with flame radiation. The convective heat transfer coefficient is multiplied by a blowing factor to account for the effect of the volatiles leaving the surface. Ignition is assumed to occur when the calculated total heat release rate reaches 30 kW/m^2 which is the minimum heat release rate required to maintain a flame on the surface. The use of this ignition criterion will be discussed in

section 7. The flame is extinguished when the calculated heat release rate again drops below 30 kW/m² at the end of the flaming phase. Only the heat release rate during the flaming phase is treated by this model.

The mass retention fraction Z_i for slice i is defined by

$$Z_i = m_i / m_i^0 = \frac{\rho}{\rho_0} l_x l_y l_z \quad (2-1)$$

where m_i is the mass of slice i on an oven dry basis, ρ is its density, and l_x , l_y , and l_z are the contraction factors (i.e. the ratios of the thickness, width and height of the slice to their original values). The superscript and subscript o refer to the initial values.

The contributions of the individual wood components (e.g. cellulose, hemicellulose and lignin) are additive so that

$$Z_i = \sum_{k=1}^n Z_{i,k} \quad (2-2)$$

where $Z_{i,k}$ is the mass of the k th component of slice i divided by the original mass of the whole slice. It is necessary to know the reaction rate and heat of combustion of the volatiles for each component as a function of the temperature, T_i , and the component mass retention fraction, $Z_{i,k} / Z_k^0$. Here Z_k^0 is original mass fraction of the k th component.

The moisture is taken into account by assigning a moisture retention fraction

$$Z_{w_i} = m_{w_i} / m_i^0 \quad (2-3)$$

where m_{w_i} is the mass of adsorbed water located in slice i at any time. The water produced by chemical decomposition is accounted for in the Z term.

The mass loss rate on a dry basis and heat release rate per unit area of the original specimen are calculated by the following formulas:

$$\dot{m}'' = \rho_0 \frac{\Delta X_0}{\Delta t} \sum_{i=1}^N (Z_i^t - Z_i^{t + \Delta t}) \quad (2-4)$$

where $Z^t \equiv Z(t)$ and ΔX_0 is the original thickness of each slice (assumed to be identical)

and

$$\dot{q}_{rel}'' = \rho_0 \frac{\Delta X_0}{\Delta t} \sum_{i=1}^N F_i^t (Z_i^t - Z_i^{t + \Delta t}) \quad (2-5)$$

where the heat of combustion of the volatiles is given by

$$F_i^t = \sum_{k=1}^n F_{i,k}^t Z_{i,k}^t / Z_i^t \quad (2-6)$$

since $Z_i^t = Z_i(t)$ and $Z_{i,k}^t = Z_{i,k}(t)$ then $F_i^t = F_i(t)$.

The energy equation is first solved for the temperature. Then the rate equations are used to update the mass retention fraction for each component in each slice. The total mass retention fraction, Z_i , for each slice is then determined, the property values are updated and the energy equation is solved for the temperature at the next time step.

The increase in enthalpy of an interior slice is equal to the heat conducted in minus the heat conducted out minus the heat absorbed by the pyrolysis gases passing through on their way to the front surface minus or plus the heat absorbed or generated by pyrolysis and evaporation. The energy equation for an interior slice can be written as

$$\begin{aligned}
& \rho_o \Delta X_o (Z_i^{t+\Delta t} C_i + Z_{w_i}^{t+\Delta t} C_{w_i}) T_i^{t+\Delta t} - (Z_i^t C_i + Z_{w_i}^t C_{w_i}) T_i^t \\
&= K_i \frac{T_{i-1}^{t+\Delta t} - T_i^{t+\Delta t}}{\Delta X} - \frac{T_i^{t+\Delta t} - T_{i+1}^{t+\Delta t}}{\Delta X} \Delta t l_y l_z \\
&+ (C_{g_i} \dot{m}_{i+1}'' + C_{w_i} \dot{m}_{w_{i+1}}'') \frac{T_{i+1}^{t+\Delta t} + T_i^{t+\Delta t}}{2} \Delta t \\
&- (C_{g_i} \dot{m}_i'' + C_{w_i} \dot{m}_{w_i}'') \frac{T_i^{t+\Delta t} + T_{i-1}^{t+\Delta t}}{2} \Delta t \\
&- h_{p_i} \rho_o \Delta X_o (Z_i^t - Z_i^{t+\Delta t}) - L_v \rho_o \Delta X_o (Z_{w_i}^t - Z_{w_i}^{t+\Delta t}) \tag{2-7}
\end{aligned}$$

where $\dot{m}_i'' = \frac{\rho_o \Delta X_o}{\Delta t} \sum_{j=i}^N (Z_j^t - Z_j^{t+\Delta t})$. (2-8)

14

Assuming instantaneous mass transfer,

$$\dot{m}_{w_i}'' = \frac{\rho_o \Delta X_o}{\Delta t} \sum_{j=i}^N (Z_{w_j}^t - Z_{w_j}^{t+\Delta t}) \tag{2-9}$$

$$\text{and } h_{p_i} = \sum_{k=1}^n \frac{Z_{i,k}^t}{Z_i^t} h_{p_k} \quad (2-10)$$

Here \dot{m}'' refers to the mass flow per unit original area of the specimen, not the contracted area. The heat of pyrolysis of the slice, h_{p_i} , is equal to the weighted averages of the heat of pyrolysis of each component.

Since $Z^{t+\Delta t}$ is not known ahead of the calculation of the temperature the time step must be small enough to ensure that the approximations

$$Z_i^t - Z_i^{t+\Delta t} \approx Z_i^{t-\Delta t} - Z_i^t \quad (2-11)$$

and

$$Z_{w_i}^t - Z_{w_i}^{t+\Delta t} \approx Z_{w_i}^{t-\Delta t} - Z_{w_i}^t \quad (2-12)$$

are valid. In the storage term (l.h.s. of equation (2-7)) it is easier to consider the heat-up of all of the mass present in the slice at the beginning of the time step including that lost by pyrolysis and evaporation during the time step. This mass loss then must not be added to the pyrolysis gases flowing through the slice as far as transpiration cooling of that layer is concerned. Thus the mass flow rate through each slice is uniform, and equal to \dot{m}''_{i+1} .

When the energy equation is modified to take the two approximations in equations (2-11) and (2-12) into account and is divided through by $\rho_0 \Delta X_0 C_i$ it can be rewritten as

$$\begin{aligned}
& \left(Z_i^t + Z_{w_i}^t \frac{C_{w_i}}{C_i} \right) (T_i^{t+\Delta t} - T_i^t) = \\
& \frac{K_i \Delta t \ell_y \ell_z}{\rho_o C_i (\Delta X_o)^2 \ell_x} \left(T_{i-1}^{t+\Delta t} + T_{i+1}^{t+\Delta t} - 2 T_i^{t+\Delta t} \right) \\
& + \left[\frac{C_{g_i}}{2C_i} \sum_{j=i+1}^N (Z_j^{t-\Delta t} - Z_j^t) + \frac{C_{w_i}}{2C_i} \sum_{j=i+1}^N (Z_{w_j}^{t-\Delta t} - Z_{w_j}^t) \right] (T_{i+1}^{t+\Delta t} - T_{i-1}^{t+\Delta t}) \\
& - \frac{h_{p_i}}{C_i} (Z_i^{t-\Delta t} - Z_i^t) - \frac{L_v}{C_i} (Z_{w_i}^{t-\Delta t} - Z_{w_i}^t) \tag{2-13}
\end{aligned}$$

It is noted that $\Delta X = \ell_x \Delta X_o$.

Let

$$P_i \equiv \frac{K_i \ell_y \ell_z \Delta t}{\rho_o C_i (\Delta X_o)^2 \ell_x} \tag{2-14}$$

and rewrite the energy equation in matrix format for solution of a set of algebraic equations for $T_i^{t+\Delta t}$ using an implicit method:

$$\begin{aligned}
& \left[-P_i + \frac{C_{g_i}}{2C_i} \sum_{j=i+1}^N (Z_j^{t-\Delta t} - Z_j^t) + \frac{C_{w_i}}{2C_i} \sum_{j=i+1}^N (Z_{w_j}^{t-\Delta t} - Z_{w_j}^t) \right] T_{i-1}^{t+\Delta t} \\
& + (2P_i + Z_i^t + Z_{w_i}^t \frac{C_{w_i}}{C_i}) T_i^{t+\Delta t} + \left[-P_i - \frac{C_{g_i}}{2C_i} \sum_{j=i+1}^N (Z_j^{t-\Delta t} - Z_j^t) - \frac{C_{w_i}}{2C_i} \sum_{j=i+1}^N (Z_{w_j}^{t-\Delta t} - Z_{w_j}^t) \right] T_{i+1}^{t+\Delta t} \\
& = \left(Z_i^t + Z_{w_i}^t \frac{C_{w_i}}{C_i} \right) T_i^t - \frac{h_p}{C_i} (Z_i^{t-\Delta t} - Z_i^t) - \frac{L_v}{C_i} (Z_{w_i}^{t-\Delta t} - Z_{w_i}^t) . \tag{2-15}
\end{aligned}$$

There is no mass flow of volatiles through the rear face which forms the rear boundary of slice N. Hence equation (2-15) for $i=N$ reduces to

$$\begin{aligned}
 & - P_N T_{N-1}^{t+\Delta t} + \left(P_N + Z_N^t + Z_{wN}^t \frac{C_{wN}}{C_N} \right) T_N^{t+\Delta t} \\
 & = \left(Z_N^t + Z_{wN}^t \frac{C_{wN}}{C_N} \right) T_N^t - \frac{h_{pN}}{C_N} (Z_N^{t-\Delta t} - Z_N^t) - \frac{L_v}{C_N} (Z_{wN}^{t-\Delta t} - Z_{wN}^t) \quad (2-16)
 \end{aligned}$$

Radiative and convective heat transfer must be taken into account at the front surface which forms the front boundary of slice 1. Absorption and emission of radiation within the depth of the specimen is assumed to be negligible. Prior to ignition the surface is cooled by laminar free convection. After ignition it is heated by the flame. The front surface temperature, T_s , for these calculations is obtained by linear extrapolation from the center points of the two slices nearest the surface,

$$T_s = \frac{3}{2} T_1 - \frac{1}{2} T_2 \quad (2-17)$$

The reradiation from the surface is given by

$$\alpha \sigma (T_s^4 - T_o^4) = \alpha \sigma (T_s^2 + T_o^2) (T_s + T_o) (T_s - T_o) \quad (2-18)$$

The energy flow across the front surface is given by

$$\dot{q}_{net}'' = \dot{q}_e'' + \dot{q}_{fR}'' - \omega (T_s - T_o) + h_f (T_f - T_s) B / (\exp(B) - 1) \quad (2-19)$$

where

$$\omega = \alpha\sigma (T_s^2 + T_o^2) (T_s + T_o) + hB/(\exp(B) - 1) \quad (2-20)$$

and

$$B = \dot{m}'' (h + h_f)/C_g$$

where h is the convective heat transfer coefficient from the surface to the ambient air which drops to zero after ignition, h_f is the convective heat transfer coefficient for the flame to the surface which is equal to zero prior to ignition, T_f is the flame temperature, \dot{m}'' is the mass flux through the front face, C_g is the heat capacity of the gas, and B is the mass transfer number introduced by Spalding [14], which is proportional to the mass loss rate and thus accounts for blowing. Prior to ignition the radiant heat flux from the flame, \dot{q}_{fR}'' , is zero.

The energy equation for the first slice is given by a slight extension of equation (2-7)

$$\rho_o \Delta X_o \left[(Z_1^{t+\Delta t} C_1 + Z_{w_1}^{t+\Delta t} C_{w_1}) T_1^{t+\Delta t} - (Z_1^t C_1 + Z_{w_1}^t C_{w_1}) T_1^t \right] =$$

$$\left[\dot{q}_e'' + \dot{q}_{fR}'' - \omega \left(\frac{3}{2} T_1^{t+\Delta t} - \frac{1}{2} T_2^{t+\Delta t} - T_o \right) \right.$$

$$\left. + h_f T_f - \frac{3}{2} T_1^{t+\Delta t} + \frac{1}{2} T_2^{t+\Delta t} \right] B/(\exp(B)-1) - K_1 l_z l_y \frac{T_1^{t+\Delta t} - T_2^{t+\Delta t}}{\Delta X} \Delta t$$

$$\begin{aligned}
& + (C_{g_1} \ddot{m}_2 + C_{w_1} \ddot{m}_{w_2}) \frac{T_2^{t+\Delta t} + T_1^{t+\Delta t}}{2} \Delta t - (C_{g_1} \dot{m}_1 + C_{w_1} \dot{m}_{w_1}) \frac{3}{2} T_1^{t+\Delta t} - \frac{1}{2} T_2^{t+\Delta t} \Delta t \\
& - h_{p_1} \rho_o \Delta X_o (Z_1^t - Z_1^{t+\Delta t}) - L_v \rho_o \Delta X_o (Z_{w_1}^t - Z_{w_1}^{t+\Delta t}) \quad (2-21)
\end{aligned}$$

In final form this becomes

$$\begin{aligned}
& Z_1^t + Z_{w_1}^t \frac{C_{w_1}}{C_1} + P_1 \left[1 + \frac{3}{2} \frac{\ell_x \Delta X_o}{K \ell_y \ell_z} \omega + h_f B / (\exp(B) - 1) \right] + \frac{C_{g_1}}{C_1} \sum_{j=2}^N (Z_j^{t-\Delta t} - Z_j^t) \\
& + \frac{C_{w_1}}{C_1} \sum_{j=2}^N (Z_{w_j}^{t-\Delta t} - Z_{w_j}^t) T_1^{t+\Delta t} \\
& + -P_1 \left[1 + \frac{1}{2} \frac{\Delta X_o}{K \ell_y \ell_z} \ell_x \omega + h_f B / (\exp(B) - 1) \right] - \frac{C_{g_1}}{C_1} \sum_{j=2}^N (Z_j^{t-\Delta t} - Z_j^t) \\
& - \frac{C_{w_1}}{C_1} \sum_{j=2}^N (Z_{w_j}^{t-\Delta t} - Z_{w_j}^t) T_2^{t+\Delta t} \\
& = (Z_1^t + Z_{w_1}^t \frac{C_{w_1}}{C_1}) T_1^t + P_1 \frac{\Delta X_o \ell_x}{K \ell_y \ell_z} \ddot{Q}_e + \ddot{Q}_f + \omega T_o + h_f T_f B / (\exp(B) - 1) \\
& - \frac{h_{p_1}}{C_1} (Z_1^{t-\Delta t} - Z_1^t) - \frac{L_v}{C_1} (Z_{w_1}^{t-\Delta t} - Z_{w_1}^t) \quad (2-22)
\end{aligned}$$

The change in mass retention fraction for each component of slice i during the time step is given by

$$Z_{i,k}^{t+\Delta t} - Z_{i,k}^t = - (Z_{i,k}^t - Z_{f,k}^t) A_k \exp(-E_k / RT_i^{t+\Delta t}) \Delta t \quad (2-23)$$

where $Z_{f,k}$ is the residual mass fraction of component k when pyrolysis is completed in an inert atmosphere, and A_k and E_k are the frequency factor and activation energy for component k . The total mass retention fraction for slice i is then given by

$$Z_i^{t+\Delta t} = Z_i^t - \sum_{k=1}^n (Z_{i,k}^{t+\Delta t} - Z_{i,k}^t). \quad (2-24)$$

The mass retention fraction for water is given by

$$Z_{w_i}^{t+\Delta t} = Z_{w_i}^t (1 - A_w \exp(-E_w/RT_i^{t+\Delta t}) \Delta t) \quad (2-25)$$

The parameters - K , ρ , C , C_w , C_g , α , A_k , A_w , E_k , E_w , F_k , h_{p_k} , L_v , l_x , l_y , and l_z - are needed as inputs to the model. While some of these data can be obtained within the accuracy needed by consulting the literature, the thermo-physical properties K , ρ , C , α , l_x , l_y , and l_z and the thermochemical properties A_k , E_k , F_k , and h_{p_k} must be determined experimentally for the material of concern. Most of these parameters vary with temperature and the mass retention fraction.

3. THERMOCHEMICAL PROPERTIES

3.1 Pyrolyzer

The pyrolyzer shown in figure 3 was constructed to obtain the kinetic constants A_k and E_k and the heat of combustion F_k required by the model. A small cavity is created in the center of the aluminum block by bolting three sections together. The block is heated to a constant and uniform temperature

by a hot plate and is insulated by 50 mm thick fiberglass batts. After a constant temperature is reached, a 50 mm diameter 1 mm thick specimen is inserted by placing it in the circular cutout in the sliding aluminum plate shown in figure 4. When the plate is slid into position it effectively seals off the insertion channel except for a small groove through which a 10 mil chromel alumel thermocouple passes. There are also notches in the circular portion of the plate to allow easy flow of nitrogen into the specimen chamber. The thermocouple is attached to the specimen by threading it through a series of holes and pulling the junction tight against the surface. A nitrogen stream sweeps the volatile pyrolysis products up into a lean methane/oxygen flame. The increase in CO₂ and H₂O and the drop in O₂ measured by the analyzers are used to calculate the carbon, hydrogen, and oxygen content of the volatiles according to the procedures outlined in Appendix C. The mass loss rate necessary to calculate the kinetic constants A_k and E_k is then given by

$$\dot{m} = \dot{m}_C + \dot{m}_H + \dot{m}_O \quad (3-1)$$

The heat release rate is calculated by determining the external oxygen requirement for complete combustion to water and carbon dioxide and multiplying by 13100 kJ/kg. It takes 8 grams of oxygen to convert 1 gram of hydrogen to water and 8/3 grams of oxygen to convert 1 gram of carbon to carbon dioxide. The mass of oxygen present in the volatiles must be subtracted from the total required to completely oxidize the hydrogen and carbon in order to determine the external oxygen requirement. It is assumed that 13100 kJ of heat is released for each kilogram of oxygen consumed [15]. This approximation is good to within ± 5% for most organic compounds. Thus

$$\dot{q}_{rel} = 13100 \left(8 \dot{m}_H + \frac{8}{3} \dot{m}_C - \dot{m}_O \right) \quad (3-2)$$

The heat of combustion is simply

$$\Delta H = \dot{q}_{rel} / \dot{m} \quad (3-3)$$

At the time of this status report the gas analysis system is not completely operative and thus alternate methods have been used to obtain these data. Specimens were pyrolyzed for prescribed periods of time, removed from the pyrolyzer, and weighed to obtain the mass loss rate data. The dimensional changes were measured to obtain the contraction factors l_x , l_y , and l_z as a function of the mass retention fraction.

3.2 Heat of Combustion of Pyrolysis Vapor

The gross heat of combustion of charred and uncharred specimens of Douglas fir particle board were determined with the oxygen bomb calorimeter. These data are plotted as open circles in figure 5. The data point on the vertical axis is pure carbon which might be considered to be the ideal end point in the charring process. However, in a fire situation it is the net heat of combustion, which refers to the case where the water remains as a vapor in the final state, that is important. From the overall chemical composition of the wood the amount of water produced during complete combustion can be determined. Thus the heat of evaporation of the water can be taken into account in order to obtain the net heat of combustion of the virgin wood. The upper dashed curve is the net heat of combustion assuming a linear drop in the correction factor for water as the final char is approached.

The heat of combustion of the volatiles is equal to the total heat released during combustion of the wood minus the total heat released during combustion of the char divided by the difference in mass between the wood and the char. The instantaneous heat of combustion of the volatiles is given by

$$F = \frac{d(m\Delta H)}{dm} = \Delta H + \left(\frac{m}{m_0}\right) \frac{d\Delta H}{d\left(\frac{m}{m_0}\right)} . \quad (3-4)$$

The derived values appear as closed circles in figure 5.

Using a linear approximation to the points between $Z = 0.4$ and 1.0 the heat of combustion of the volatiles can be represented over the range of concern by

$$\begin{aligned} F &= 20 [1.24 - Z] \text{ MJ/kg} & Z \geq 0.26 \\ &= 33.6 & Z < 0.26 \end{aligned} \quad (3-5)$$

which is expressed by the lower dashed curve. Although the calculated points demonstrate some curvature, the uncertainty in the assumed correction factor for water does not justify the inclusion of additional terms in eq. (3-5).

3.3 Calculation of Kinetic Constants from Mass Loss Data at Constant Temperature

Although there are several wood components present, each with different kinetic constants, it was decided to try to fit the decomposition of particle board to a single first-order reaction. This is the normal assumption for the mass loss rate models. In that case for specimens at a constant temperature

$$\frac{dm}{dt} = - (m - m_f) A \exp (- E/RT) \quad (3-6)$$

so that

$$\ln \frac{(m - m_f)}{(m_o - m_f)} = - t A \exp (- E/RT)$$

and

$$\ln \left[- \frac{1}{t} \ln \left(\frac{\frac{m}{m_o} - \frac{m_f}{m_o}}{1 - \frac{m_f}{m_o}} \right) \right] = \ln A - \frac{E}{R} \frac{1}{T} \cdot \quad (3-7)$$

The final char fraction m_f/m_o was found to be 0.225 after heating a specimen wrapped in aluminum foil in an oven for 5 minutes at 560°C. The intercept and slope of the plot of the l.h.s. of equation (3-5) against $1/T$ yields a frequency factor A of $5.9 \times 10^7 \text{ s}^{-1}$ and an activation energy E_a of 121 kJ/mol for the Douglas fir particle board, as seen in figure 6. The constancy of the l.h.s. of equation (3-7) for a given value of T depends on the assumption of a single first order reaction. Since this assumption is not completely valid, the expression in the brackets will vary for different combinations of m and t even at a fixed temperature and thus could be responsible for some of the scatter in figure 6. While the data need to be analyzed in terms of more than one reaction the constants determined in figure 6 are used in the initial checkout of the computer model for heat release rate.

3.4 Contraction Factors

The contraction factors measured along the surface (i.e., l_y and l_z) for southern pine are plotted in figure 7. The contraction is seen to be much greater across the grain than it is along the grain. In addition, the thickness of each specimen was measured with a micrometer. There was considerably more scatter in the latter data but they tended to center around the lower curve. The contraction factors for Douglas fir particle board are displayed in figure 8. The contraction is independent of direction and is midway between the contraction factors for southern pine. The data for Douglas fir particle board can be represented by the expressions,

$$l_x = l_y = l_z = 1 \quad \text{for } 0.65 \leq Z \leq 1.0 \quad (3-8)$$

$$l_x = l_y = l_z = 1 - (0.65 - Z)^2 \quad \text{for } Z < 0.65 \quad (3-9)$$

3.5 Heat of Pyrolysis

While differential scanning calorimeter (DSC) data has been taken on both southern pine and particle board to determine the heat of pyrolysis, these data have not been fully analyzed yet. The heat of pyrolysis is suspected to be small and has been therefore set equal to zero in the model. Atreya [13] has found that the results of his mass loss model for wood were relatively insensitive to the heat of pyrolysis. That sensitivity was also checked on this project by making a run with the model assuming a heat of pyrolysis of 400 kJ/kg which is approximately the value for alpha cellulose. The peak heat release rate was reduced by 20%.

3.6 Parameters Dealing with Moisture

Atreya found his mass loss rate model to be very sensitive to the moisture content [13]. He determined the frequency factor and activation energy for the desorption of water experimentally to be $4.5 \times 10^3 \text{ s}^{-1}$ and 43.9 kJ/mole. The heat of vaporization of water is 2.4 MJ/kg. These values were used in the present model.

4. THERMOPHYSICAL PROPERTIES

4.1 Heat Capacity

The specific heat of wood does not depend on density or even significantly on the species. However, it does depend rather strongly on temperature. In 1912 Dunlap [16] described this temperature dependence up to 106°C for 20 different species of wood as

$$C = 1.11 + 0.00486 T \quad (4.1)$$

In 1969 Koch [17] found that

$$C = 1.11 + .0042 T \quad (4-2)$$

for spruce pine between 60°C and 140°C where T is in °C and C is in kJ/kg°K. The present model simply extends the linear relationship in equation (4-2) to the highest temperature at which the wood retains its chemical structure. For moist specimens the heat capacity of the wood and the heat capacity of the

moisture are linearly combined. The heat capacity of charcoal is reported to be 0.67 kJ/kg ·K [16]. For the purposes of the initial running of the model the heat capacity has been assumed to vary linearly between wood and final char and to have the same temperature dependence as for wood. Thus

$$C = (1.11 + 0.0042 T) (0.43 + 0.57 Z) \quad (4-3)$$

for oven-dry wood and char.

4.2 Thermal Conductivity Data from the Literature

A universal formula for the thermal conductivity of wood (normal to the grain) and plywood (across the thickness) as a function of density and moisture content was established experimentally by MacLean [18]. This is given by

$$K = [237 + 2.00 \rho (1 - .020 M)] \times 10^{-7} \text{ kW/m}\cdot\text{K}. \quad (4-4)$$

The density, ρ , is expressed in kg/m^3 over a range of 300-800 kg/m^3 and the moisture content, m , in percent by weight over a range of 0-40%. This formula was also found to hold for charred wood up to a 37% mass loss. It is noted that when ρ goes to zero, k is equal to the thermal conductivity of air.

The ratio of the thermal conductivity along the grain to that across the grain will depend on the fibril angle. A typical ratio is 2.5. The more nearly aligned the fibers are along the length of the cell wall the higher the thermal conductivity in grain direction.

Thermal conductivity data on oven dry fiberboard and particle board at 24°C was obtained by Lewis [19] and is presented in Table 1.

Using these data and assuming that the contributions of the water and air were the same in the fiberboard and particle board as they were in the wood, equations of the same form as equation (4-3) were obtained for these materials. For fiberboard

$$K = [237 + 1.11 \rho (1 + .036 M)] \times 10^{-7} \text{ kW/m}\cdot\text{K} \quad (4-5)$$

and for particle board

$$K = [237 + 1.37 \rho (1 + .029 M)] \times 10^{-7} \text{ kW/m}\cdot\text{K}. \quad (4-6)$$

Lewis also reported average increases in thermal conductivity of 1.37×10^{-7} and 2.41×10^{-7} per deg C, respectively, for fiberboard and particle board. The temperature dependence of the thermal conductivity of wood was given by Kollmann [20] as

$$K = K_0 [1 + (1.1 - 9.8 \times 10^{-4} \rho) (T - T_0)/100] \text{ kW/m}\cdot\text{K} \quad (4-7)$$

The upper limit for this formula is 100°C.

4.3 Thermal Conductivity Measurements

The thermal conductivity was measured on this project as a function of temperature up to 250°C by exposing vertical specimens of thicknesses between 1 and 2 mm, which are at least 40 mm wide and high, to a radiant panel. Thermocouples were attached to the front and rear surfaces. At equilibrium the heat flowing through the specimen is lost from the rear face. Thus

$$K (T_1 - T_2)/D = \alpha\sigma (T_2^4 - T_o^4) + h_2 (T_2 - T_o)$$

or

$$K = \left[\alpha\sigma (T_2^4 - T_o^4) + h_2 (T_2 - T_o) \right] D / (T_1 - T_2) \quad (4-8)$$

where T_1 and T_2 are the front and rear surface temperatures, respectively. The only unknown on the r.h.s. (i.e., h_2) could be calculated assuming laminar free convection. Thus according to Schlichting [21],

$$h = 0.636 x^{-1/4} \frac{\lambda}{\sqrt{v}} \left(\frac{T - T_o}{T} \right)^{1/4} \quad (4-9)$$

where x is the distance from the bottom of the specimen to the thermocouple.

It can also be calculated from the energy balance:

$$\alpha\dot{q}_e'' = \alpha\sigma (T_1^4 + T_2^4 - 2T_o^4) + h_1 (T_1 - T_o) + h_2 (T_2 - T_o). \quad (4-10)$$

Thus

$$h_2 = \frac{\alpha \dot{q}_e'' - \alpha \sigma (T_1^4 + T_2^4 - 2T_o^4)}{T_2 - T_o + \frac{h_1}{h_2} (T_1 - T_o)} \quad (4-11)$$

If the temperature difference, $T_2 - T_1$, is small enough that λ and ν are the same at both faces and the thermocouple junctions are at the same height, the ratio h_1/h_2 is found from equation(4-9) to be

$$\frac{h_1}{h_2} = \left[\left(\frac{T_1 - T_o}{T_2 - T_o} \right) \frac{T_2}{T_1} \right]^{1/4} \quad (4-12)$$

As seen in figure 9 the 5 mil (0.127 mm) diameter thermocouples attached to the front and rear surface provide support for the specimen. The junctions are held firmly against the surface by threading them through small diameter holes and pulling tight. Improved thermal contact as well as a high and known absorptivity is achieved by coating both surfaces of the specimen with a spray coat of Krylon 1602* which has an absorptivity of 0.94 [22]. The effect of the extra thickness provided by the paint has not been investigated yet. The wires then go to a digital thermocouple readout with a built-in electronic cold junction.

The external radiant flux incident on the front face is controlled by varying the distance from the panel. Equilibrium is established in less than one minute thereby allowing the specimen to go to relatively high temperatures without significant decomposition as opposed to the standard guarded hot plate method which takes many hours to establish thermal equilibrium. At each distance the external heat flux and surface temperatures are recorded. A

*The product name is given for identification purposes only and does not constitute an endorsement.

small computer program was written to calculate the thermal conductivity from the above input data. The convective heat transfer coefficient is also calculated by the program as a check on the system.

Table 2 shows the results for a 1.27 mm thick oven dry specimen of southern pine while table 3 shows similar data for a charred specimen. These data are plotted in figure 10. The lines represent a least squares fit. The extrapolated value of the thermal conductivity at 20°C is 1.22×10^{-4} kW/m ·K compared to 1.23×10^{-4} kW/m ·K predicted by MacLean's formula (4-4) using the measured density of southern pine which is 498 kg/m³. The calculated values from eq. (4-4) for both charred and uncharred pine are included in the figure.

The measured density of the char is 207 kg/m³. However, the calculated temperature coefficient using Kollman's formula (4-7) is an order of magnitude higher than the measured one. The thermal conductivity data plotted in figure 10 can be expressed by the formula

$$K = 1.20 (1 + 0.0026 (1.35 - Z) T) (0.71 Z + 0.29) \times 10^{-4} \text{ kW/m}\cdot\text{K} \quad (4-13)$$

where the temperature is in °C.

The experimentally determined thermal conductivity of uncharred and charred Douglas fir particle board is listed in tables 4 and 5 and plotted in figure 11. The value of the thermal conductivity of uncharred particle board at 20°C in figure 11 was determined with a guarded hot plate. The upper line was obtained by a least squares fit. Because of the larger scatter and the limited temperature range of the data the use of a least squares fit for the

lower line led to an unreasonably high value of the thermal conductivity of the char at ambient temperature. Thus the lower line was passed through the center of gravity of the data points and the calculated value of the thermal conductivity using eq. (4-6) with the measured char density. The thermal conductivity represented by the lines in figure 11 can be expressed as

$$K = 1.16 (1 + 0.0058 (1.6 - Z) T) (0.84 Z + 0.16) \times 10^{-4} \text{ kW/m}\cdot\text{K} \quad (4-14)$$

Equation (4-14) was used in the computer model. This equation was determined for the temperature range over which wood could be expected to exist in its original form and is simply extrapolated into the high temperature region. High temperature data on charred specimens are needed to accurately predict the thermal conductivity over the full temperature range required. The measured value of the thermal conductivity at 20°C using eq. (4-14) for extrapolation is 1.24×10^{-4} kW/mK compared to 1.21×10^{-4} kW/m ·K calculated from equation (4-6) using a density of 709 kg/m³ for Douglas fir particle board. The calculated and measured temperature coefficients were within 20% for the particle board.

The rear surface convective heat transfer coefficient was calculated for comparison with the measured values reported in table 2. At the highest heat flux the rear surface temperature for uncharred southern pine was 234°C. In this case the average film temperature in the boundary layer was 127°C. The thermal conductivity and kinematic viscosity at this temperature are 3.37×10^{-5} kW/mK and 25.9×10^{-6} m²/s [21], respectively. The thermocouple junction was 0.02 m above the lower edge and the ambient temperature was 30°C. When these data were substituted into equation (4-9) the heat transfer

than the measured value. In addition to experimental errors, the flow may not correspond to the ideal condition required by equation (4-8). On the other hand the height of the particle board specimens was twice that of the pine yielding a calculated coefficient at 230°C of 0.0079 which is 30% higher than the measured value in table 4. These 30% differences only lead to a 10% error in the thermal conductivity at 230°C.

5. CALCULATIONS OF HEAT RELEASE RATE USING THE MODEL

The computer program requires input data for a number of parameters. Some of these have been experimentally determined on the project, some have been taken from the literature and some are simply assumed at this stage. These parameters along with their assigned values and sources are listed in Table 6. The front and rear surface temperature, the mass loss rate (equation (2-4)), the heat release rate (equation (2-5)), the char depth, and the effective heat of combustion are all calculated as a function of time during the test. The effective heat of combustion is simply equal to the ratio of the heat release rate and the mass loss rate. The char depth is equal to ΔX_0 multiplied by the number of slices for which Z is less than 0.95. Some of these outputs are plotted in figures 12 to 19 for different external radiant heat fluxes, specimen thicknesses, and moisture contents. The baseline case is for an oven dry 12.7 mm thick specimen of Douglas fir particle board exposed to an external radiant heat flux of 50 kW/m². In all cases the rear surface is assumed to be insulated and impervious to the flow of volatile pyrolysis products and water vapor.

The program has been set up on a Tektronix 4052 terminal using BASIC. The total number of slices is limited to 60 by the capacity of the micro-computer. The longest acceptable time step is one second at an incident flux of 25 kW/m^2 , and 0.1 second at an incident flux of 100 kW/m^2 . This can be increased later on in the run. These critical times were determined by using successively smaller time steps until there were no further changes in the output data curves. The calculations require about 30 seconds per time step. A typical run takes about 4 hours.

The calculated front and rear surface temperatures for a dry 12.7 mm specimen of Douglas fir particle board exposed at an external radiant flux of 50 kW/m^2 are shown in figure 12. The front surface temperature shows a cusp at 45 seconds, when ignition occurred. It approaches 700°C by the time the flame goes out. Figure 13 shows the predicted progression of the char front into the material. The char front here is taken to be located at the center point of the slice whose mass retention fraction has just dropped to 0.95. After an initial rapid penetration the charring rate becomes nearly constant until the rear surface temperature starts to rise. Then it increases abruptly. The apparently constant rate may depend on specimen thickness. Figure 14 shows the predicted mass flow through the front surface. The second large peak occurs when the thermal wave is reflected from the insulated rear face. This second peak would be missing altogether if the rear surface were maintained at some low temperature. Figure 15 shows the calculated heat release rate curve. Its features are similar to the mass loss rate curve except that it rises abruptly from zero to 30 kW/m^2 at ignition and the ratio of the second and first peak is higher for the heat release rate curve. The first peak is about 240 kW/m^2 . The effective heat of combustion is plotted in

figure 16. It is relatively constant over the first part of the curve decaying only slightly to a minimum and then rising abruptly when the rear surface begins to char. The magnitude during the early part of the curve is 12 MJ/kg versus 20 MJ/kg for the gross heat of combustion of the uncharred particle board determined by the oxygen bomb calorimeter. The bump in the curve around 400 s is an artifact caused by a change in the time step size at that point.

Throughout the above calculations, the heat of pyrolysis has been set equal to zero. The effect of the heat of pyrolysis on the heat release rate curve is displayed in figure 17 where it has been set equal to 400 kJ/kg which is approximately the value for alpha cellulose. This resulted in a 20% drop in the peak heat release rate and a substantially larger drop in the second peak. Figure 18 shows the effect of a 7% moisture content. This is the equilibrium value for Douglas fir conditioned at 50% RH at 23°C. This results in a drop in the peak heat release rate of about 10%. The value of the first peak is relatively unaffected by decreasing the thickness of the slab but the second peak is much higher and earlier in time as seen in figure 19. Lowering the irradiance to 25 kW/m² lowers the first peak and extends the time scale as seen in figure 20. The calculated heat release rate curves for 75 and 100 kW are presented in figures 21 and 22.

6. HEAT RELEASE RATE MEASUREMENTS IN THE CONE CALORIMETER

Heat release rate measurements were made on oven dry specimens of Douglas fir particle board at external radiant flux levels of 25, 50, 75, and 100 kW/m². The specimens were all 12.7 mm thick. The measurements were made in the vertical orientation in the NBS cone calorimeter [7] and are shown in figures 23 through 26.

The heat release rates are determined using the standard method for this calorimeter which is based only on the oxygen concentration and the volume flow measured in the exhaust duct. A standard estimated correction is made to account for the difference between the molar flow of air into the system and the molar flow of gas in the exhaust duct due to chemical reaction. The mass loss rate is determined from the load cell.

The first peaks of the measured heat release rate curves increase with the incident radiant flux but are about 20% lower than the calculated ones. The second peaks are lower than the first peaks for the measured curves. This is probably due to the absorption of some heat by the insulation material in contact with the rear surface. The first peaks fall off faster and the second peaks occur later for the calculated curves. This discrepancy could be due to inadequate data on the thermal properties of the char at high temperature or unrealistic kinetics defined by the assumption of a single first order reaction. The calculated heat of combustion is close to the measured values and is independent of the incident radiant flux. See for example figures 16 and 27-30. The early segments of these experimental curves to the left of the dashed lines are due to instrumental problems and should be ignored.

The three analyzer method of calculating the heat release rate and effective heat of combustion in the cone calorimeter relies on the concentrations measured in the carbon dioxide and water vapor analyzers as well as the oxygen analyzer.

The density of the exhaust gases is determined from the concentrations of oxygen, carbon dioxide and water vapor in the analyzers according to Appendix

A. This density along with the exhaust temperature and pressure drop across the orifice plate in the duct determine the nitrogen flow through the system according to Appendix B. The nitrogen flow along with the above concentrations were used in the calculation of the mass flows of carbon, hydrogen and oxygen from the specimen using Appendix C. The latter quantities were used to determine the mass loss rate and heat release rate and hence the effective heat of combustion using the methods of section 3.2. The calculation of heat release rate using all three analyzers is based on the assumption that the fuel vapors generated by the burning specimen are composed only of carbon, hydrogen, and oxygen and that combustion is complete. It is not recommended for the determination of heat release rates in general. The heat release rate and the effective heat of combustion determined by the three analyzer method are shown in figures 31 and 32 for the 50 kW/m^2 external radiant flux. These curves depart from those determined by the standard method early in the exposure because of as yet unresolved problems with the time response of the water vapor measurement system.

7. DISCUSSION

The prediction of the heat release rate of wood involves (1) the development of a suitable computer program which includes all of the important physics with acceptable assumptions and approximations and which converge to the exact solution of the formulated equations and (2) the gathering of the required input data on the properties of the particular wood specimen over a large temperature and decomposition range.

The computer model includes a description of the heat transfer at the surfaces, an ignition criterion, the formulation of an energy equation in the interior along with rate equations for the various chemical species which make up the solid wood, a means of accounting for the shrinkage of the char, and a way of dealing with the fissures formed by the shrinkage. This model only applies during the flaming phase. It is assumed that during this period the oxygen is completely excluded from the surface so that there is no oxidation of the char and the pyrolysis takes place in an inert atmosphere.

The heat transfer to the surface includes a specified external radiant flux, radiation from the surface and convective heat losses assuming laminar free convection. Laminar flow seems reasonable for the 100 mm high specimens in the cone calorimeter which is used to check out the model. Turbulence will have to be included in dealing with the heat release rate from a burning wall. After ignition the convective loss term is replaced by flame radiation and convective heat transfer to the surface. The radiation to the surface was assumed to be 10 kW/m^2 based on measurements by Tewarson [8]. This would only be expected to apply to small surfaces. The convective heat transfer coefficient was obtained by measuring the total flux to a 3 mm diameter water cooled heat flux gage embedded in the surface. The 10 kW/m^2 flame radiation was subtracted from the 30 kW/m^2 measured by the gauge. This difference was divided by the difference between the flame temperature, which was measured by a 2 mil thermocouple to be 1200°C , and the water temperature of 20°C . This yielded a convective heat transfer coefficient of $0.017 \text{ kW/m} \cdot \text{K}$. Any temperature dependence was neglected. However, the coefficients both before and after ignition are modified by a blowing factor. This depends on the B number which is equal to the product of the mass loss rate times the heat capacity of

the volatiles divided by the appropriate heat transfer coefficient. The heat capacity of the volatiles was assumed to be the same as that of air. Emission and absorption of radiation at the surface of the specimen depends on the surface emissivity. This was determined to be 0.80 from the ratio of the derivatives of the surface temperature with respect to the square root of the time at the beginning of the exposure for unblackened and blackened specimens exposed to a gas-fired radiant panel. Any change in spectral emissivity with wave length was neglected. A state of the art flame heat transfer model needs to be incorporated into the heat release rate model.

The piloted ignition criterion adopted here was the attainment of a calculated heat release rate which would be sufficient to maintain a flame over the entire surface of the specimen. For lower heat release rates the shortening of the flame will lead to extinction. In the analysis of the Steiner tunnel [23] it was found that this critical value was approximately 50 kW/m^2 . However, prior to ignition when the test calculation is made there is no flame heat transfer. Hence the calculated heat release rate would be less than 50 kW/m^2 at the time just prior to piloted ignition. It was reduced to 30 kW/m^2 so that ignition could be achieved in the model at an external radiant heat flux of 25 kW/m^2 which is sufficient to cause ignition of this material in the cone calorimeter. This choice could have considerable impact on the time to ignition but probably a minor effect on the heat release rate beyond the very early part of the curve. In any event this is another part of the model which needs to be improved.

It was necessary to use a difference formulation for the energy equation because the dimensions of the slices and the material properties change during

the burning period and are, in general, different for each slice. A grid of 60 slices was necessary to prevent oscillations in the calculated heat release rate versus time curve for the 12.7 mm Douglas fir specimens. This grid size required a time step no greater than 1 second at an external radiant flux of 25 kW/m² and 0.1 second for 100 kW/m². However, after the minimum in the heat release rate curve the time step could be increased. The maximum permissible time step was found by reducing it until there was no perceptible difference in the generated heat release rate curve. The time step determined this way did not satisfy the usual convergence criterion,

$$\frac{K\Delta t}{\rho C(\Delta X)^2} \leq 1/2, \quad (7-1)$$

in the case of the larger time steps. If the oscillations referred to above were due to the violation of the convergence criterion, the effect of reducing the grid spacing would be to aggravate the problem. They are more likely to be due to intolerably large changes in z or in the material properties over the distance Δx .

An important element of this model is the ability to consider the rate equation, heat of pyrolysis, heat of combustion of the volatiles generated during pyrolysis, and heat capacity separately for each chemical component present in the solid wood. However, as a practical consideration it is necessary to lump in so far as possible all of the species with similar properties and ignore those that are present in very small quantities. Thus wood might be considered to consist of three components - cellulose, lignin and hemicellulose - although hemicellulose consists of a number of different carbohydrates and there is a small quantity of miscellaneous extractives present.

To make use of the additional detail it is necessary to measure the properties of the individual components. Since this has not been done as yet, it has been necessary to consider wood as a single chemical species in this report. Assigning a single first order reaction to wood has not been very satisfactory as can be seen in figure 6 where different combinations of m and t at a fixed temperature do not lead to the same value for the ordinate as they would if the rate were given by equation (3-6).

The char shrinkage normal to the surface is easily handled by the energy equation by taking the change in slice dimensions into account. The reduction in spacing results in higher temperature gradients which increase heat conduction. Shrinkage parallel to the surface, while the specimen width is maintained by the rigidity of the remaining virgin wood, sets up stresses which relieve themselves by the formation of fissures. These are visible as deep cracks in the surface. The reduction in the area of the region of the surface between the fissures represents a reduction in the area through which heat is conducted and also in the area normal to the external heat flux and the heat flux from the flame. This results in a reduction in heat transfer. However, the radiant flux can now penetrate deep within the specimen in the area of the fissures. This is counteracted by the easy outflow of volatiles through the fibers parallel to the surface. They flow into the fissures and carry the excess heat with them as they exhaust through the cracks. Up until the time of the fissure formation the volatiles cool the char layer as they pass through it. Then the cooling is shut off as the layer is by-passed. The depth of the fissures is taken to be the middle of the slice whose mass retention factor has just dropped to $Z_f + 0.05 (1 - Z_f)$. This is where 95% of the mass that can be lost is lost.

The bulk properties required as input to the model include the thermal conductivity, heat capacity, char contraction factors, kinetic constants, and the heat of combustion and heat capacity of the volatiles generated during pyrolysis. Sensitivity tests with the model indicated that the shape of the heat release rate versus time curve was strongly dependent on the thermal conductivity. Thermal conductivity data on this project were limited to temperatures below 250°C which is the temperature at which the lower molecular weight species in wood start to decompose. It will be necessary to extend these data up to 700°C on char. The measurements must be done in an inert atmosphere to avoid glowing combustion of the char. The general formula for the thermal conductivity of wood, equation (4-3), as a function of its density and moisture content is probably adequate at room temperature. However, the temperature dependence given by equation (4-6) does not appear to be adequate particularly beyond its reported range of validity which is only up to 100°C. At the present time it will be necessary to measure the temperature dependence for each species of wood at its applicable density. It does appear, however, that it may be possible to construct a temperature dependent heat conduction model in which there is solid phase heat conduction through the fiber walls and gas phase heat conduction and radiation through the pore spaces.

The general formula for the heat capacity of wood, equation (4-1), does appear to apply to all woods over the temperature range for which they are stable. However, data on the heat capacity of char at high temperatures is needed. The heat capacity of the volatiles can be deduced from the measurements of the heat capacity of the char.

Figures 15 and 17 show the calculated heat release rates at an external flux of 50 kW/m^2 for assumed heats of pyrolysis of 0 and 400 kJ/kg, respectively. The effect on the shape and amplitude of the curve is significant. Therefore, the heat of pyrolysis must be measured.

Comparison of figures 15 and 20 with figures 24 and 23 show that the calculated ignition times are nearly twice as long as the measured ones. It should be noted that the model assumes a constant absorptivity of 0.8 for the incoming radiation. As the surface layer begins to char the absorptivity should approach unity for the real specimen in the cone calorimeter and thus a shorter measured time to ignition would be expected. The calculated char depth (see figure 13) shows that the calculated time at which the surface layer loses 5% of its mass is close to the time that the actual specimen ignites. The calculated ignition temperature, indicated by the cusp in figure 12, was 420°C which is somewhat higher than the 380°C reported by Quintiere and Harkleroad [24] for Douglas fir particle board. Choosing a critical calculated heat release rate of less than 30 kW/m^2 would have lowered the calculated ignition temperature and shortened the calculated time to ignition. As indicated earlier, the ignition criterion in the model must be improved. It should also be noted that the effect of diathermancy is neglected in the model. It is difficult to judge its impact on the time to ignition.

One of the motivating factors for the introduction of a heat release rate model over that of a mass loss rate model was the variation in the effective heat of combustion during the burning period. However, the calculated effective heat of combustion for dry Douglas fir particle board can be represented by 12 MJ/kg to within $\pm 10\%$ over the first three quarters of the burning

period for all fluxes between 25 and 100 kW/m². The constancy of the effective heat of combustion is also demonstrated by the similarity of the calculated heat and mass loss rate curves in figures 14 and 15. This is so in spite of a large variation in the heat of combustion of the vapors over the full range of decomposition for a single layer within the specimen. This finding is in agreement with the measurements in the cone calorimeter. Thus a constant effective heat of combustion might be used in the flame spread models after all, at least for Douglas fir particle board. However, it is necessary to measure the effective heat of combustion for the material rather than use the gross heat of combustion measured in the oxygen bomb calorimeter. The calculations demonstrate that the low values of the measured effective heat of combustion of wood are not due to incomplete combustion but rather to the difference in the carbon:hydrogen:oxygen ratio in the vapors from that of the virgin wood.

The formulas developed in Appendices A, B, and C are included here primarily because they will be used to determine the kinetic constants and the heat of combustion of the vapors on this project in the future. The three analyzer method used to obtain the heat release rate and the effective heat of combustion of the specimen in the cone calorimeter, as shown in figure 31 and 32, serves as a partial demonstration of their use. It is unfortunate that the water vapor analysis system was not functioning properly during the initial phase of the project. The three analyzer method also provides a means of determining the effective overall chemical composition of the volatiles in the cone calorimeter using the formulas of Appendix C.

8. SUMMARY

This is a status report on the prediction of the heat release rate of wood. While much remains to be done in order to obtain a completely satisfactory model, a first cut on the overall problem has been completed. A computer program has been written, laboratory test methods have been devised to obtain the critical input data, calculations have been made using the model and comparisons have been made with experimentally determined heat release rates from the cone calorimeter. For the limited comparisons made, the predicted and measured effective heats of combustion over most of the burning period are within 25% and the peak heat release rates are within 20%. The shape of the calculated and measured heat release rate curves are similar but the time scales are substantially different. This may be due to inadequate data on the thermal properties of char at high temperatures. The second peak of the measured heat release rate curve is considerably smaller than the measured one. This may be due to heat conduction into the marineite backing board.

The computer model is unique in that it (1) accounts for the change in the heat of combustion of the volatiles generated during the pyrolysis period, (2) accounts for char shrinkage, and (3) provides for different reaction rates for the different components of wood. However this last capability was not exercised during this first test of the model where a single first order reaction was assumed. This is the standard assumption used in the kinetic mass loss rate models.

New experimental techniques have been devised to measure the heat of combustion of the volatile pyrolysis products and the thermal conductivity of

wood and wood char at higher temperatures than can be attained for pyrolyzing materials using the standard methods. During the next stage of the project the thermal conductivity measurements on the char must be carried to higher temperatures still. Also high temperature data on the heat capacity of char must be obtained. The experimental data obtained on the above properties were determined from a limited number of tests and have not been subjected to a rigorous error analysis. Therefore they must be regarded as preliminary data at this point.

9. FUTURE PLANS

As this work continues improvements will be made in the model and in the experimental methods employed to obtain the input data. Furthermore a much broader data base will be obtained on the thermophysical and thermochemical properties of wood and wood char, particularly at high temperature. In order to reliably describe the kinetic constants for the thermal decomposition of wood and the effective heat of combustion of its volatile pyrolysis products as a function of time, it will be necessary to make these determinations on the individual wood components (i.e., cellulose, hemicellulose, and lignin). The prediction techniques will also need to be extended to include other wood products such as fiber board, hardboard, and plywood. The effect of fire retardants will also be included.

Improvements to be made to the computer model will include (1) the reduction in grid size and in the time of calculation by transferring the program to a larger computer, (2) a state of the art model for the flame heat transfer to the front surface, (3) an improved ignition criterion, (4) modification of

the boundary condition at the rear surface to simulate the marinite block typically used to back the specimen in the heat release rate calorimeter or the simulation of the wall cavity during a room fire, and (5) a model for calculating the impact of the fissures.

In the verification tests with the calorimeter some restraint system will have to be used to hold the specimen in place as long as possible in order to extend the period over which the calculated and measured heat release rates can be compared. At present the warping of the specimen near the end of the test allows flames to move around to the rear surface; or the specimen may fall out of the holder altogether. For selected tests the specimen will be instrumented with thermocouples to check the calculated temperature profiles. Some effort will be devoted to measuring the heat flux from the flame to the surface in the calorimeter.

Improvements in the pyrolyzer will be aimed at better heat transfer to the specimen to reduce the amount of decomposition that it undergoes by the time it reaches a constant pyrolysis temperature. Other problems with the present pyrolyzer will only become apparent when it is finally used in the gas analysis mode; those tests should begin soon. It will be beneficial to have determined the critical thermochemical properties by two entirely different methods.

10. ACKNOWLEDGMENTS

This work was supported in part by FEMA. Henry Tovey served as the technical monitor. In addition I am grateful to Bill Twilley who constructed the pyrolyzer and helped on many of the other facets of the project.

11. REFERENCES

1. Babrauskas, V., "Estimating Room Flashover Potential," Fire Technology, Vol. 16, No. 2, May 1980, pp 94-103.
2. McCaffrey, B.J., Quintiere, J.G. and Harkleroad, M.F., "Estimating Room Temperatures and the Likelihood of Flashover Using Fire Data Correlations," Fire Technology, Vol. 17, No. 2, May 1981, pp 98-119.
3. Smith, E.E., "Heat Release Rate of Building Materials," ASTM Special Technical Publication 502, June 1972.
4. Parker, W.J. and Long, M.E., "Development of a Heat Release Rate Calorimeter at NBS," ASTM Special Technical Publication 502, June 1972.
5. Tewarson, A., "Heat Release Rate from Burning Plastics," J. Fire and Flammability, 8, 115, 1977.
6. Tordella, J.P. and Twilley, W.H., "Development of a Calorimeter for Simultaneously Measuring Heat and Mass Loss," NBSIR 83-2708, Nat. Bur. Stand. (U.S.), June 1983.
7. Babrauskas, V., "Development of the Cone Calorimeter -- A Bench-Scale Heat Release Rate Apparatus Based on Oxygen Consumption," NBSIR 82-2611, Nat. Bur. Stand. (U.S.), Nov. 1982.
8. Tewarson, A., "Physico-Chemical and Combustion, Pyrolysis Properties of Polymeric Materials," NBS-GCR-80-295, Nat. Bur. Stand. (U.S.).
9. Tang, W.K. and Neil, W.K., "Effect of Flame Retardants on Pyrolysis and Combustion of α -Cellulose," J. of Polymer Sci.: C, 65 (1964).
10. Kanury, A.M., "Rate of Burning of Wood (A Simple Thermal Model)," Combustion Science and Technology, Vol. 5, 1972.
11. Kung, H.C., "A Mathematical Model of Wood Pyrolysis," Combustion and Flame, Vol. 18, pp 185-195 (1972).
12. Tamanini, F., "A Study of the Extinguishment of Wood Fires," Ph.D. Thesis, Harvard University, May 1974.
13. Atreya, A., "Pyrolysis, Ignition, and Fire Spread on Horizontal Surfaces of Wood, Ph.D. Thesis, Harvard University, May 1983.
14. Spalding, D.B., Intern. J. Heat Mass Transfer, Vol. 1, pp. 192-207, 1960.
15. Huggett, C., "Estimation of Rate of Heat Release by Oxygen Consumption Measurements", Fire and Materials, Vol. 4, pp. 61-65 (1980).
16. Dunlap, F., "The Specific Heat of Wood", U.S. Dep. Agr. Bull. No. 110, Washington, DC, 1912.

17. Koch, P., "Specific Heat of Oven-Dry Spruce Pine Wood and Bark," Wood Sci. 1:203-214, 1969.
18. MacLean, J.D., "Thermal Conductivity of Wood," Heating, Piping and Air Conditioning 13:380-391, 1941.
19. Lewis, W. C., "Thermal Conductivity of Wood-Base Fiber and Particle Panel Materials," USDA Forest Serv. Res. Pap. FPL-77, 12 pp, Forest Prod. Lab., Madison Wisconsin 1967.
20. Kollmann, F.F.P. and Cote, W.A., "Principles of Wood Science and Technology, Volume I: Solid Wood", Springer-Verlag, New York, 1984, p. 250.
21. Schlichting, H., "Boundary Layer Theory," 4th Edition, McGraw Hill, 1960, pp 332-334.
22. Brown, R.J. and Young, B.G., "Spectral Emission at Ambient Temperatures", Applied Optics, Vol. 14, No. 12, Dec. 1975, p. 2927.
23. Parker, W.J., "An Assessment of Correlations Between Laboratory and Full Scale Experiments for the FAA Aircraft Fire Safety Program, Part 3: ASTM E84", NBSIR 82-2564, Nat. Bur. Stand. (U.S.), Aug. 1982.
24. Quintiere, J.Q. and Harkleroad, M., "New Concepts for Measuring Flame Spread Properties", NBSIR 84-2943.

Table 1

Thermal Conductivity of Fiberboard and Particle Board

Density (kg/m ³)	Thermal Conductivity x 10 ⁴ (kW/m .K)	
	Fiberboard	Particle Board
200	0.50	0.52
400	0.66	0.75
600	0.82	1.04
800	1.05	1.35
1000	1.40	1.70

Table 2

Thermal Conductivity of Oven Dry
Southern Pine as a Function of Temperature*

External Heat Flux (kW/m ²)	Front Surface Temp. (°C)	Rear Surface Temp. (°C)	Average Temp. (°C)	Thermal Conductivity x 10 ⁴ (kW/m .K)	Rear Surface Convective Heat Transfer Coefficient (kW/m ² .K)
3.6	122	107	114	1.28	.010
4.6	139	121	130	1.35	.011
5.6	158	137	148	1.41	.011
6.8	181	155	168	1.36	.011
9.1	213	180	197	1.42	.012
12.4	255	211	233	1.41	.013
15.7	287	234	261	1.46	0.014

*Specimen is 1.27 mm thick and has a density of 498 kg/m³.

Table 3

Thermal Conductivity of a Charred Specimen of
Southern Pine as a Function of Temperature*

External Heat Flux (kW/m ²)	Front Surface Temp. (°C)	Rear Surface Temp. (°C)	Average Temp. (°C)	Thermal Conductivity x 10 ⁴ (kW/m · K)	Rear Surface Convective Heat Transfer Coefficient (kW/m ² · K)
3.6	124	101	113	0.75	0.010
4.6	148	120	134	0.78	0.010
5.6	165	131	148	0.77	0.011
6.8	187	148	168	0.81	0.011
9.1	222	172	197	0.82	0.012
12.4	265	204	235	0.91	0.012
15.7	303	233	268	0.99	0.013

*Specimen is 1.22 mm thick and has a density of 207 kg/m³.

Table 4

Thermal Conductivity of Oven Dry Douglas Fir Particle
Board as a Function of Temperature*

External Heat Flux (kW/m ²)	Front Surface Temp. (°C)	Rear Surface Temp. (°C)	Average Temp. (°C)	Thermal Conductivity x 10 ⁴ (kW/m/°K)	Rear Surface Convective Heat Transfer Coefficient (kW/m ² ·K)
1.8	83	74	79	1.50	0.007
2.7	109	96	103	1.64	0.007
3.6	133	116	125	1.64	0.007
5.4	170	148	159	1.77	.006
7.2	205	177	191	1.98	.007
7.6	209	178	194	1.85	.008
8.9	233	199	216	1.95	.007
11.0	267	230	249	2.24	.006
12.0	288	249	269	2.28	.005

* Specimen is 1.96 mm thick and has a density of 709 kg/m³

Table 5

Thermal Conductivity of a Charred Specimen of Douglas Fir
Particle Board as a Function of Temperature*

External Heat Flux (kW/m ²)	Front Surface Temp. (°C)	Rear Surface Temp. (°C)	Average Temp. (°C)	Thermal Conductivity × 10 ⁴ (kW/m/ .K)	Rear Surface Convective Heat Transfer Coefficient (kW/m ² .K)
5.2	155	140	147	1.44	.010
6.2	168	151	159	1.53	.011
7.2	187	166	177	1.44	.011
9.7	221	195	208	1.60	.012
10.5	234	206	220	1.53	.011
11.4	251	222	236	1.60	.010
12.7	270	237	253	1.56	.010

*Thickness is 0.99 mm

Mass retention factor is 0.513.

Table 6

Input Data for Running the Model for Douglas Fir Particle Board

Property	Value	Source
<u>Wood</u>		
Activation Energy	121 kJ/mol	1
Pre-Exponential Factor	$5.94 \times 10^7 \text{ s}^{-1}$	1
Heat of Pyrolysis	0	2
Original Density	709 kg/m ³	1
Heat Capacity	$1.11 (1 + 0.0067 T) \times (0.54 + 0.46Z) \text{ kJ/kg} \cdot \text{K}$	3
Thermal Conductivity	$1.24 \times 10^{-4} (0.35 + 0.65Z) \times (1 + (T - T_0) 6.8 \times 10^{-4}) \text{ kW/m} \cdot \text{K}$	1
Absorptivity	0.8 $Z \geq 0.75$; 1.0 $Z < 0.75$	1
Contraction Factors	$\lambda_x = \lambda_y = \lambda_z = 1$ for $0.65 < Z < 1$ $= 1 - (0.65 - Z)^2$ for $Z < 0.65$	1
Final Char Yield	0.225	1
<u>Volatile Pyrolysis Products</u>		
Heat Capacity	$1.05 + 1.80 \times 10^{-4} (T - T_0) \text{ kJ/kg} \cdot \text{K}$	4
Heat of Combustion	20000 [1.24 - Z] kJ/kg	1
<u>Water</u>		
Activation Energy	44 kJ/mol	4
Pre-Exponential Factor	$4.5 \times 10^3 \text{ s}^{-1}$	4
Heat of Vaporization	2400 kJ/kg	4
Heat Capacity	$4.19 \text{ kJ/kg} \cdot \text{K}$, $T < 100^\circ\text{C}$ $4.19 + 3.1 \times 10^{-5} \times (T - 100) \text{ kJ/kg} \cdot \text{K}$, $T \geq 100^\circ\text{C}$	5
<u>Flame</u>		
Temperature	1200°C	1
Radiation	10 kW/m ²	7
Total Heat Flux to Cold Surface	30 kW/m ²	1

1. Experimentally determined on project.
 2. Assumed.
 3. Temperature Dependence - Koch [17]; dependence on charring assumed based on published value for charcoal.
 4. Atreya [13].
 5. Handbook of Chemistry and Physics.
 6. Calculated.
 7. Tewarson [8]
- * Used in basic computer program

APPENDIX A

CALCULATION OF THE DENSITY OF THE GAS IN THE EXHAUST DUCT

In order to determine the volume and mass flows in the exhaust duct using an orifice plate or a pitot static tube it is necessary to know the density of the gas. The total mass flow through the duct is given by

$$\dot{m} = \rho_{N_2} \dot{V}_{N_2} + \rho_{O_2} \dot{V}_{O_2} + \rho_{CO_2} \dot{V}_{CO_2} + \rho_{H_2O} \dot{V}_{H_2O} \quad (A-1)$$

assuming complete combustion. Here nitrogen is taken to include all of the gases in the atmosphere except oxygen, carbon dioxide, and water. For simplicity its molecular weight will still be taken to be 28.

Hence the density is given by

$$\rho = \frac{\dot{m}}{\dot{V}^S} = \rho_{N_2} x_{N_2}^S + \rho_{O_2} x_{O_2}^S + \rho_{CO_2} x_{CO_2}^S + \rho_{H_2O} x_{H_2O}^S \quad (A-2)$$

Since

$$x_{N_2}^S = 1 - x_{O_2}^S - x_{CO_2}^S - x_{H_2O}^S, \quad (A-3)$$

equation (A-2) can be written

$$\rho = \rho_{N_2} + (\rho_{O_2} - \rho_{N_2}) x_{O_2}^S + (\rho_{CO_2} - \rho_{N_2}) x_{CO_2}^S + (\rho_{H_2O} - \rho_{N_2}) x_{H_2O}^S. \quad (A-4)$$

The density of each species is equal to its molecular weight divided by the molar volume at the reference temperature. At 0°C equation (A-4) becomes

$$\rho = (28 + 4 x_{O_2}^S + 16 x_{CO_2}^S - 10 x_{H_2O}^S) / 22.4 \quad (A-5)$$

Use will now be made of the relationships between the volume fractions measured in the analyzers and those existing in the exhaust duct. These are derived in Appendix C. Since water vapor is trapped out of the CO₂ analyzer,

$$x_{CO_2}^S = (1 - x_{H_2O}^S) x_{CO_2}^A \quad (C-20)$$

If water vapor is trapped but CO₂ is not trapped out of the oxygen analyzer,

$$x_{O_2}^S = (1 - x_{H_2O}^S) x_{O_2}^A \quad (C-23)$$

In the cone calorimeter both water vapor and CO₂ are trapped out of the oxygen analyzer so that

$$x_{O_2}^S = (1 - x_{H_2O}^S) (1 - x_{CO_2}^A) x_{O_2}^A \quad (C-25)$$

Combining equations (A-5), (C-20) and (C-25), one finds that the density of the exhaust gases expressed in terms of the volume fractions measured in the analyzers is given by

$$\rho = \left[4.5 + (1 - x_{H_2O}^S) \left[6.5 - (1 - x_{CO_2}^A) (4 - x_{O_2}^A) \right] \right] / 5.6 \quad (A-6)$$

in the case of the cone calorimeter.

If the CO₂ is not trapped then equations (A-5), (C-20) and (C-23) are combined instead to yield

$$\rho = [4.5 + (1 - x_{\text{H}_2\text{O}}^{\text{S}}) (2.5 + x_{\text{O}_2}^{\text{A}} + 4 x_{\text{CO}_2}^{\text{A}})] / 5.6 \quad (\text{A-7})$$

APPENDIX B

CALCULATION OF THE FLOW OF NITROGEN THROUGH THE EXHAUST DUCT

The formulas for the calculation of carbon, hydrogen and oxygen release rates, to be derived in Appendix C, require input data on the nitrogen flow in the exhaust duct. The formulas for the nitrogen flow will be derived in this section.

The mass flow of gas through the exhaust duct of the cone calorimeter is measured with an orifice plate using the equation

$$\dot{m}^s = C \sqrt{\frac{\Delta p}{T_e}} \quad (B-1)$$

If the orifice plate conforms to ASTM specifications, the pipe is straight for a sufficient length on each side and the gas is air, $C = 0.031 \text{ kg}\cdot\text{s}^{-1}\cdot\text{K}^{1/2}\cdot\text{Pa}^{-1/2}$. Here Δp is the pressure drop across the orifice plate in Pascals and T_e is the absolute temperature of the exhaust in K. The orifice plate was calibrated (not on this project) with a known flow rate of CO_2 and C was found to be 0.028. Since C is proportional to the square root of the density of the gas we can define a new calibration factor,

$$C^* = \sqrt{\rho/\rho_{\text{air}}} C \quad (B-2)$$

and use it in place of C in eq. (B-1). All densities and volume flows in these appendices are referred to standard conditions (760 mm Hg and 0°C). Nitrogen is taken to include all of the gases in the atmosphere other than oxygen, carbon dioxide and water. The mass flow of nitrogen is given by

$$\begin{aligned}
\dot{m}_{N_2} &= \rho_{N_2} X_{N_2} \dot{V}^S = \rho_{N_2} X_{N_2} \dot{m} / \rho \\
&= \frac{\rho_{N_2}}{\rho} X_{N_2} C^* \sqrt{\Delta p / T_e} \\
&= \frac{\rho_{N_2}}{\rho} X_{N_2} C \sqrt{\frac{\rho}{\rho_{air}}} \sqrt{\frac{\Delta p}{T_e}} \\
&= \frac{\rho_{N_2}}{\sqrt{\rho} \rho_{air}} (1 - x_{O_2}^S - x_{CO_2}^S - x_{H_2O}^S) C \sqrt{\frac{\Delta p}{T_e}} \tag{B-3}
\end{aligned}$$

Using equations (C-20) and (C-23) of Appendix C for the case where CO₂ is not trapped, we find that this can be written in terms of the analyzer concentrations as

$$\dot{m}_{N_2} = \frac{\rho_{N_2}}{\sqrt{\rho} \rho_{air}} (1 - x_{H_2O}^S) (1 - x_{O_2}^A - x_{CO_2}^A) C \sqrt{\frac{\Delta p}{T_e}} \tag{B-4}$$

Using equations (C-20) and (C-25) of Appendix C for the cone calorimeter where CO₂ is trapped out of the oxygen analyzer, we find

$$\dot{m}_{N_2} = \frac{\rho_{N_2}}{\sqrt{\rho} \rho_{air}} (1 - x_{H_2O}^S) (1 - x_{CO_2}^A) (1 - x_{O_2}^A) C \sqrt{\frac{\Delta p}{T_e}} \tag{B-5}$$

The density of the exhaust gas is given by either equation (A-6) or (A-7) from Appendix A while the densities ρ_{N_2} and ρ_{air} are 1.25 and 1.29 kg/m³ respectively.

APPENDIX C

CALCULATION OF CARBON, HYDROGEN, AND OXYGEN RELEASE RATES FROM BURNING WOOD

We wish to calculate the carbon, hydrogen and oxygen content of the volatile pyrolysis products of wood from the volume fractions of oxygen, carbon dioxide and water vapor in the combustion products along with the mass flow of nitrogen through the system. It is assumed that

1. Wood is composed only of carbon, hydrogen, and oxygen.
2. All of the volatiles undergo complete combustion to water vapor and carbon dioxide.

There are two situations of concern. The first is the pyrolyzer where the pyrolysis takes place in the nitrogen stream and then is swept into a methane flame where complete combustion takes place. The second situation is the cone calorimeter where there is no supply of methane and the volatiles simply burn in their own flame. The calculational procedures are identical. The flow rate of methane is simply set equal to zero for the cone calorimeter but is measured for the pyrolyzer or simply calculated from the volume fractions of O_2 , CO_2 and H_2O in the exhaust when the wood is absent.

The water vapor volume fraction, $X_{H_2O}^S$, is the same in the analyzer as it is in the exhaust duct. However, the O_2 and CO_2 volume fractions, $X_{O_2}^A$ and $X_{CO_2}^A$, in the analyzers differ from their values in the exhaust duct, $X_{O_2}^S$ and $X_{CO_2}^S$, due to trapping of water vapor from the analyzers. Furthermore $X_{O_2}^A$ will depend on whether CO_2 is also trapped out of the oxygen

analyzer as it currently is in the cone calorimeter. Since both cases arise, the following calculations will consider Case I where CO₂ is not trapped and Case II where it is trapped. It will be assumed that the molar flow ratios are the same in the analyzers as they are in the exhaust duct for those species which are present in both.

The mass flow rates will first be calculated in terms of the volume fractions in the stack or exhaust duct. Then they will be transformed for each of the two cases to be expressed in terms of the volume fractions in the analyzers. The stack volume fractions are given in terms of the molar flows by

$$x_{O_2}^S = \frac{\dot{n}_{O_2}}{\dot{n}_{N_2} + \dot{n}_{O_2} + \dot{n}_{CO_2} + \dot{n}_{H_2O}} \quad (C-1)$$

$$x_{CO_2}^S = \frac{\dot{n}_{CO_2}}{\dot{n}_{N_2} + \dot{n}_{O_2} + \dot{n}_{CO_2} + \dot{n}_{H_2O}} \quad (C-2)$$

$$x_{H_2O}^S = \frac{\dot{n}_{H_2O}}{\dot{n}_{N_2} + \dot{n}_{O_2} + \dot{n}_{CO_2} + \dot{n}_{H_2O}} \quad \text{and} \quad (C-3)$$

$$x_{N_2}^S = \frac{\dot{n}_{N_2}}{\dot{n}_{N_2} + \dot{n}_{O_2} + \dot{n}_{CO_2} + \dot{n}_{H_2O}} \quad (C-4)$$

Furthermore

$$x_{N_2}^S = 1 - x_{O_2}^S - x_{CO_2}^S - x_{H_2O}^S \quad (C-5)$$

Here nitrogen is taken to include all of the gases in the atmosphere other than oxygen, carbon dioxide, and water. For simplicity its molecular weight will still be taken to be 28.

The molar flows of the combustion products in the duct are related to the carbon, hydrogen, and oxygen content of the volatile pyrolysis products, the species present in the incoming air and the methane by the expressions,

$$\dot{n}_{\text{CO}_2} = \dot{n}_{\text{C}} + \dot{n}_{\text{CO}_2}^{\circ} + \dot{n}_{\text{CH}_4} \quad (\text{C-6})$$

$$\dot{n}_{\text{H}_2\text{O}} = \frac{1}{2} \dot{n}_{\text{H}} + \dot{n}_{\text{H}_2\text{O}}^{\circ} + 2 \dot{n}_{\text{CH}_4} \quad (\text{C-7})$$

$$\dot{n}_{\text{O}_2} = \frac{1}{2} \dot{n}_{\text{O}} + \dot{n}_{\text{O}_2}^{\circ} - (\dot{n}_{\text{CO}_2} - \dot{n}_{\text{CO}_2}^{\circ}) - \frac{1}{2} (\dot{n}_{\text{H}_2\text{O}} - \dot{n}_{\text{H}_2\text{O}}^{\circ}) \quad (\text{C-8})$$

Combining equations (C-1) to (C-8) the molar flow ratios of atomic carbon, hydrogen, and oxygen in the volatile pyrolysis products to the molecular nitrogen flowing through the system are given by

$$\frac{\dot{n}_{\text{C}}}{\dot{n}_{\text{N}_2}} = \frac{x_{\text{CO}_2}^{\text{S}}}{1 - x_{\text{O}_2}^{\text{S}} - x_{\text{CO}_2}^{\text{S}} - x_{\text{H}_2\text{O}}^{\text{S}}} - \frac{x_{\text{CO}_2}^{\circ}}{1 - x_{\text{O}_2}^{\circ} - x_{\text{CO}_2}^{\circ} - x_{\text{H}_2\text{O}}^{\circ}} - \frac{\dot{n}_{\text{CH}_4}}{\dot{n}_{\text{N}_2}} \quad (\text{C-9})$$

$$\frac{\dot{n}_{\text{H}}}{\dot{n}_{\text{N}_2}} = \frac{2 x_{\text{H}_2\text{O}}^{\text{S}}}{1 - x_{\text{O}_2}^{\text{S}} - x_{\text{CO}_2}^{\text{S}} - x_{\text{H}_2\text{O}}^{\text{S}}} - \frac{2 x_{\text{H}_2\text{O}}^{\circ}}{1 - x_{\text{O}_2}^{\circ} - x_{\text{CO}_2}^{\circ} - x_{\text{H}_2\text{O}}^{\circ}} - 4 \frac{\dot{n}_{\text{CH}_4}}{\dot{n}_{\text{N}_2}} \quad (\text{C-10})$$

and

$$\frac{\dot{n}_O}{\dot{n}_{N_2}} = \frac{2 X_{O_2}^S + 2 X_{CO_2}^S + X_{H_2O}^S}{1 - X_{O_2}^S - X_{CO_2}^S - X_{H_2O}^S} - \frac{2 X_{O_2}^O + 2 X_{CO_2}^O + X_{H_2O}^O}{1 - X_{O_2}^O - X_{CO_2}^O - X_{H_2O}^O} \quad (C-11)$$

The ambient volume fractions $X_{O_2}^O$, $X_{CO_2}^O$, and $X_{H_2O}^O$ are determined from the analyzers prior to the test with the traps bypassed.

Noting that

$$\frac{\dot{m}_C}{\dot{m}_{N_2}} = \frac{3}{7} \frac{\dot{n}_C}{\dot{n}_{N_2}} \quad (C-12)$$

$$\frac{\dot{m}_H}{\dot{m}_{N_2}} = \frac{1}{28} \frac{\dot{n}_H}{\dot{n}_{N_2}} \quad (C-13)$$

$$\frac{\dot{m}_O}{\dot{m}_{N_2}} = \frac{4}{7} \frac{\dot{n}_O}{\dot{n}_{N_2}} \quad (C-14)$$

and

$$\frac{\dot{m}_{CH_4}}{\dot{m}_{N_2}} = \frac{4}{7} \frac{\dot{n}_{CH_4}}{\dot{n}_{N_2}} \quad (C-15)$$

we find that

$$\dot{m}_C = \frac{3}{7} \left(\frac{X_{CO_2}^S}{1 - X_{O_2}^S - X_{CO_2}^S - X_{H_2O}^S} - \frac{X_{CO_2}^O}{1 - X_{O_2}^O - X_{CO_2}^O - X_{H_2O}^O} \right) \dot{m}_{N_2} - \frac{3}{4} \dot{m}_{CH_4} \quad (C-16)$$

$$\dot{m}_H = \frac{1}{14} \left(\frac{x_{H_2O}^S}{1 - x_{O_2}^S - x_{CO_2}^S - x_{H_2O}^S} - \frac{x_{H_2O}^O}{1 - x_{O_2}^O - x_{CO_2}^O - x_{H_2O}^O} \right) \dot{m}_{N_2} - \frac{1}{4} \dot{m}_{CH_4} \quad (C-17)$$

and

$$\dot{m}_O = \frac{4}{7} \left(\frac{2 x_{CO_2}^S + 2 x_{O_2}^S + x_{H_2O}^S}{1 - x_{O_2}^S - x_{CO_2}^S - x_{H_2O}^S} - \frac{2 x_{O_2}^O + 2 x_{CO_2}^O + x_{H_2O}^O}{1 - x_{O_2}^O - x_{CO_2}^O - x_{H_2O}^O} \right) \dot{m}_{N_2} \quad (C-18)$$

Equations (C-16), (C-17) and (C-18) are in terms of the volume fractions in the exhaust ducts. It is necessary to establish the relationships between the volume fractions in the analyzer and in the exhaust duct.

The concentration in the CO₂ analyzer is given by

$$x_{CO_2}^A = \frac{\dot{n}_{CO_2}}{n_{N_2} + n_{O_2} + n_{CO_2}} \quad (C-19)$$

where the molar ratios are taken to be the same in the analyzer as they are in the exhaust duct for N₂, O₂, and CO₂. Combining equations (C-2) and (C-19) yields

$$x_{CO_2}^S = (1 - x_{H_2O}^S) x_{CO_2}^A \quad (C-20)$$

If CO₂ is not trapped out of the oxygen analyzer (Case I) then

$$x_{O_2}^A = \frac{n_{O_2}}{n_{N_2} + n_{O_2} + n_{CO_2}} \quad (C-21)$$

If CO₂ is trapped (Case II) then

$$x_{O_2}^{A'} = \frac{\dot{n}_{O_2}}{\dot{n}_{N_2} + \dot{n}_{O_2}} \quad (C-22)$$

Combining equations (1) and (21) yields

$$x_{O_2}^S = (1 - x_{H_2O}^S) x_{O_2}^A \quad (C-23)$$

for Case I. Combining equations (C-1) and (C-22) yields

$$x_{O_2}^S = (1 - x_{CO_2}^S - x_{H_2O}^S) x_{O_2}^{A'} \quad (C-24)$$

for Case II. Combining equations (C-20) and (C-24) expresses the volume fraction of O₂ in the exhaust duct in terms of the volume fractions in the analyzers,

$$x_{O_2}^S = (1 - x_{H_2O}^S)(1 - x_{CO_2}^A) x_{O_2}^{A'} \quad (C-25)$$

It can be seen from equations (C-20) and (C-23) that for Case I

$$1 - x_{O_2}^S - x_{CO_2}^S - x_{H_2O}^S = (1 - x_{H_2O}^S)(1 - x_{O_2}^A - x_{CO_2}^A) \quad (C-26)$$

Substituting (C-20), (C-23) and (C-26) into (C-16), (C-17) and (C-18) yields for Case I with no trapping

$$\dot{m}_C = \frac{3}{7} \left(\frac{x_{CO_2}^A}{1 - x_{O_2}^A - x_{CO_2}^A} - \frac{x_{CO_2}^O}{1 - x_{O_2}^O - x_{CO_2}^O - x_{H_2O}^O} \right) \dot{m}_{N_2} - \frac{3}{4} \dot{m}_{CH_4} \quad (C-27)$$

$$\dot{m}_H = \frac{1}{14} \left(\frac{x_{H_2O}^S}{(1-x_{H_2O}^S)(1-x_{O_2}^A-x_{CO_2}^A)} - \frac{x_{H_2O}^O}{1-x_{O_2}^O-x_{CO_2}^O-x_{H_2O}^O} \right) \dot{m}_{N_2} - \frac{1}{4} \dot{m}_{CH_4} \quad (C-28)$$

and

$$\dot{m}_O = \frac{4}{7} \left(\frac{x_{H_2O}^S}{(1-x_{H_2O}^S)(1-x_{O_2}^A-x_{CO_2}^A)} + \frac{2(x_{O_2}^A+x_{CO_2}^A)}{(1-x_{O_2}^A-x_{CO_2}^A)} - \frac{2x_{O_2}^O+2x_{CO_2}^O+x_{H_2O}^O}{1-x_{O_2}^O-x_{CO_2}^O-x_{H_2O}^O} \right) \dot{m}_{N_2} \quad (C-29)$$

It can be seen from equation (C-20) and (C-25) that

$$1 - x_{O_2}^S - x_{CO_2}^S - x_{H_2O}^S = (1-x_{H_2O}^S)(1-x_{O_2}^{A'}) (1-x_{CO_2}^A) \quad (C-30)$$

Substituting equations (C-20), (C-25) and (C-23) into equations (C-16), (C-17) and (C-18) yields for Case II (with trapping)

$$\dot{m}_C = \frac{3}{7} \left(\frac{x_{CO_2}^A}{(1-x_{O_2}^{A'})(1-x_{CO_2}^A)} - \frac{x_{CO_2}^O}{1-x_{O_2}^O-x_{CO_2}^O-x_{H_2O}^O} \right) \dot{m}_{N_2} - \frac{3}{4} \dot{m}_{CH_4} \quad (C-31)$$

$$\dot{m}_H = \frac{1}{14} \left(\frac{x_{H_2O}^O}{(1-x_{H_2O}^S)(1-x_{O_2}^{A'})(1-x_{CO_2}^A)} - \frac{x_{H_2O}^O}{1-x_{O_2}^O-x_{CO_2}^O-x_{H_2O}^O} \right) \dot{m}_{N_2} - \frac{1}{4} \dot{m}_{CH_4} \quad (C-32)$$

$$\dot{m}_O = \frac{4}{7} \left(\frac{2(x_{O_2}^{A'}+x_{CO_2}^A)}{(1-x_{O_2}^{A'})(1-x_{CO_2}^A)} + \frac{x_{H_2O}^S}{(1-x_{H_2O}^S)(1-x_{O_2}^{A'})(1-x_{CO_2}^A)} - \frac{2x_{O_2}^O+2x_{CO_2}^O+x_{H_2O}^O}{1-x_{O_2}^O-x_{CO_2}^O-x_{H_2O}^O} \right) \dot{m}_{N_2}$$

(C-33)

Now we drop the superscripts S, A and A' and assume that the volume fractions are those measured in the analyzers, ($x_{H_2O}^S$ is the volume fraction in the water vapor analyzer). We are assuming Case II where the CO_2 is trapped.

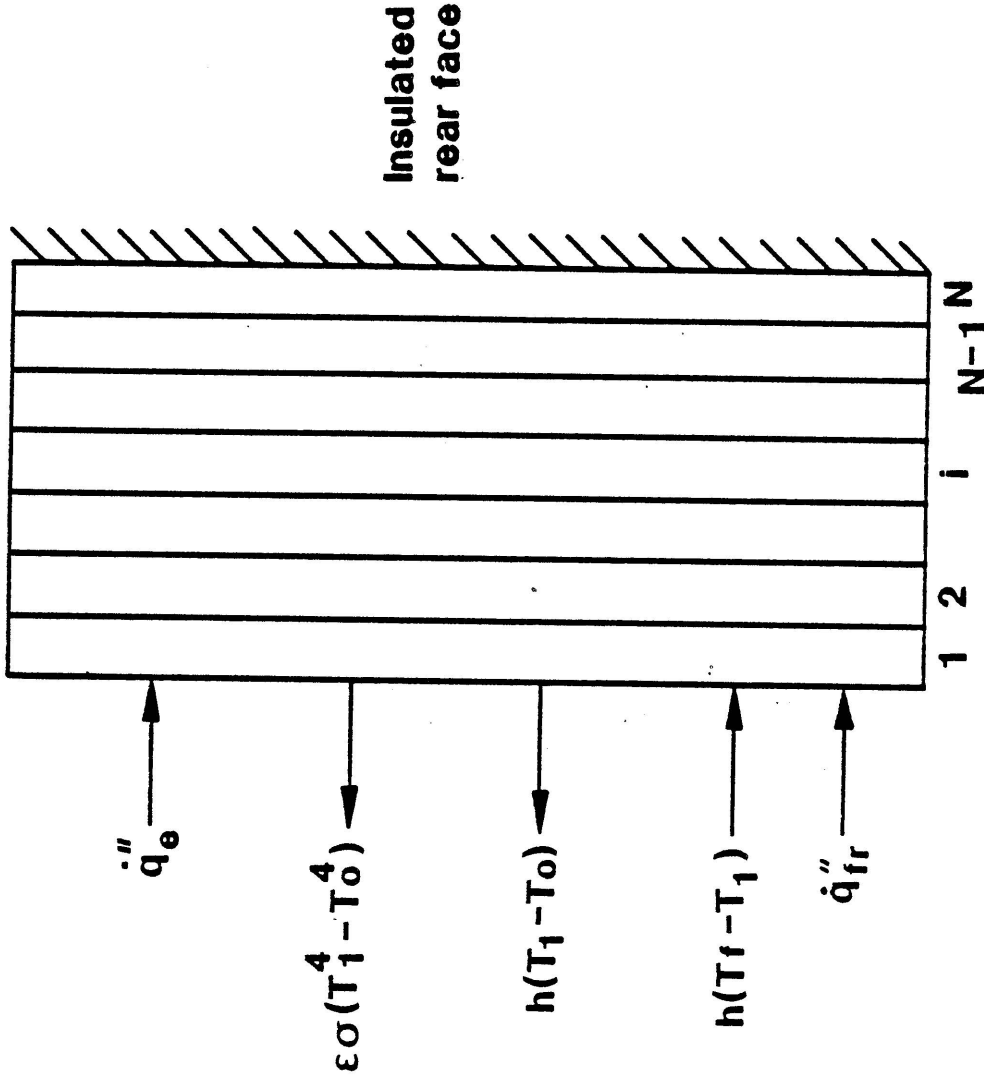
Then

$$\dot{m}_c = \frac{3}{7} \left(\frac{x_{CO_2}}{(1-x_{O_2})(1-x_{CO_2})} - \frac{x_{CO_2}^o}{1-x_{O_2}^o - x_{CO_2}^o - x_{H_2O}^o} \right) \dot{m}_{N_2} - \frac{3}{4} \dot{m}_{CH_4} \quad (C-34)$$

$$\dot{m}_H = \frac{1}{14} \left(\frac{x_{H_2O}}{(1-x_{H_2O})(1-x_{O_2})(1-x_{CO_2})} - \frac{x_{H_2O}^o}{1-x_{O_2}^o - x_{CO_2}^o - x_{H_2O}^o} \right) \dot{m}_{N_2} - \frac{1}{4} \dot{m}_{CH_4} \quad (C-35)$$

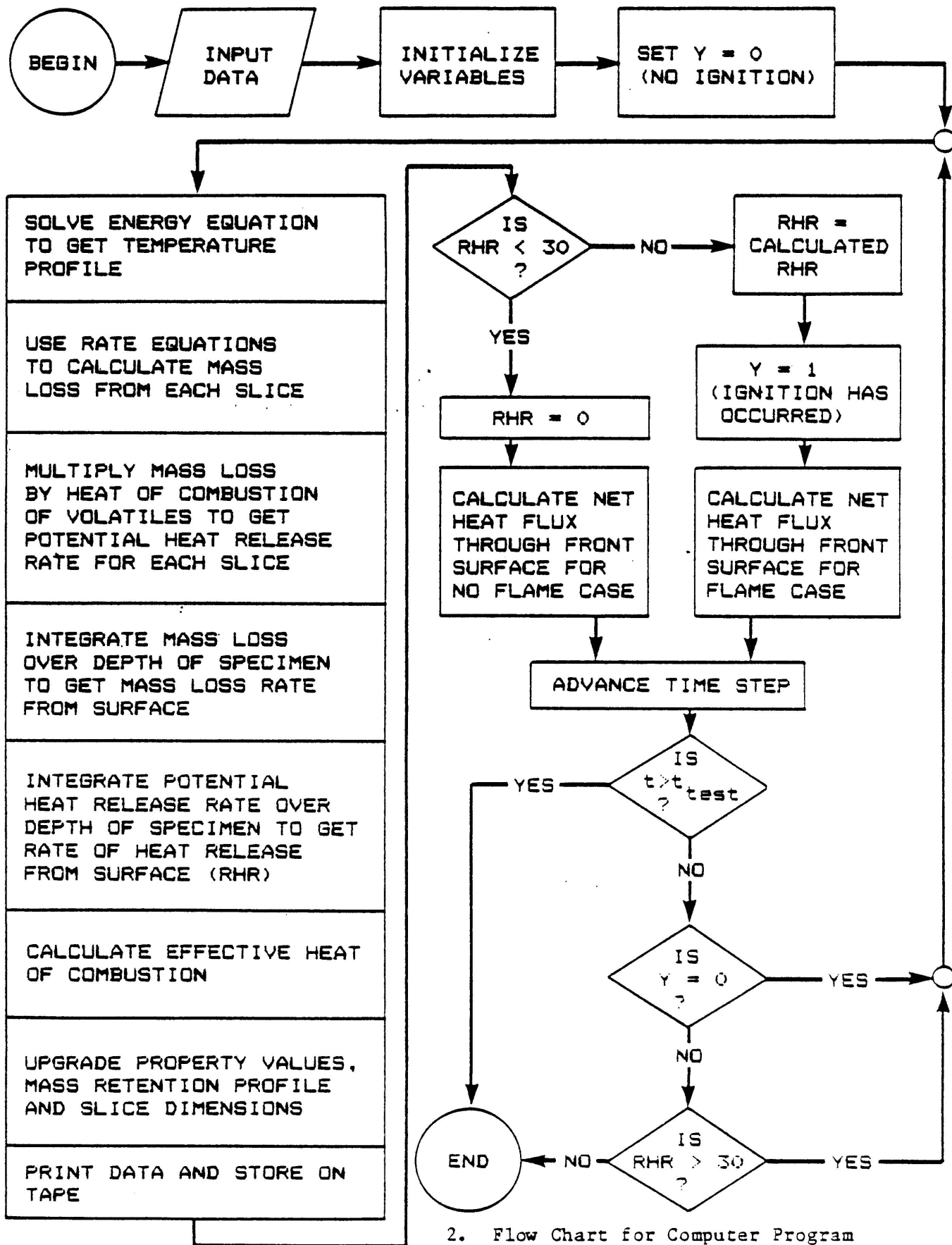
$$\dot{m}_O = \frac{4}{7} \left(\frac{2(x_{O_2} + x_{CO_2})}{(1-x_{O_2})(1-x_{CO_2})} + \frac{x_{H_2O}}{(1-x_{H_2O})(1-x_{O_2})(1-x_{CO_2})} - \frac{2(x_{O_2}^o + x_{CO_2}^o) + x_{H_2O}^o}{1-x_{O_2}^o - x_{CO_2}^o - x_{H_2O}^o} \right) \dot{m}_{N_2} \quad (C-36)$$

BURNING SLAB



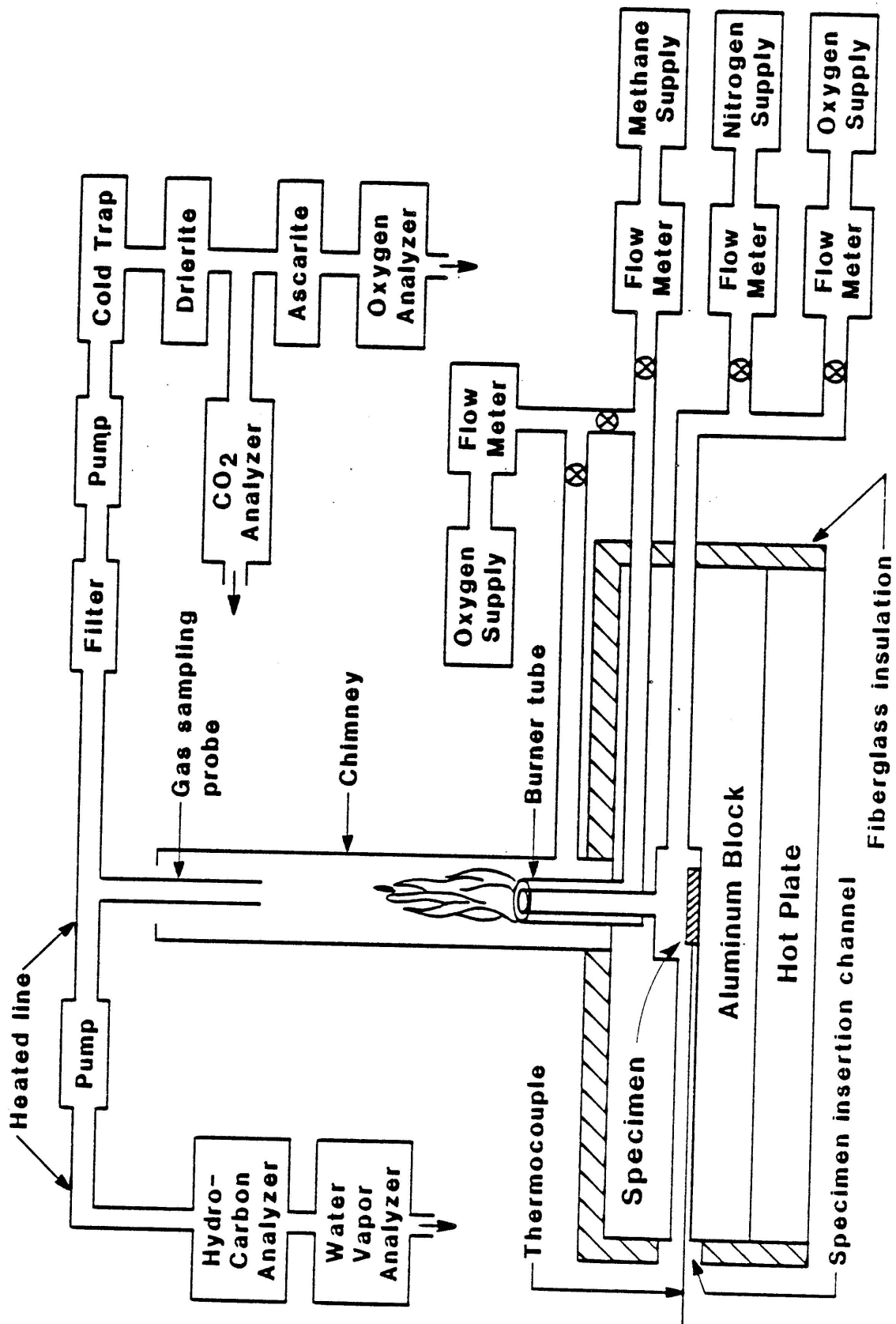
- N slices of thickness ΔX_0 of unit width and height
- Boundaries move as char shrinks

1. Boundary Conditions and Subdivision of Burning Vertical Slab



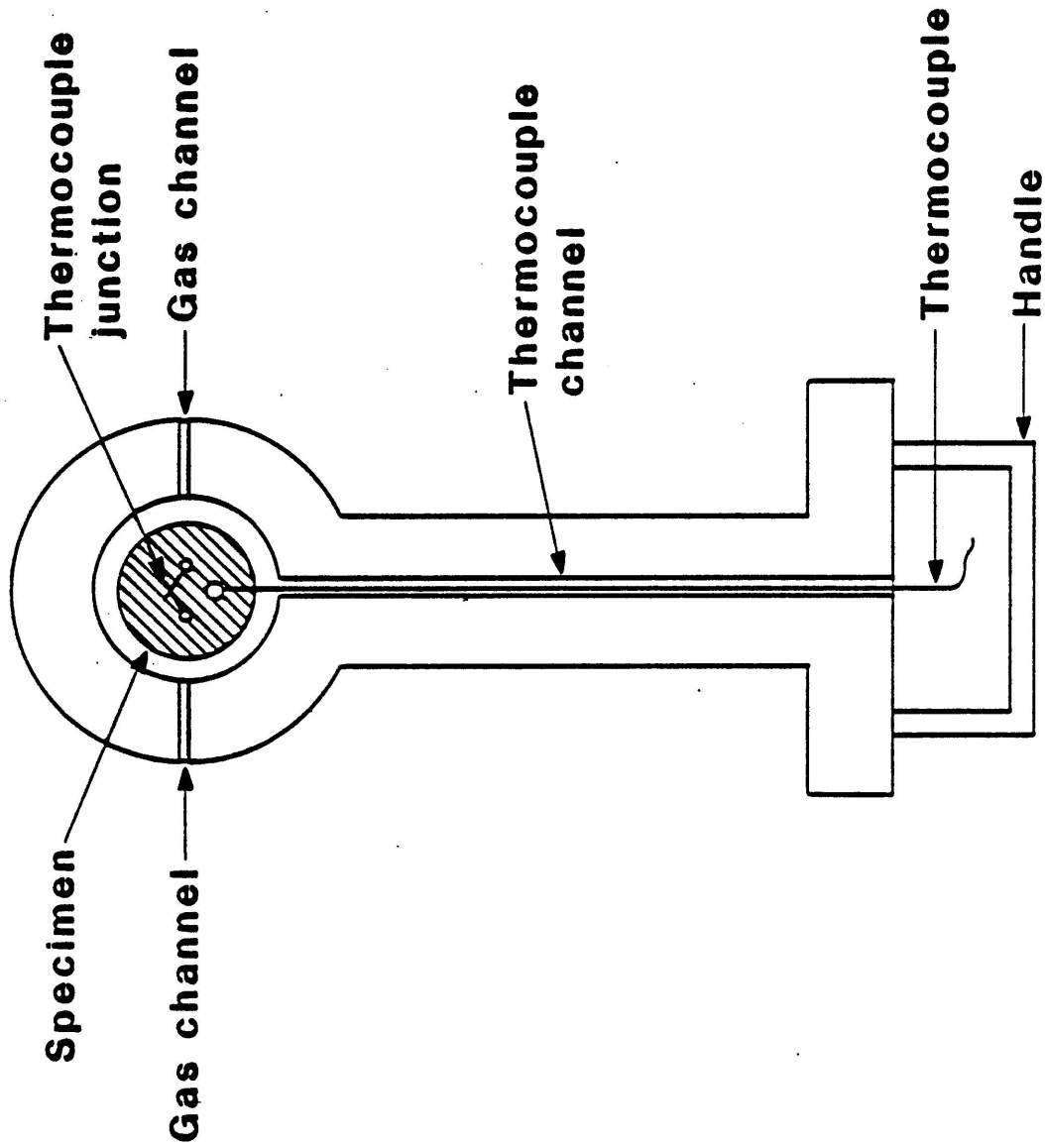
2. Flow Chart for Computer Program

PYROLYZER

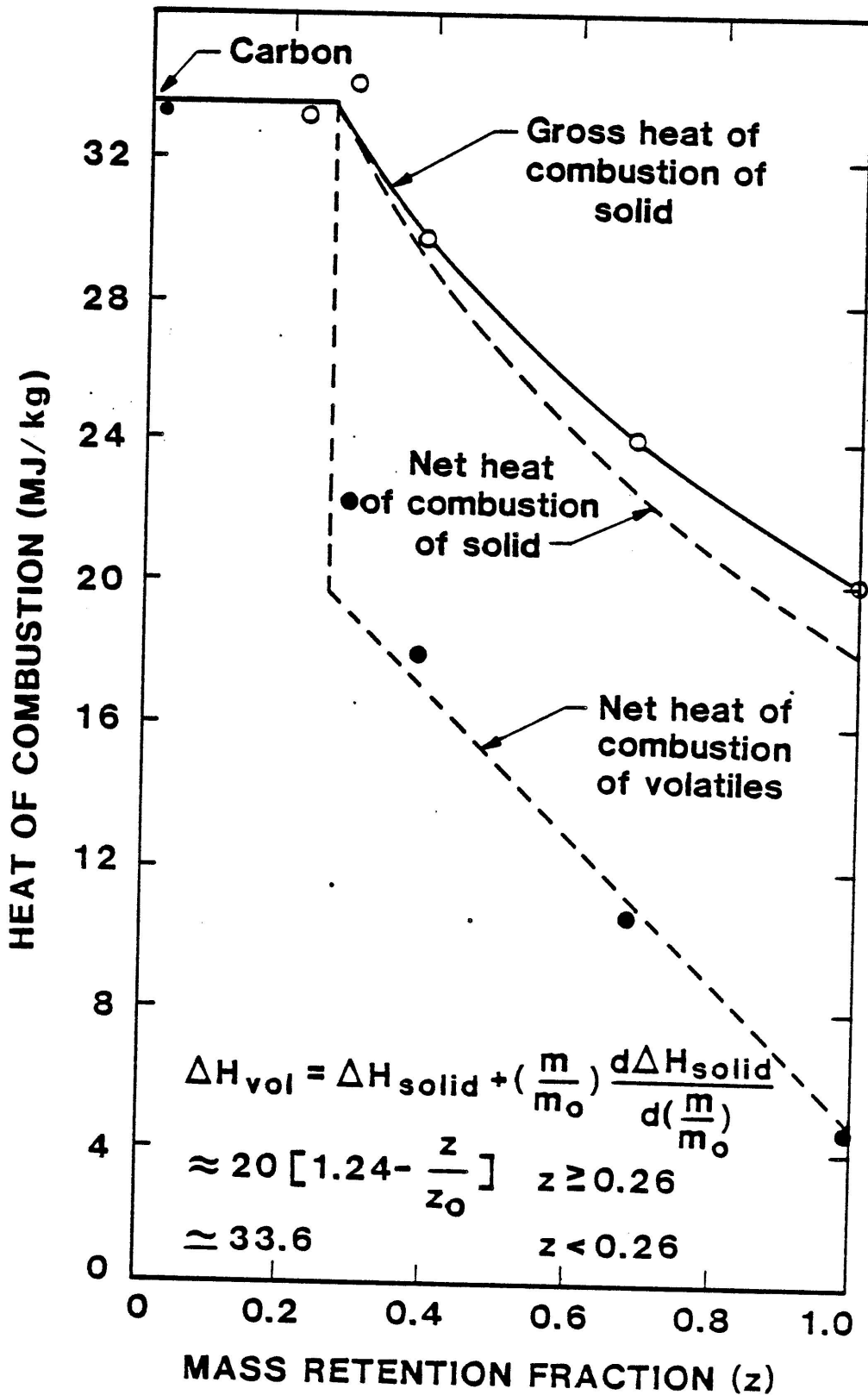


3. Pyrolyzer .

TOP VIEW OF CLOSURE SLIDE

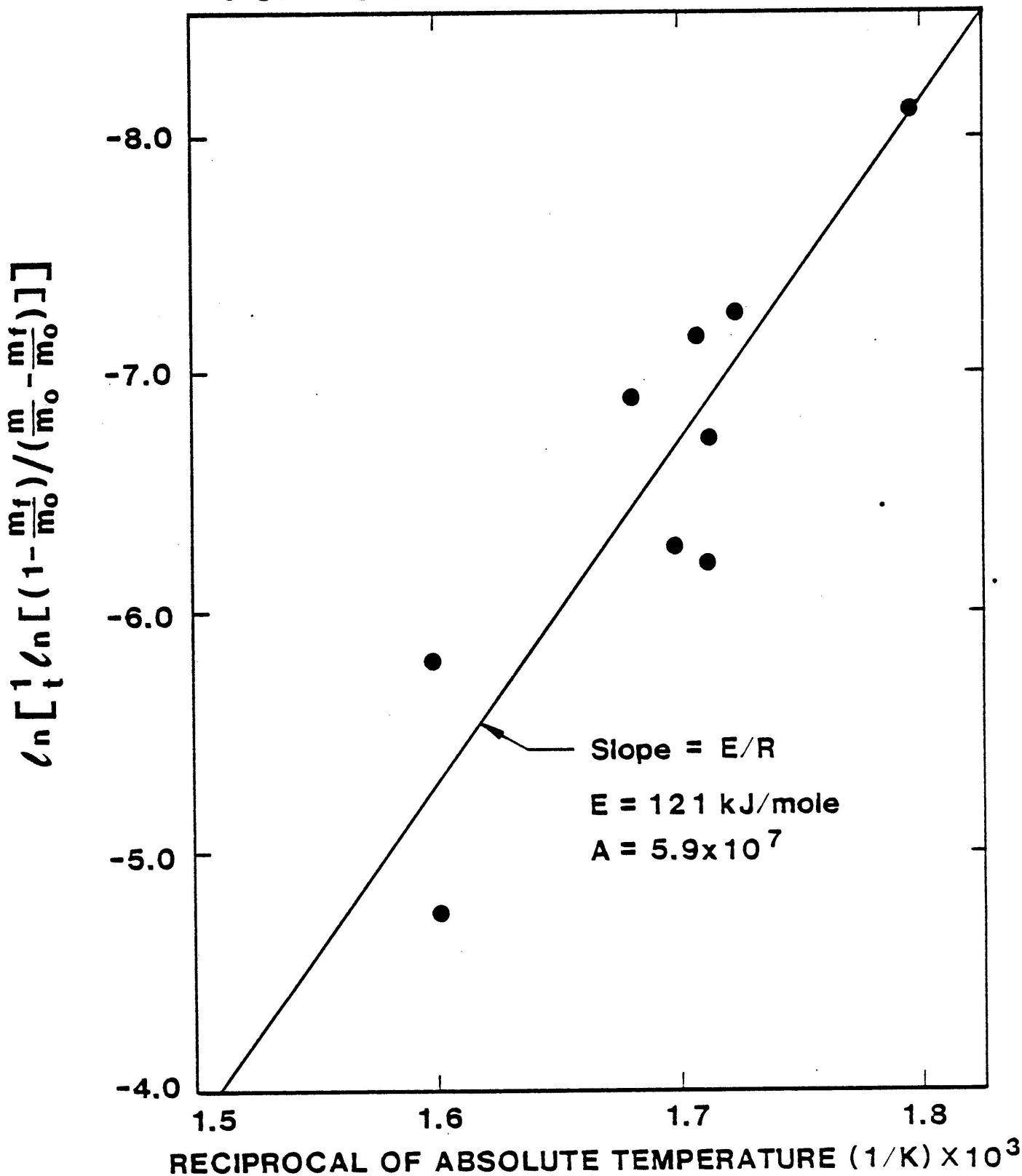


4. Closure Slide

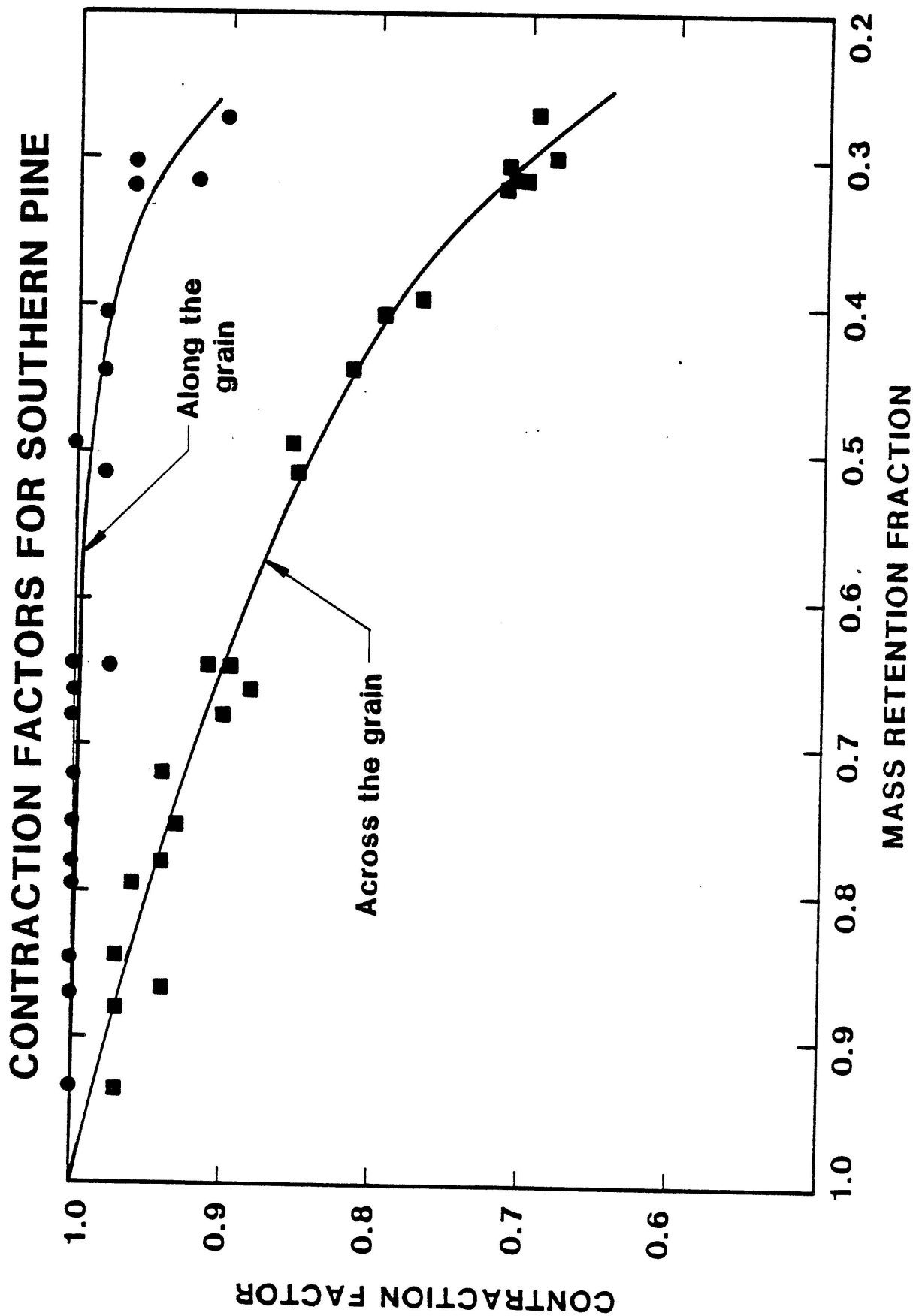


5. Heat of Combustion of Pyrolysis Vapor for Douglas Fir Particle Board

ACTIVATION ENERGY AND FREQUENCY FACTOR FOR DOUGLAS FIR PARTICLE BOARD

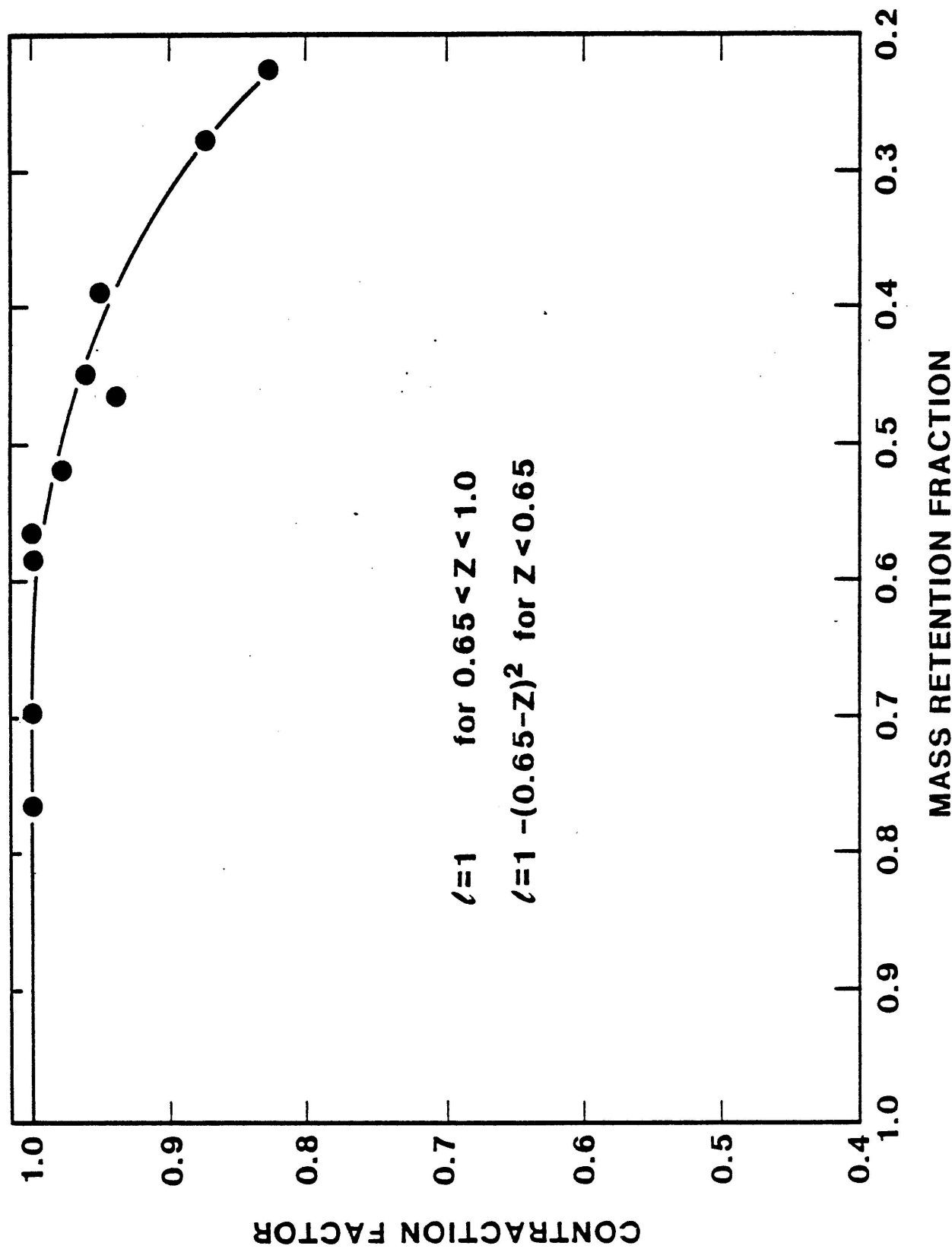


6. Arrhenius Plot for Douglas Fir Particle Board

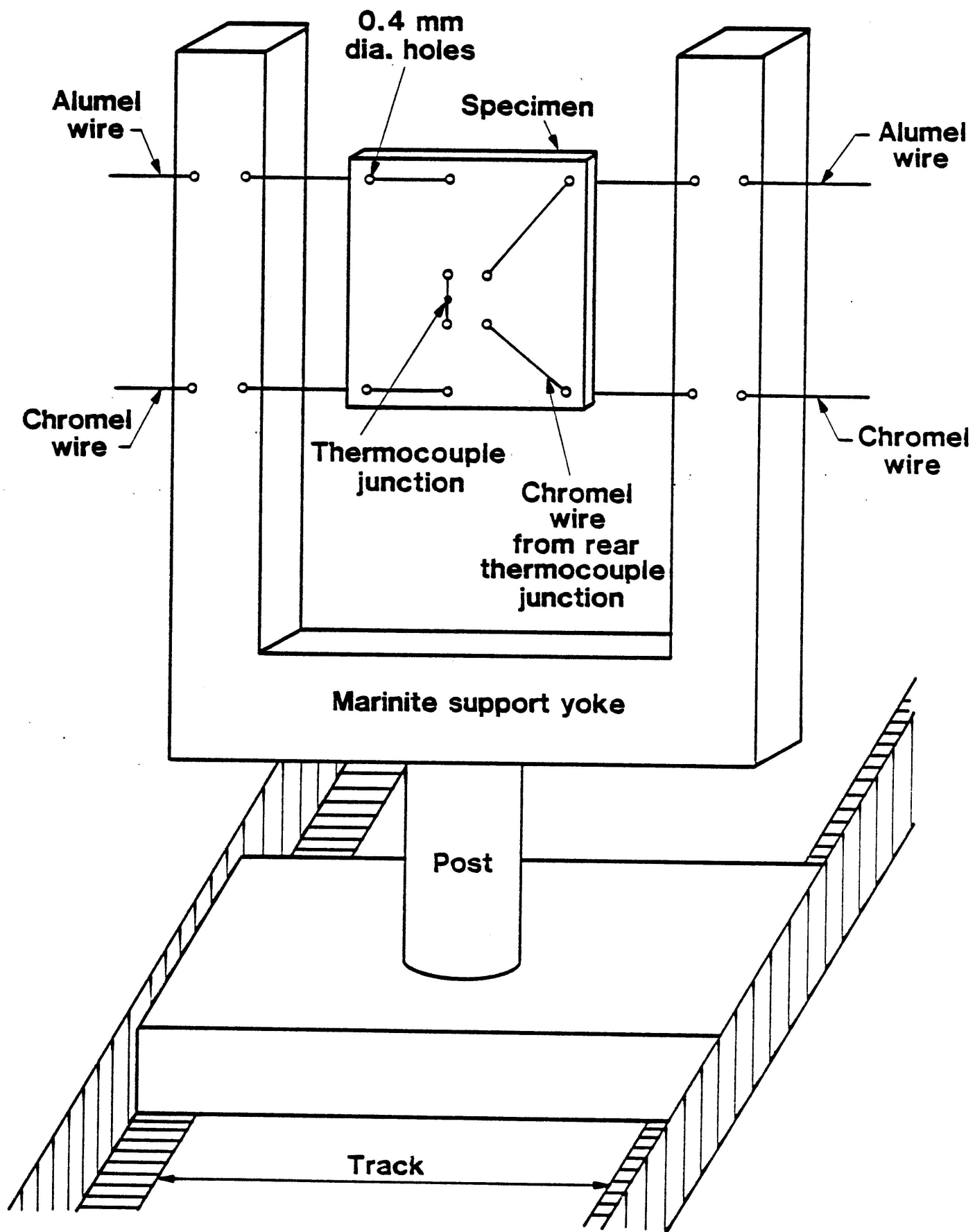


7. Contraction Factors for Southern Pine

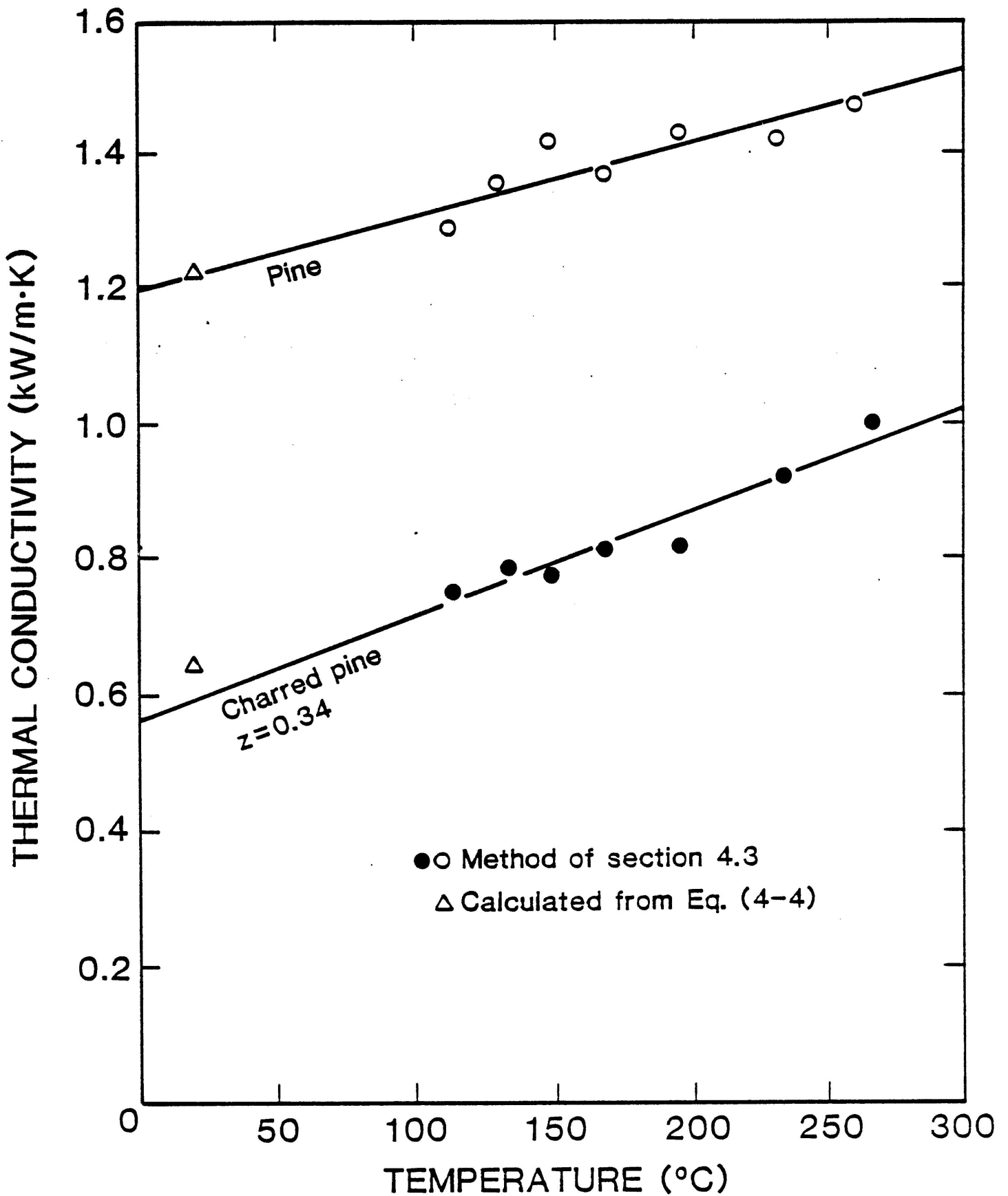
CONTRACTION FACTOR FOR PARTICLE BOARD



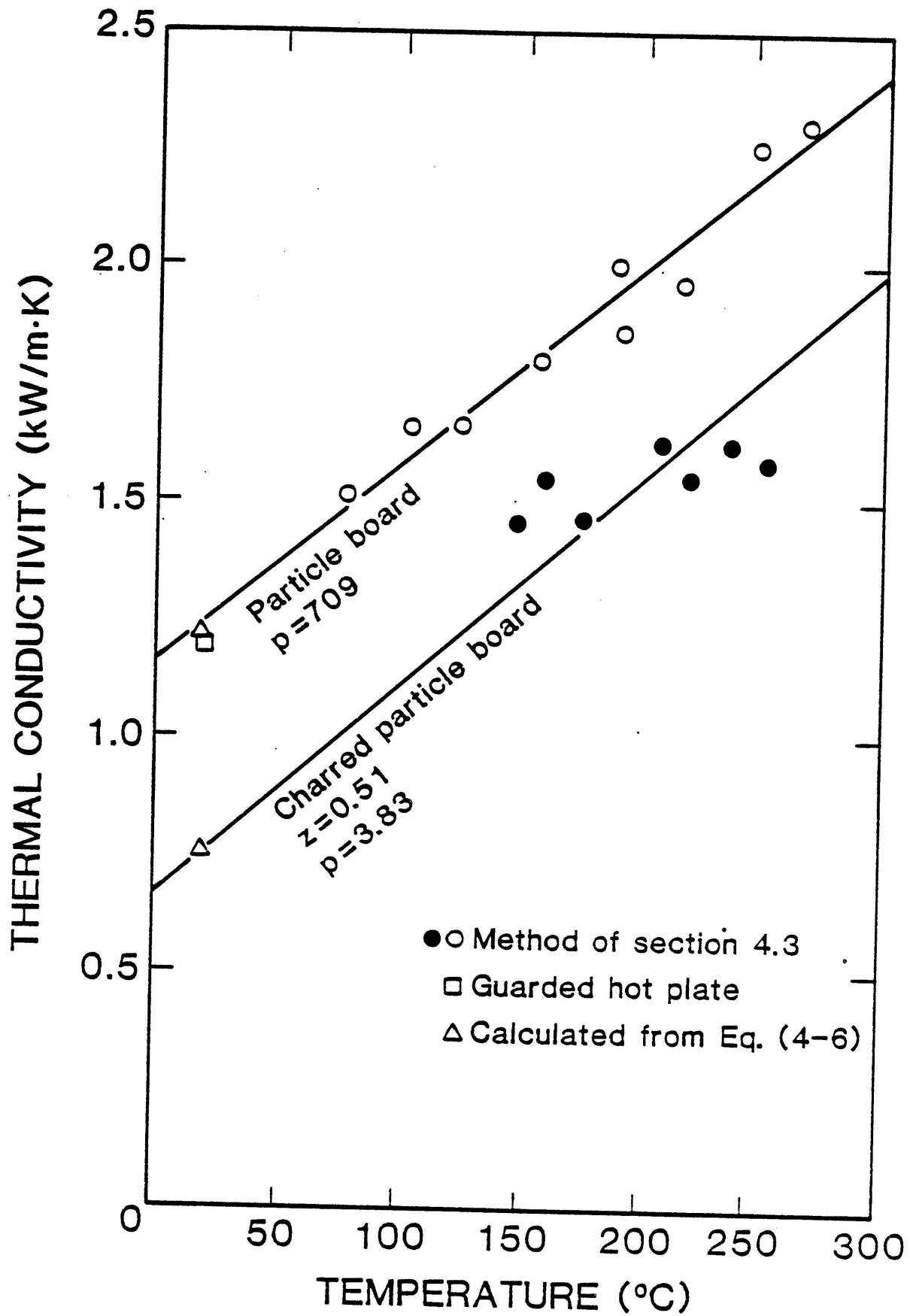
8. Contraction Factors for Douglas Fir Particle Board



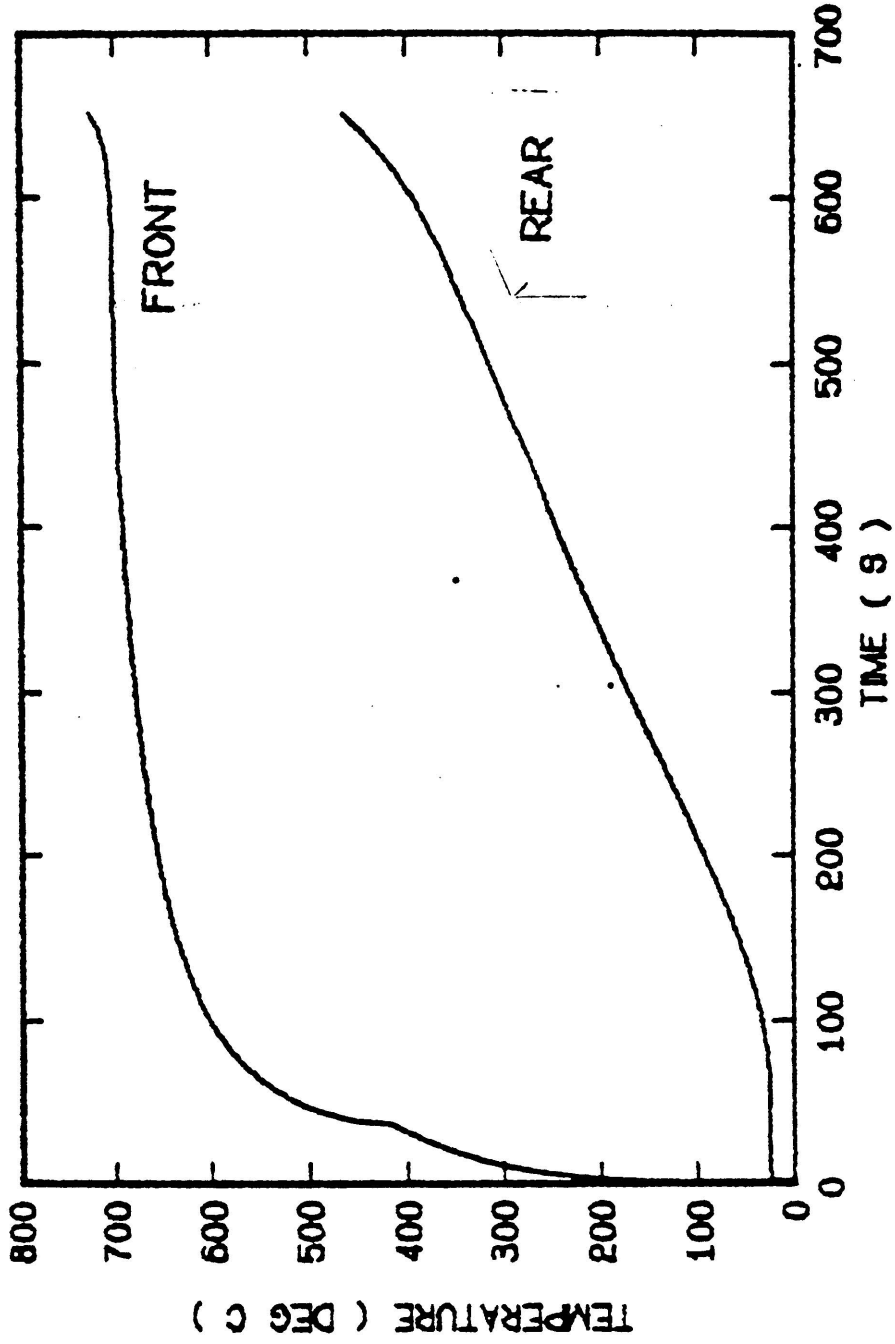
9. Experimental Setup for Determining Thermal Conductivity



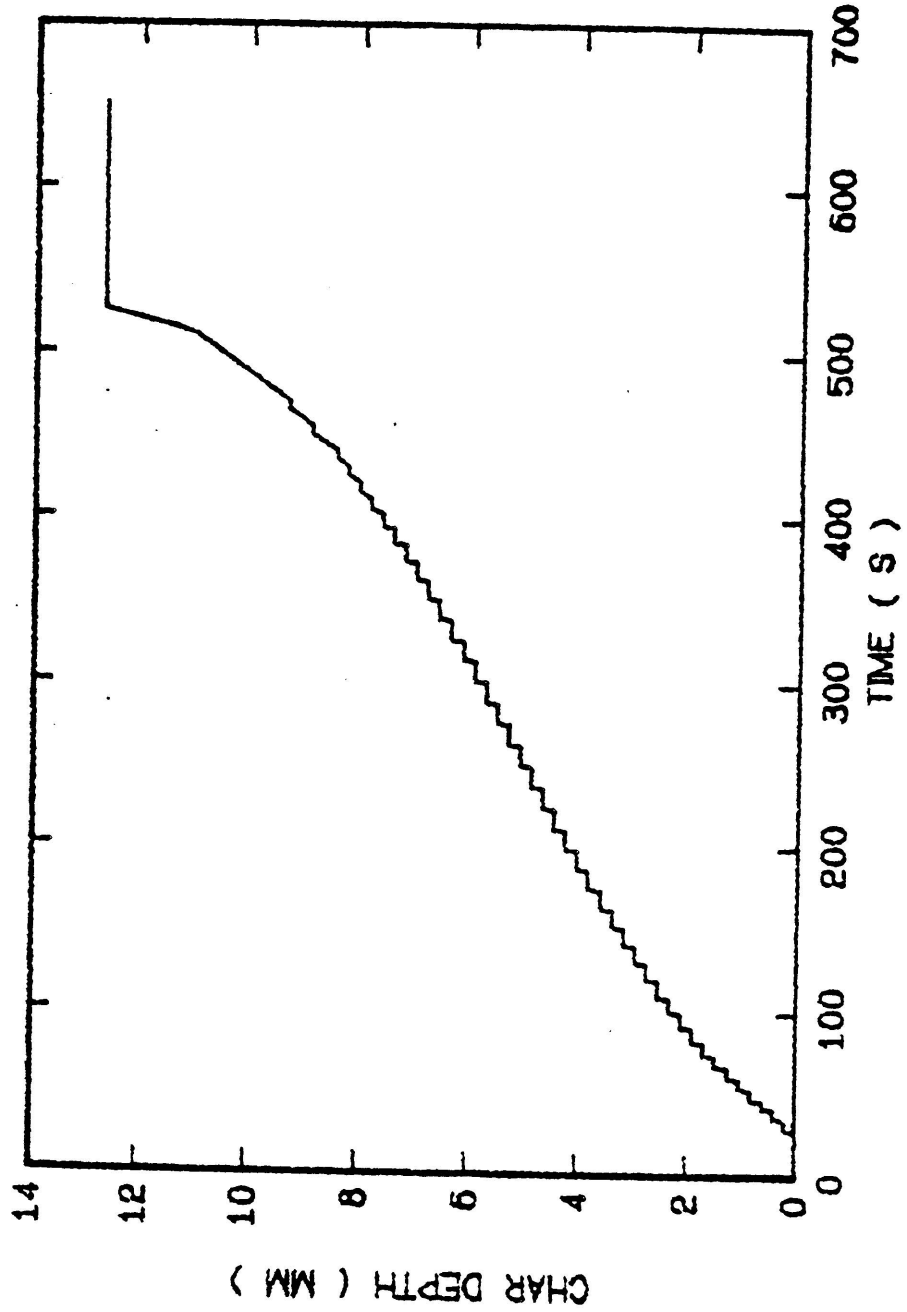
10. Thermal Conductivity as a Function of Temperature for Charred and Uncharred Specimens of Southern Pine



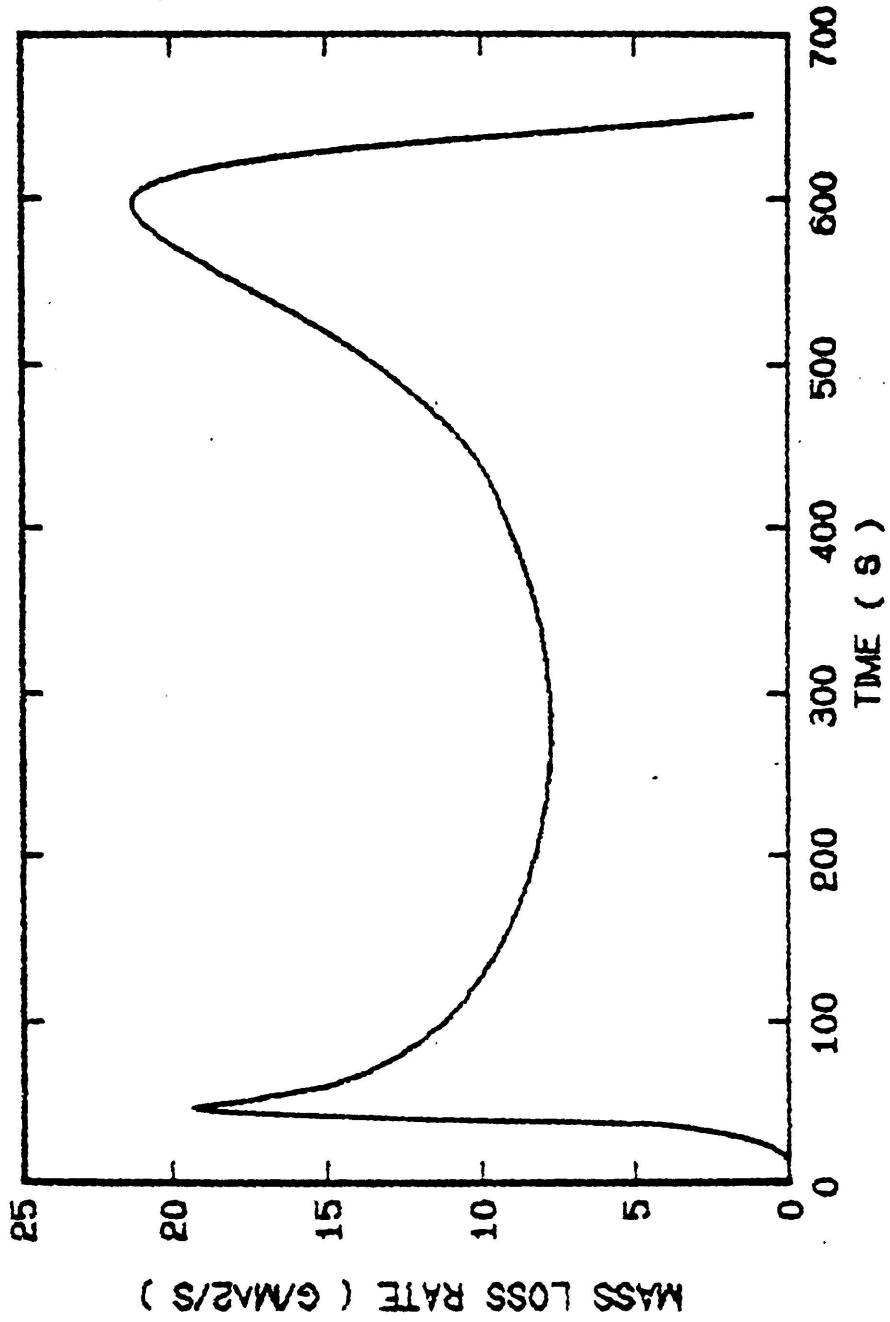
11. Thermal Conductivity as a Function of Temperature for Charred and Uncharred Specimens of Douglas Fir Particle Board



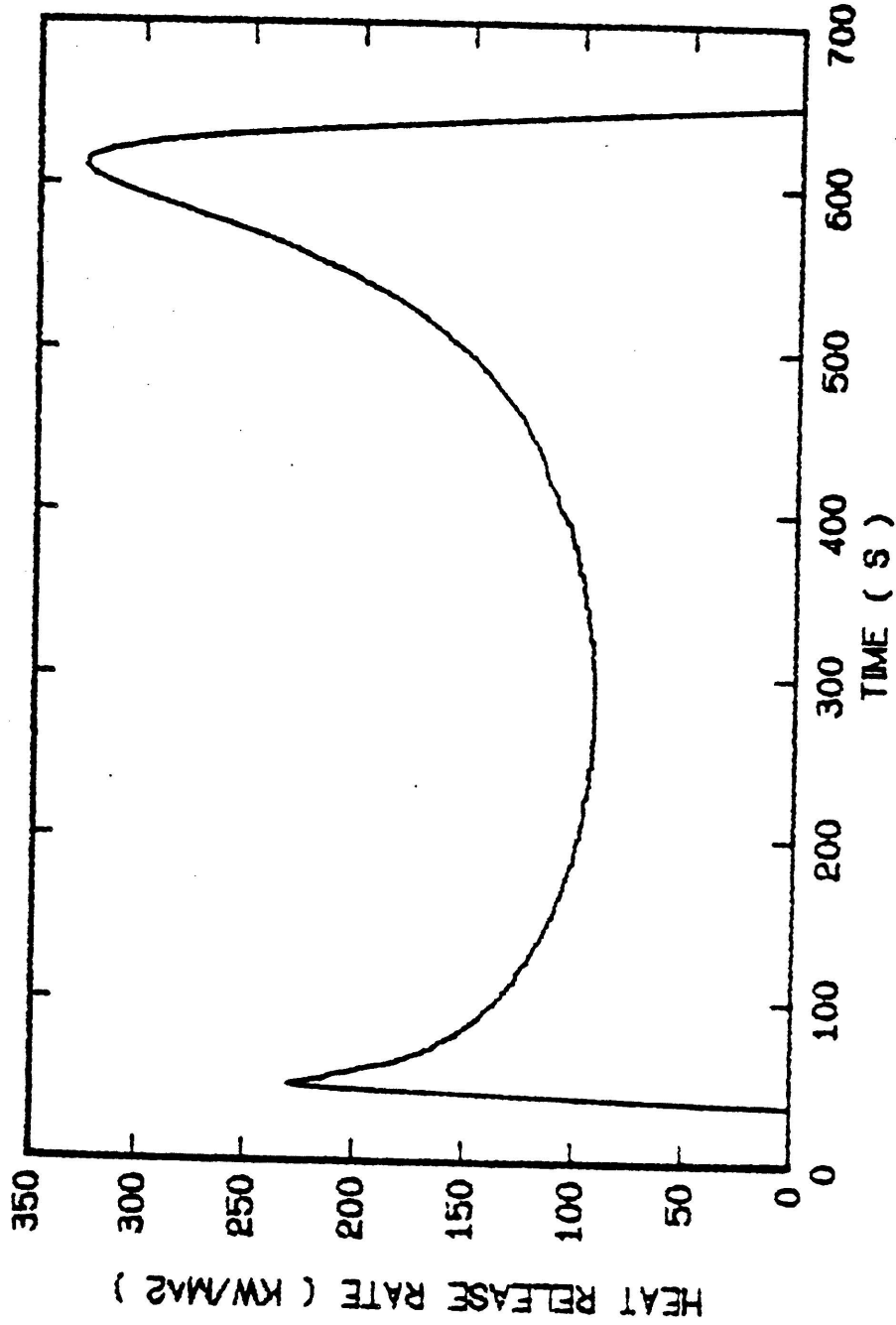
12. Calculated Front and Rear Surface Temperatures for Dry 12.7 mm Specimen of Douglas Fir Particle Board Exposed at an External Radiant Flux of 50 kW/m²



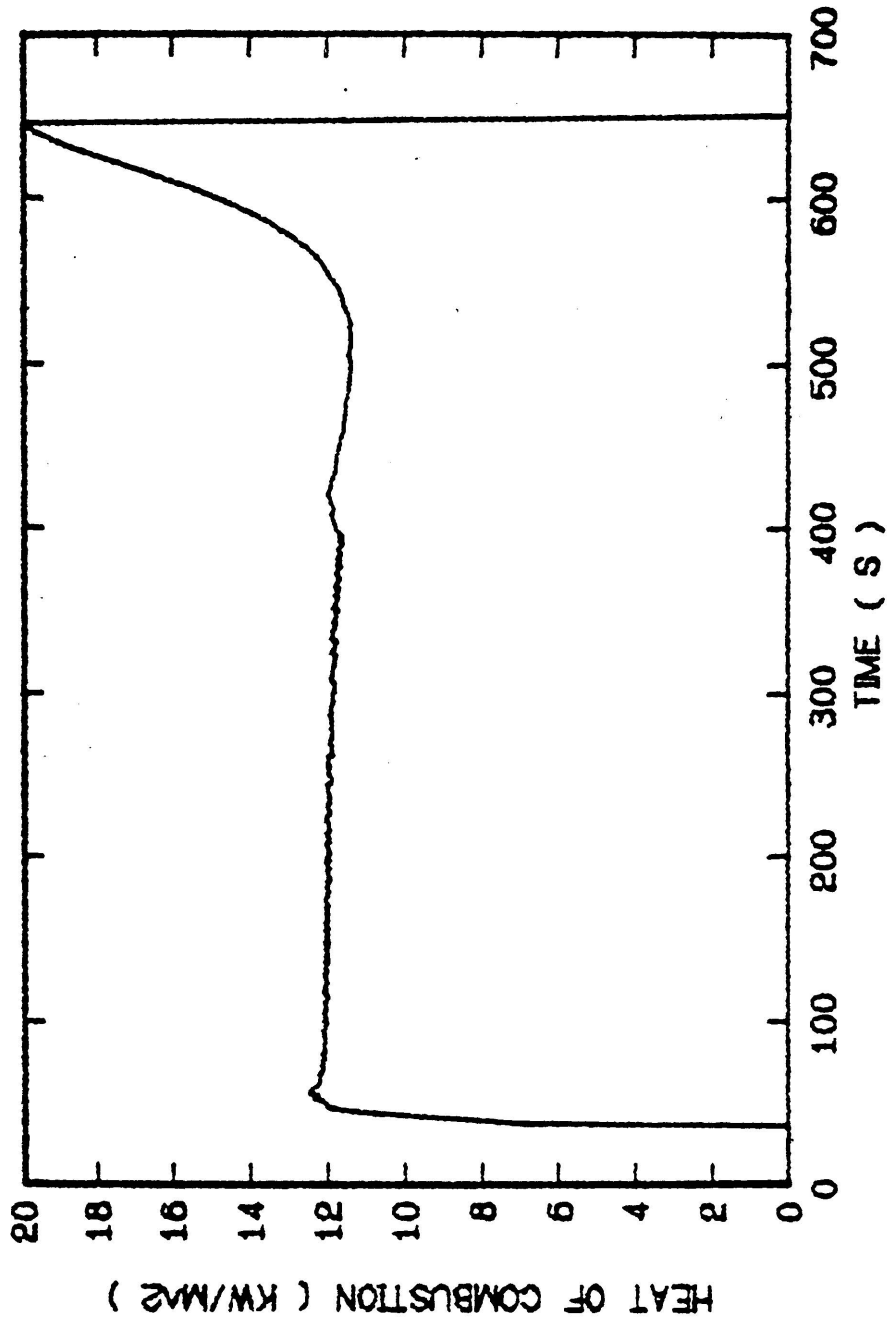
13. Calculated Char Depth for Dry 12.7 mm Specimen of Douglas Fir Particle Board Exposed at an External Radiant Flux of 50 kW/m²



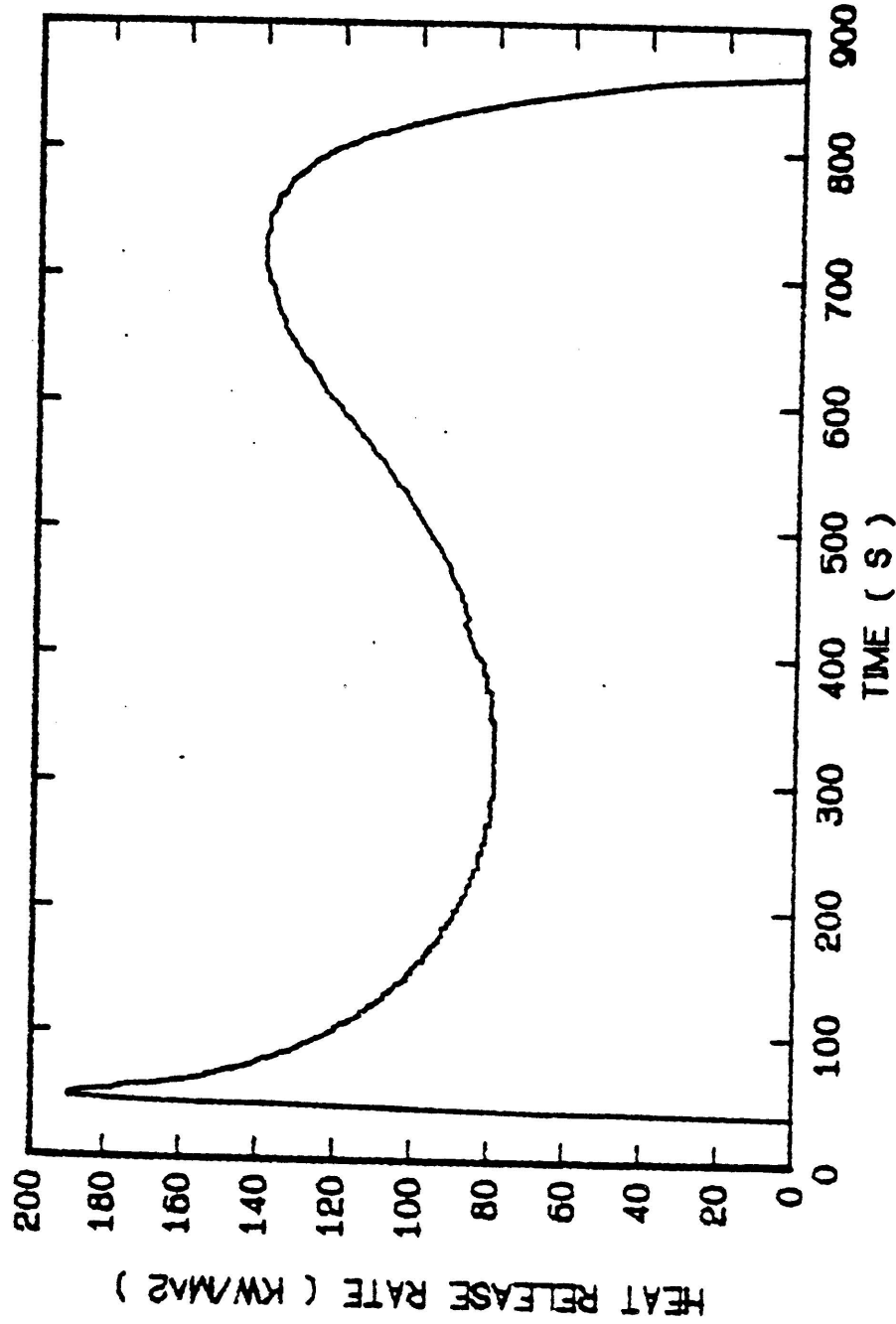
14. Calculated Mass Loss Rate for Dry 12.7 mm Specimen of Douglas Fir Particle Board Exposed at an External Radiant Flux of 50 kW/m²



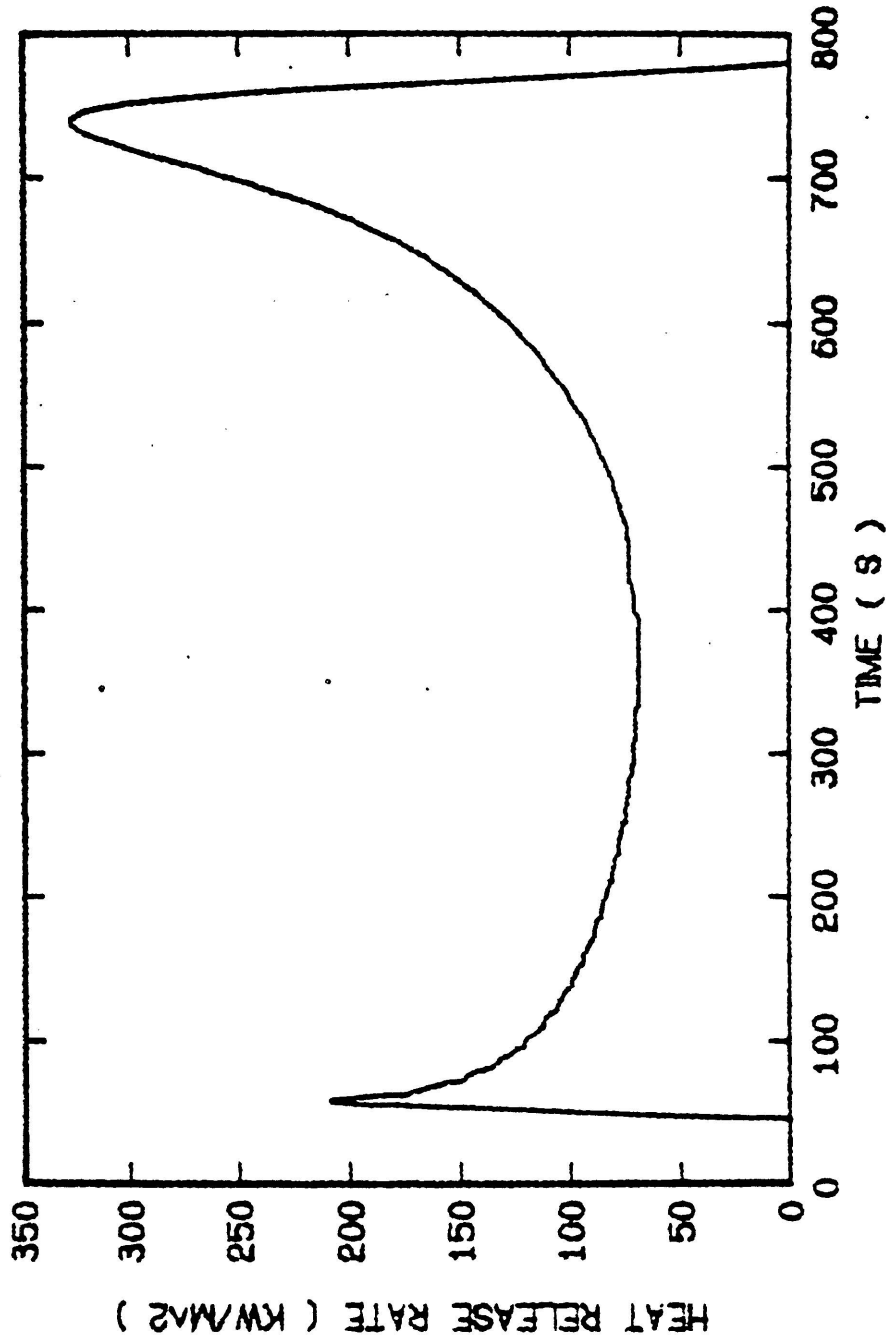
15. Calculated Heat Release Rate for Dry 12.7 mm Specimen of Douglas Fir Particle Board Exposed at an External Radiant Flux of 50 kW/m²



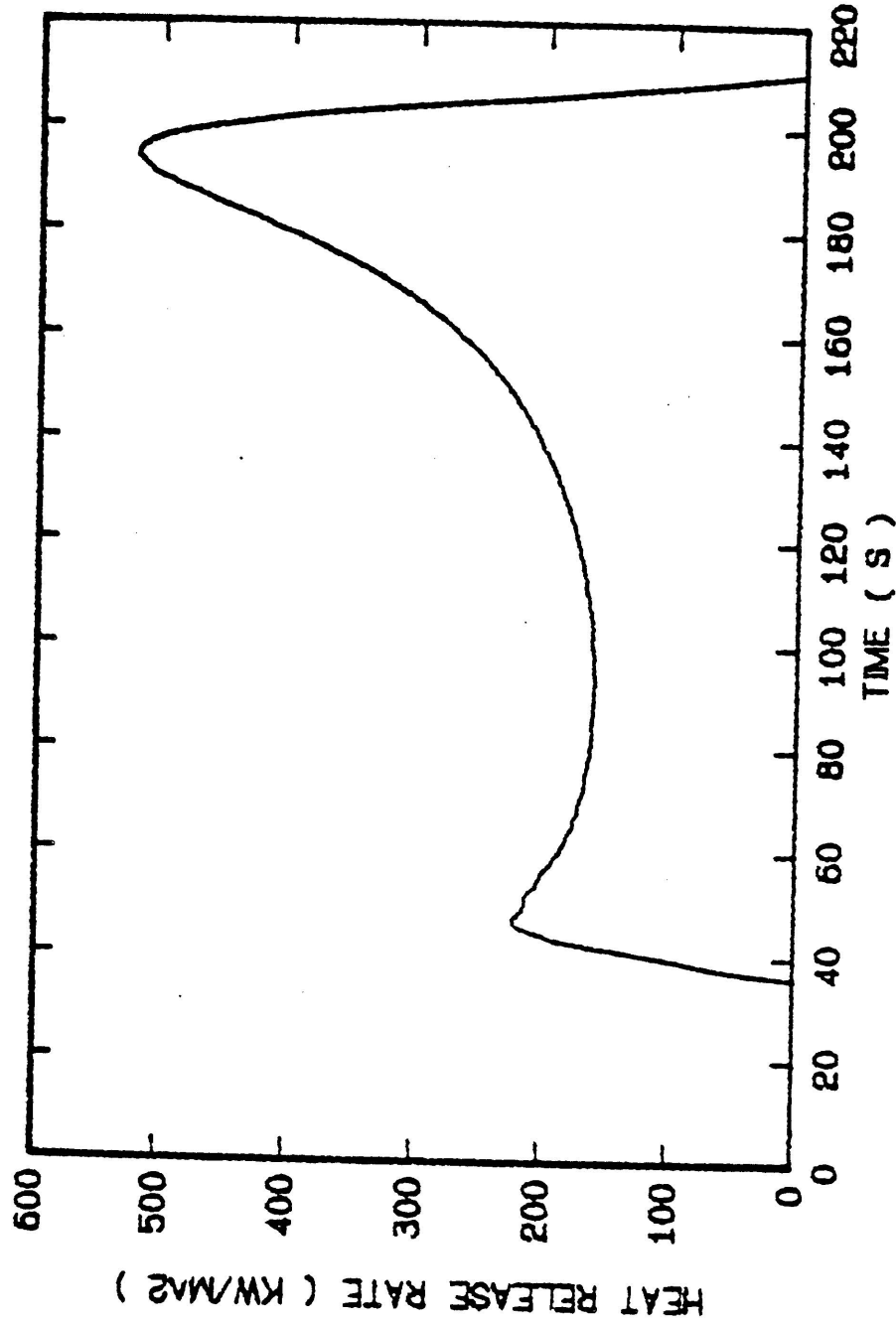
16. Calculated Effective Heat of Combustion for Dry 12.7 mm Specimen of Douglas Fir Particle Board Exposed at an External Radiant Flux of 50 kW/m²



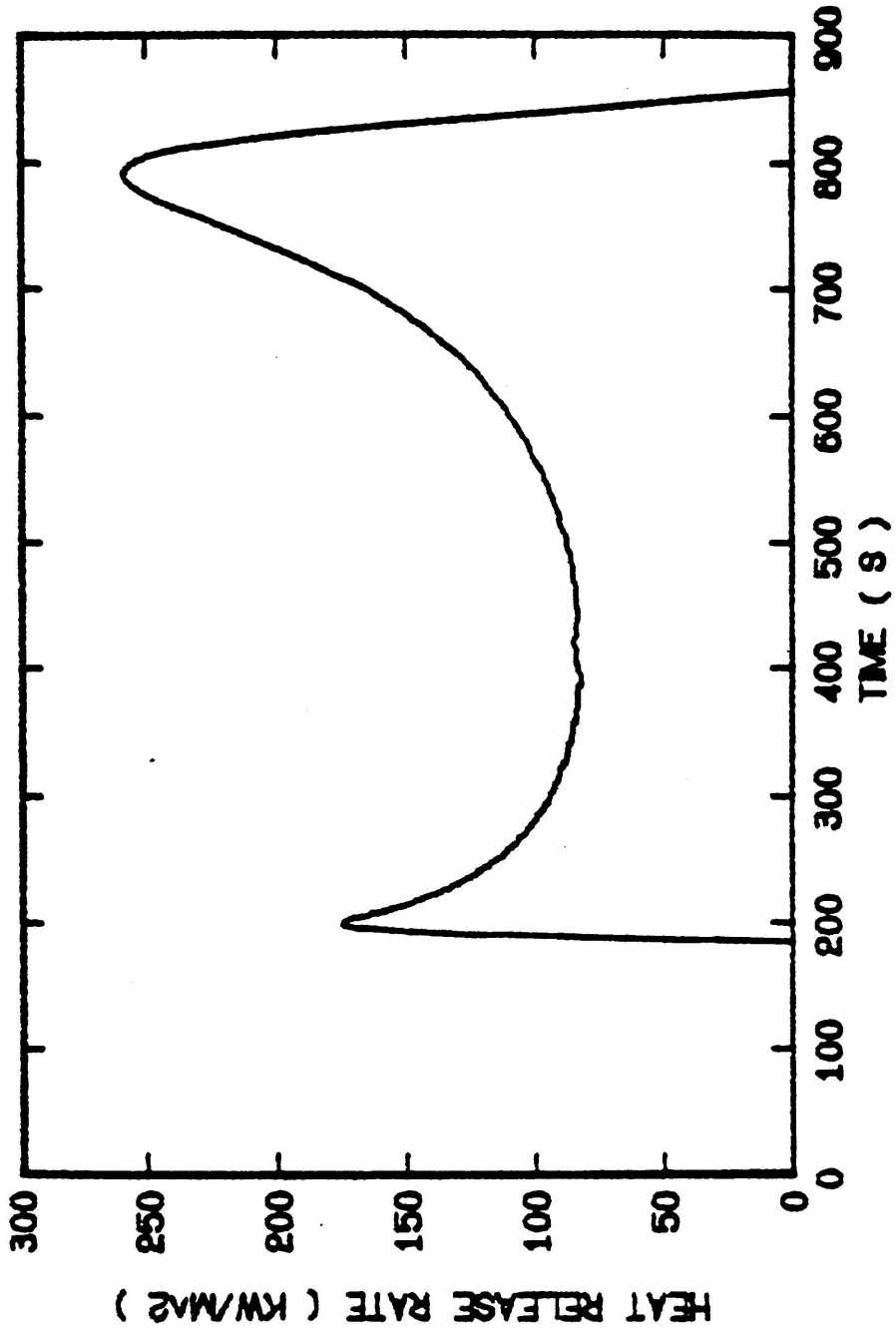
17. Calculated Heat Release Rate for Dry 12.7 mm Specimen of Douglas Fir Particle Board with an Assumed Heat of Pyrolysis of 400 kJ/kg Exposed at an External Radiant Flux of 50 kW/m²



18. Calculated Heat Release Rate for 7% Moisture Content 12.7 mm Specimen of Douglas Fir Particle Board Exposed at an External Radiant Flux of 50 kW/m²



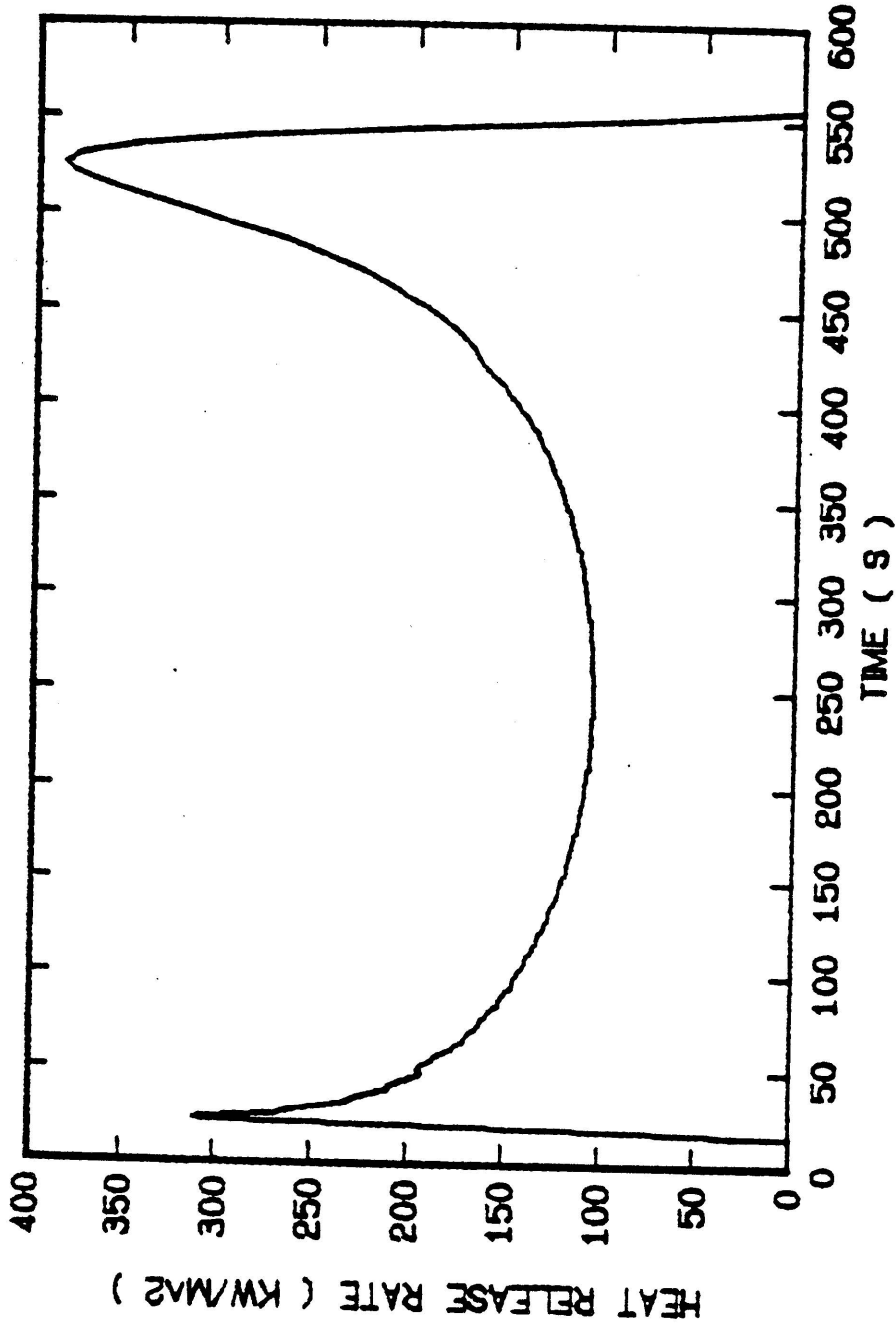
19. Calculated Heat Release Rate for Dry 6 mm Specimen of Douglas Fir Particle Board Exposed at an External Radiant Flux of 50 kW/m²



**CALCULATED HEAT RELEASE RATE AT 25 KW/M²
FOR DRY 12.5 MM DOUGLAS FIR PARTICLE BOARD**

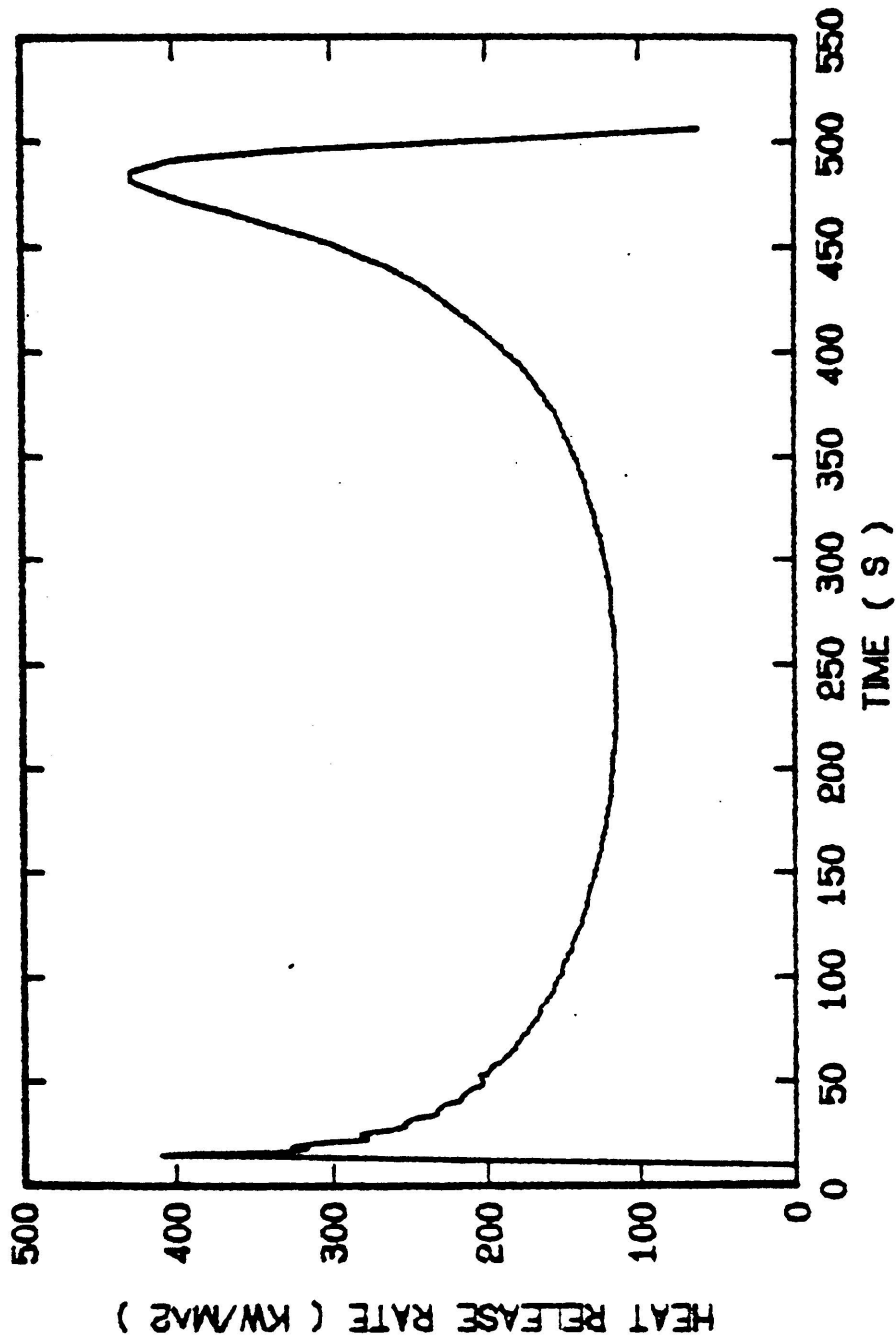
20. Calculated Heat Release Rate for Dry 12.7 mm Specimen of Douglas Fir Particle Board Exposed at an External Radiant Flux of 25 kW/m²

20

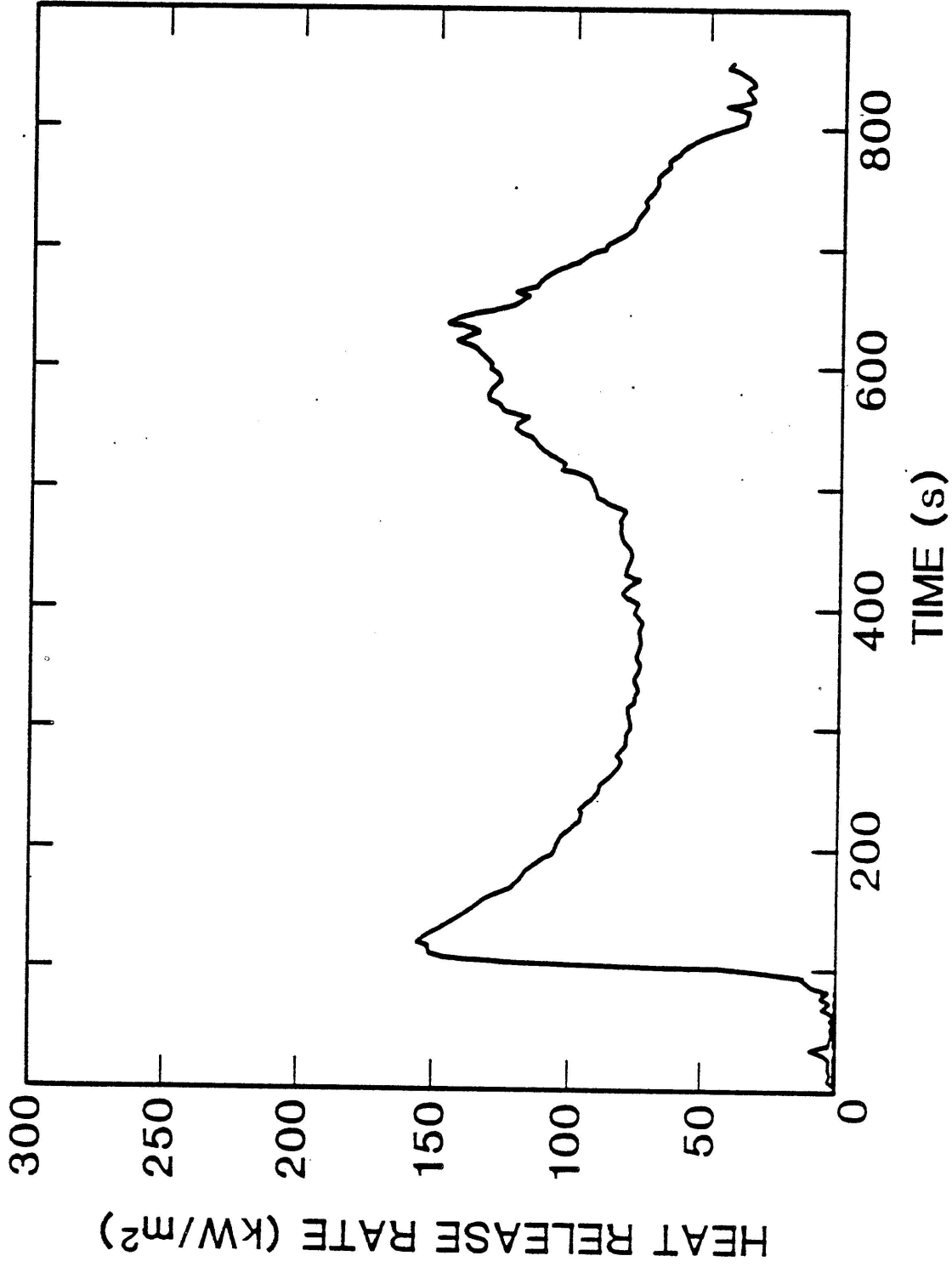


**CALCULATED HEAT RELEASE RATE AT 75 KW/M²
FOR DRY 12.6 MM DOUGLAS FIR PARTICLE BOARD**

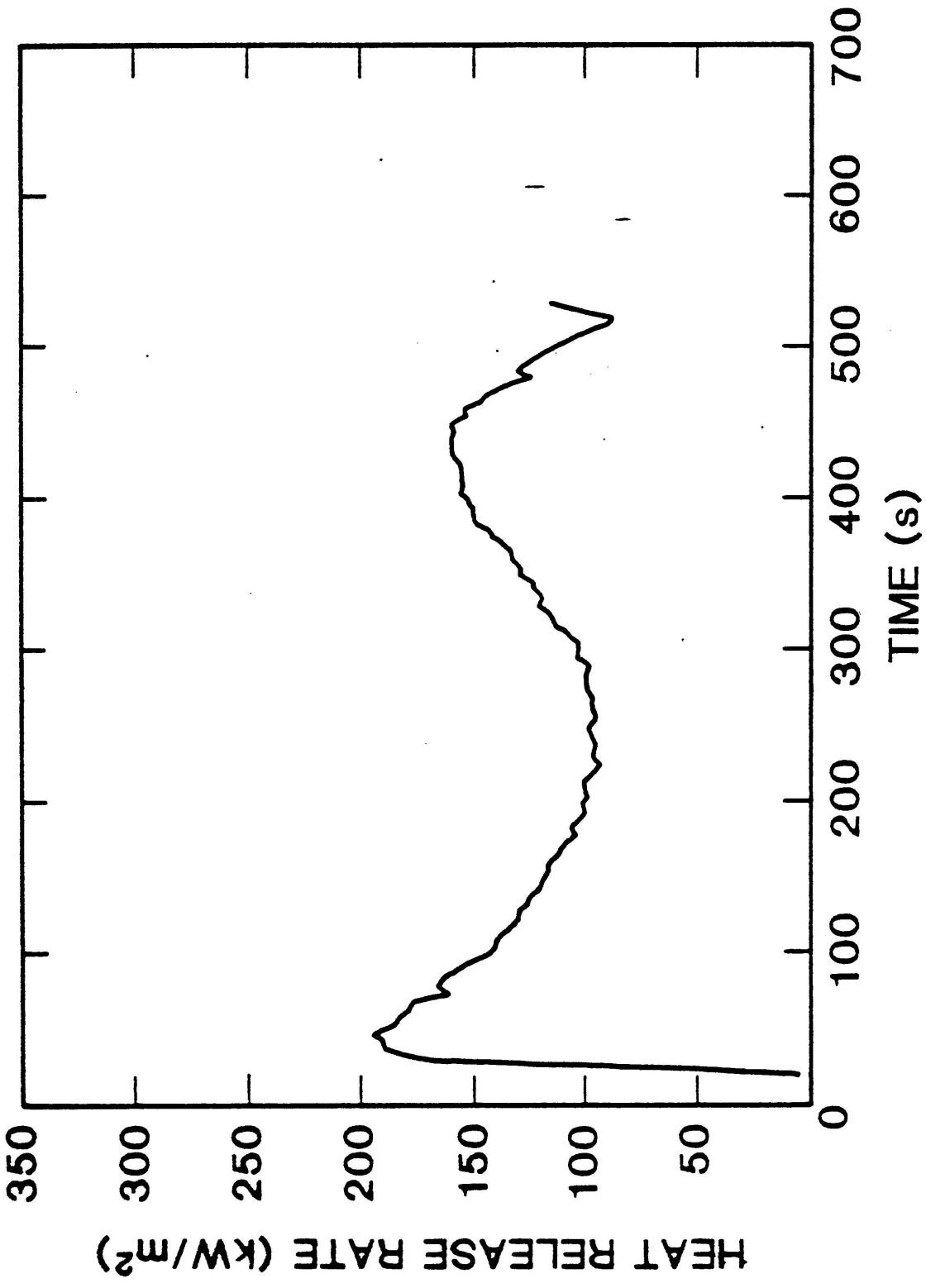
21. Calculated Heat Release Rate for Dry 12.7 mm Specimen of Douglas Fir Particle Board Exposed at an External Radiant Flux of 75 kW/m²



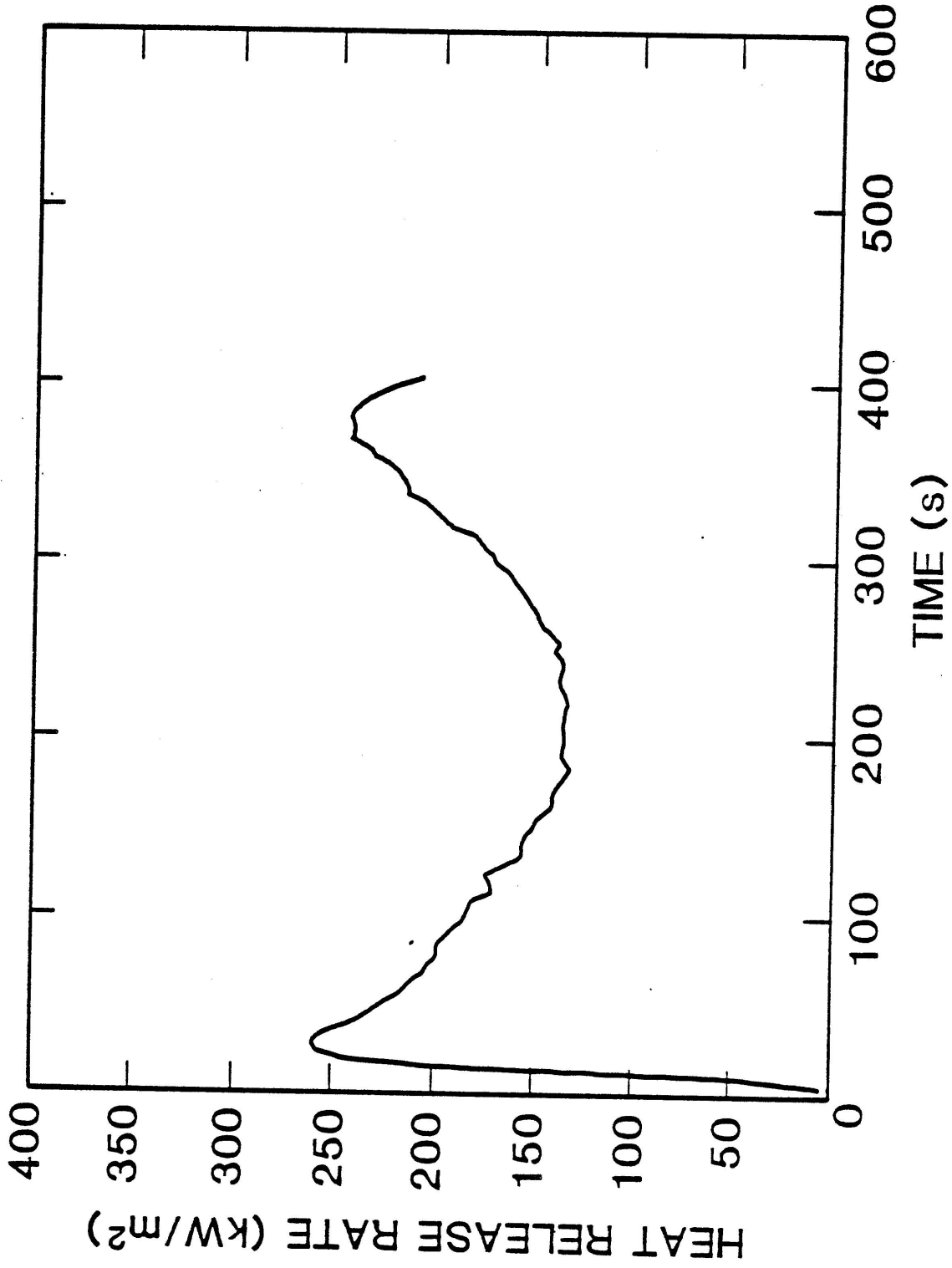
22. Calculated Heat Release Rate for Dry 12.7 mm Specimen of Douglas Fir Particle Board Exposed at an External Radiant Flux of 100 kW/m²



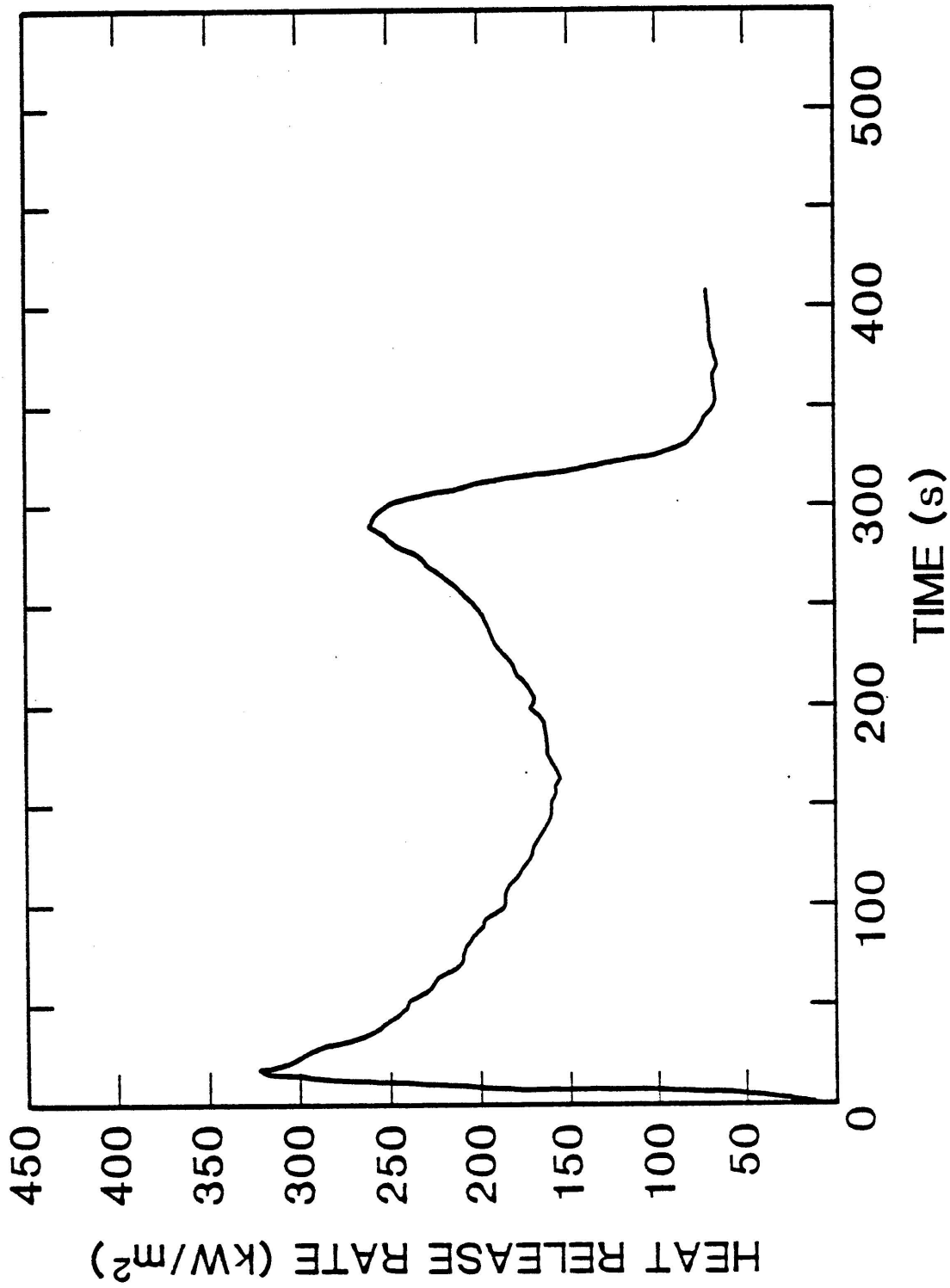
23. Measured Heat Release Rate for Dry 12.7 mm Specimen of Douglas Fir Particle Board Exposed at an External Radiant Flux of 25 kW/m²



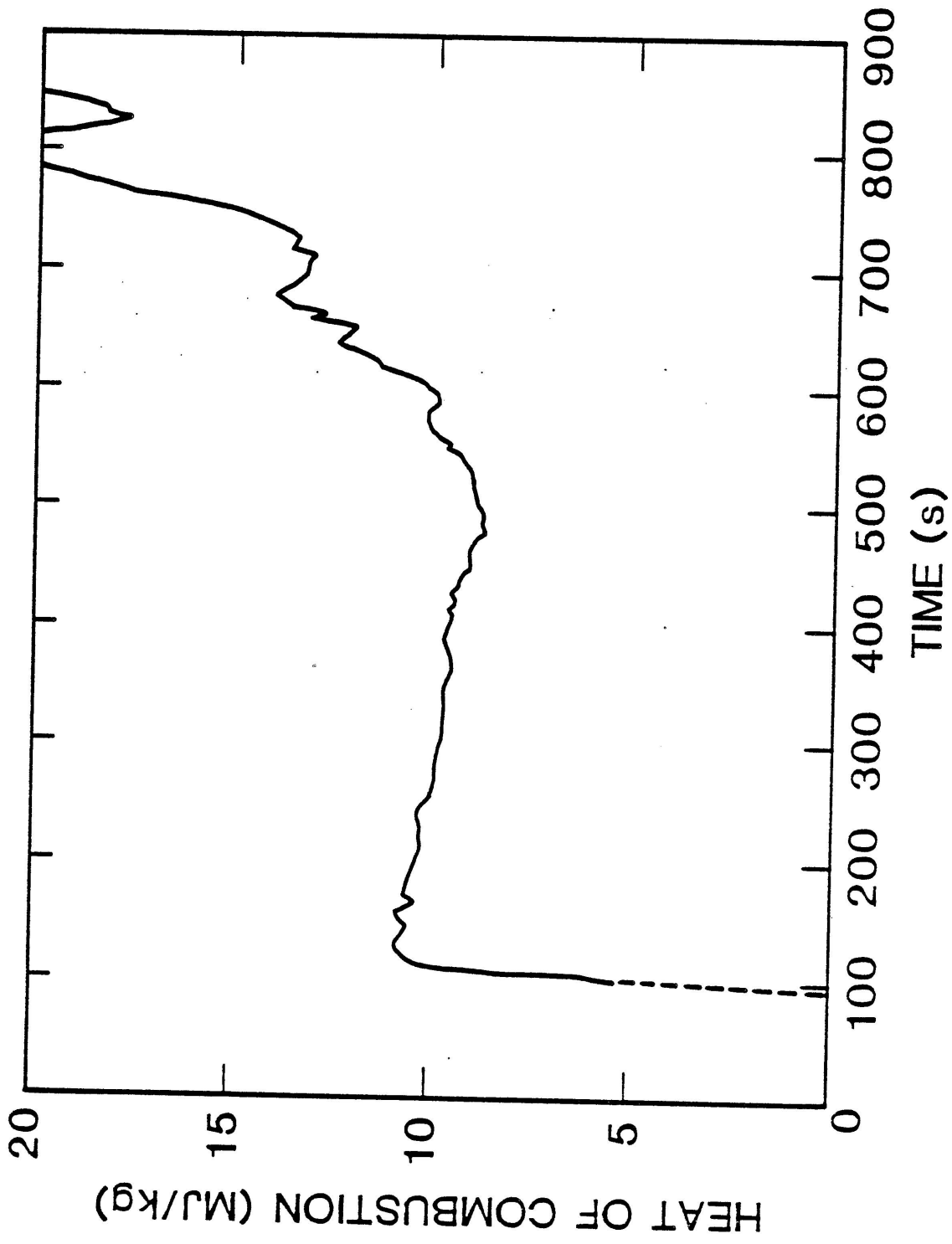
24. Measured Heat Release Rate for Dry 12.7 mm Specimen of Douglas Fir Particle Board Exposed at an External Radiant Flux of 50 kW/m²



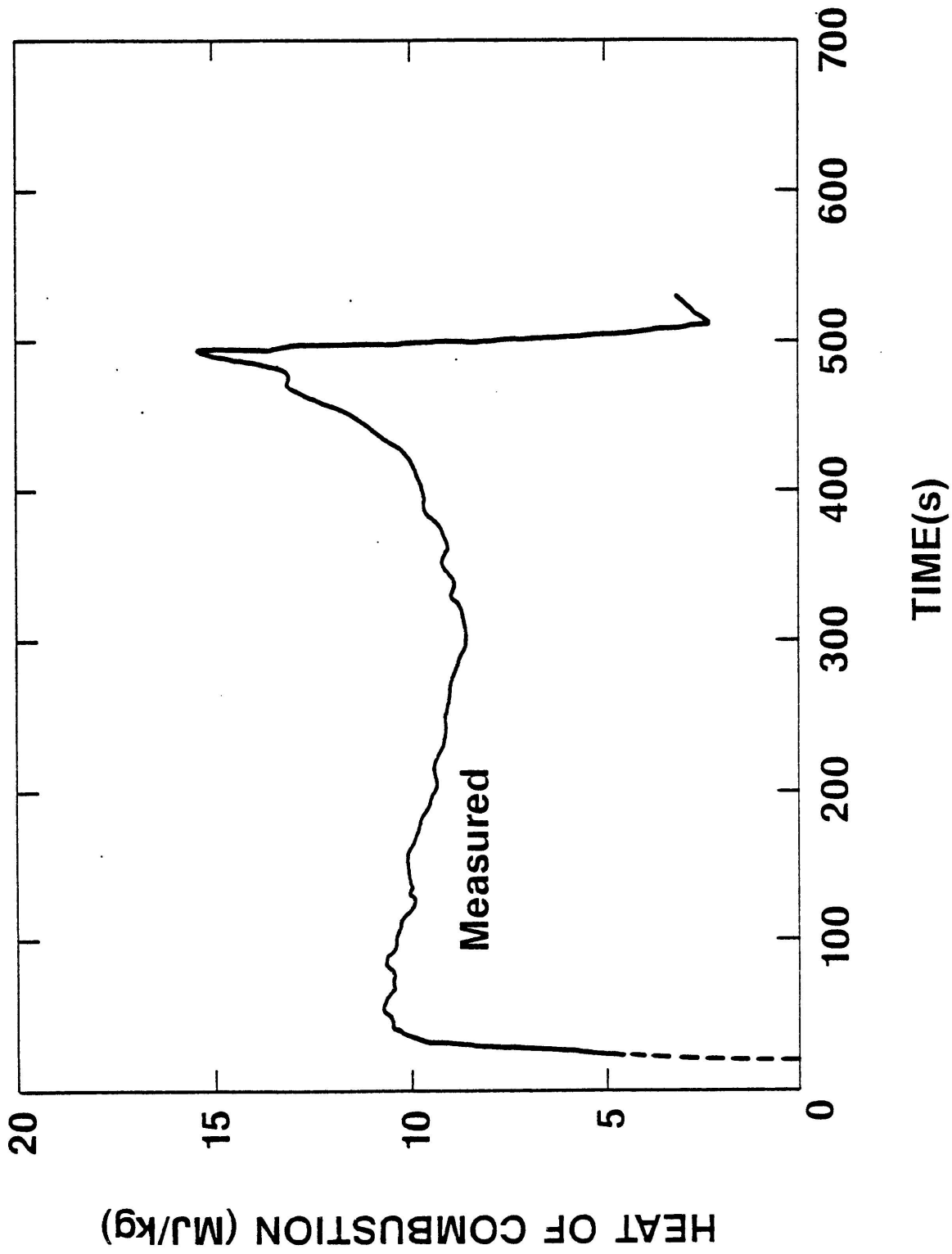
25. Measured Heat Release Rate for Dry 12.7 mm Specimen of Douglas Fir Particle Board Exposed at an External Radiant Flux of 75 kW/m²



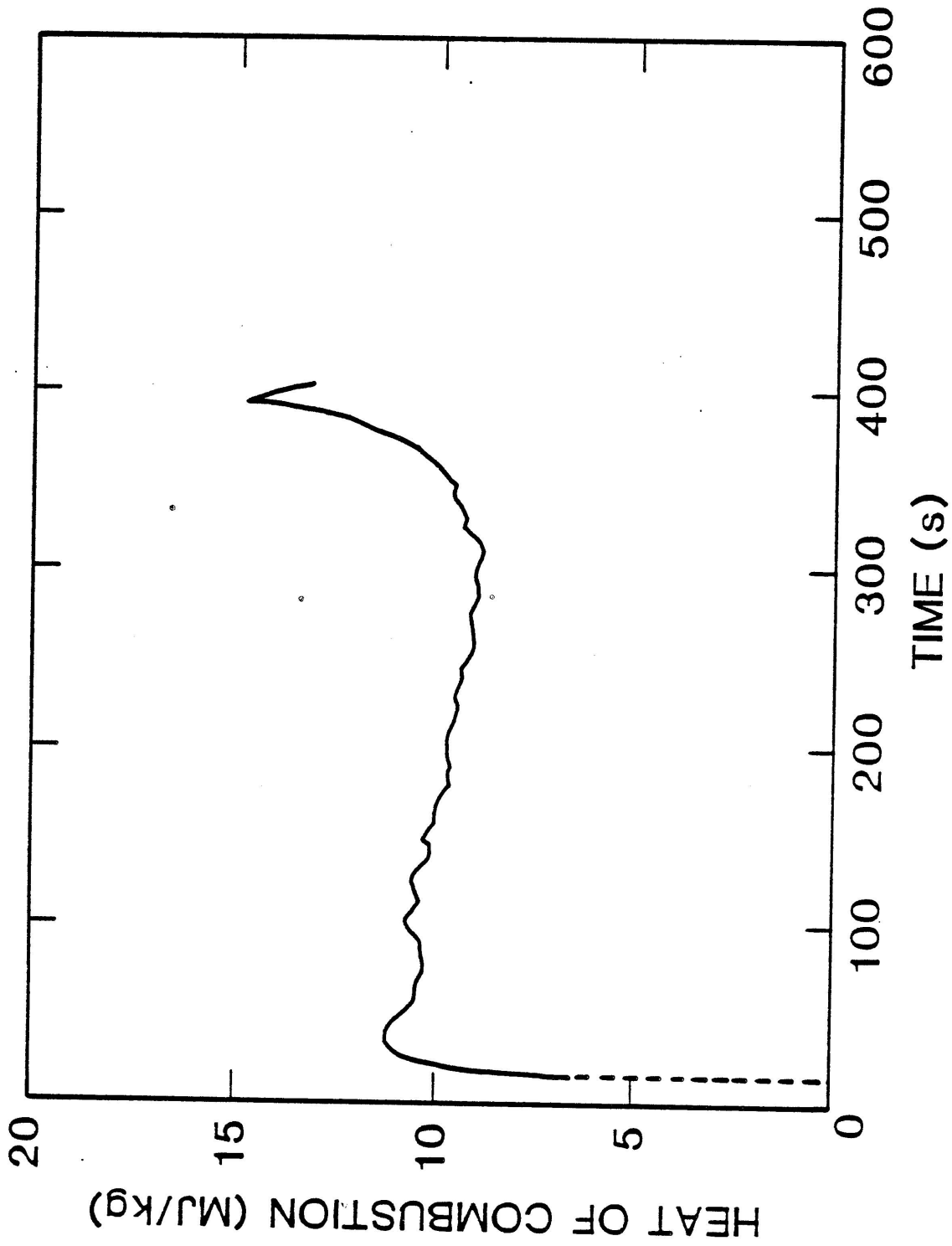
26. Measured Heat Release Rate for Dry 12.7 mm Specimen of Douglas Fir Particle Board Exposed at an External Radiant Flux of 100 kW/m²



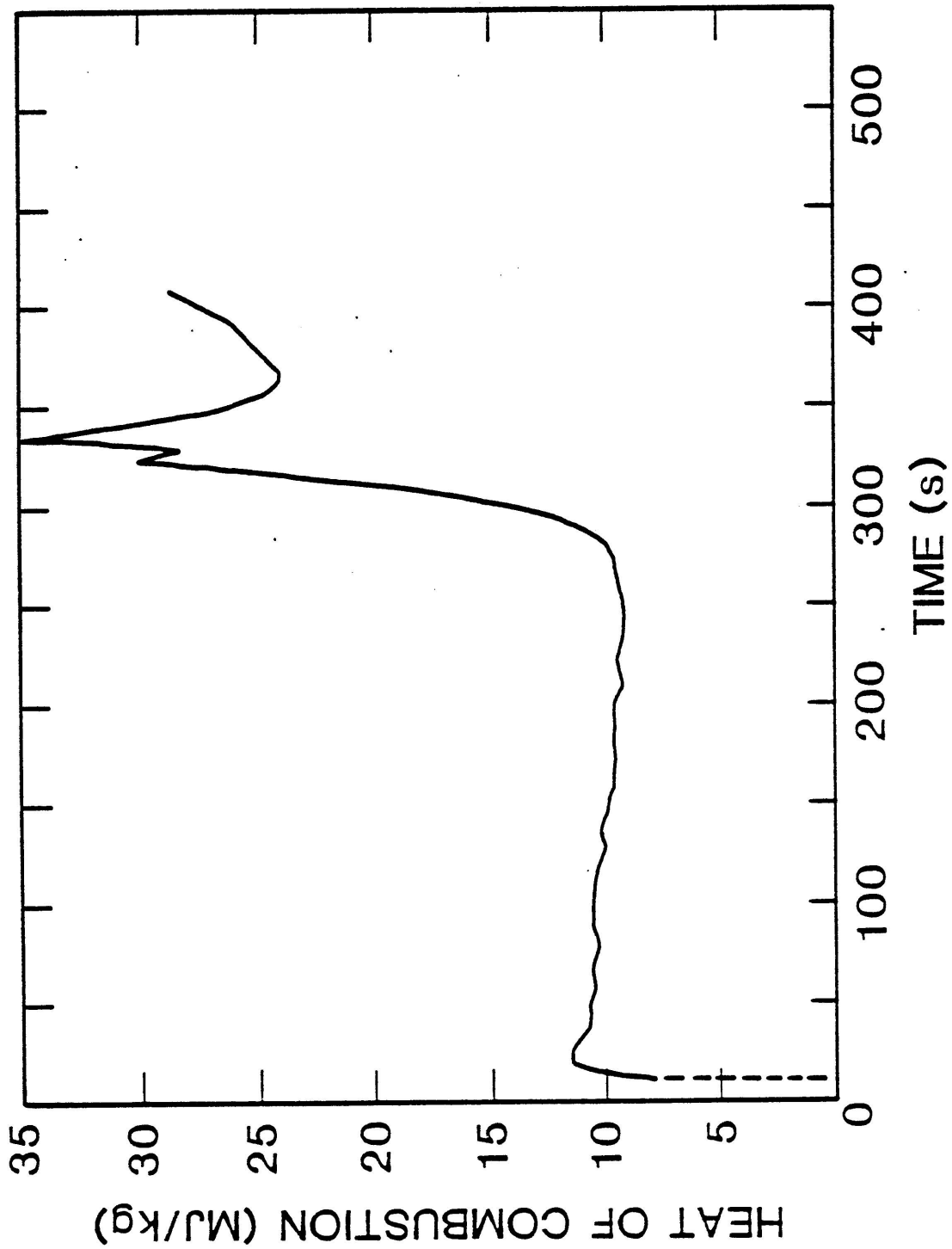
27. Measured Effective Heat of Combustion for Dry 12.7 mm Specimen of Douglas Fir Particle Board Exposed at an External Radiant Flux of 25 kW/m²



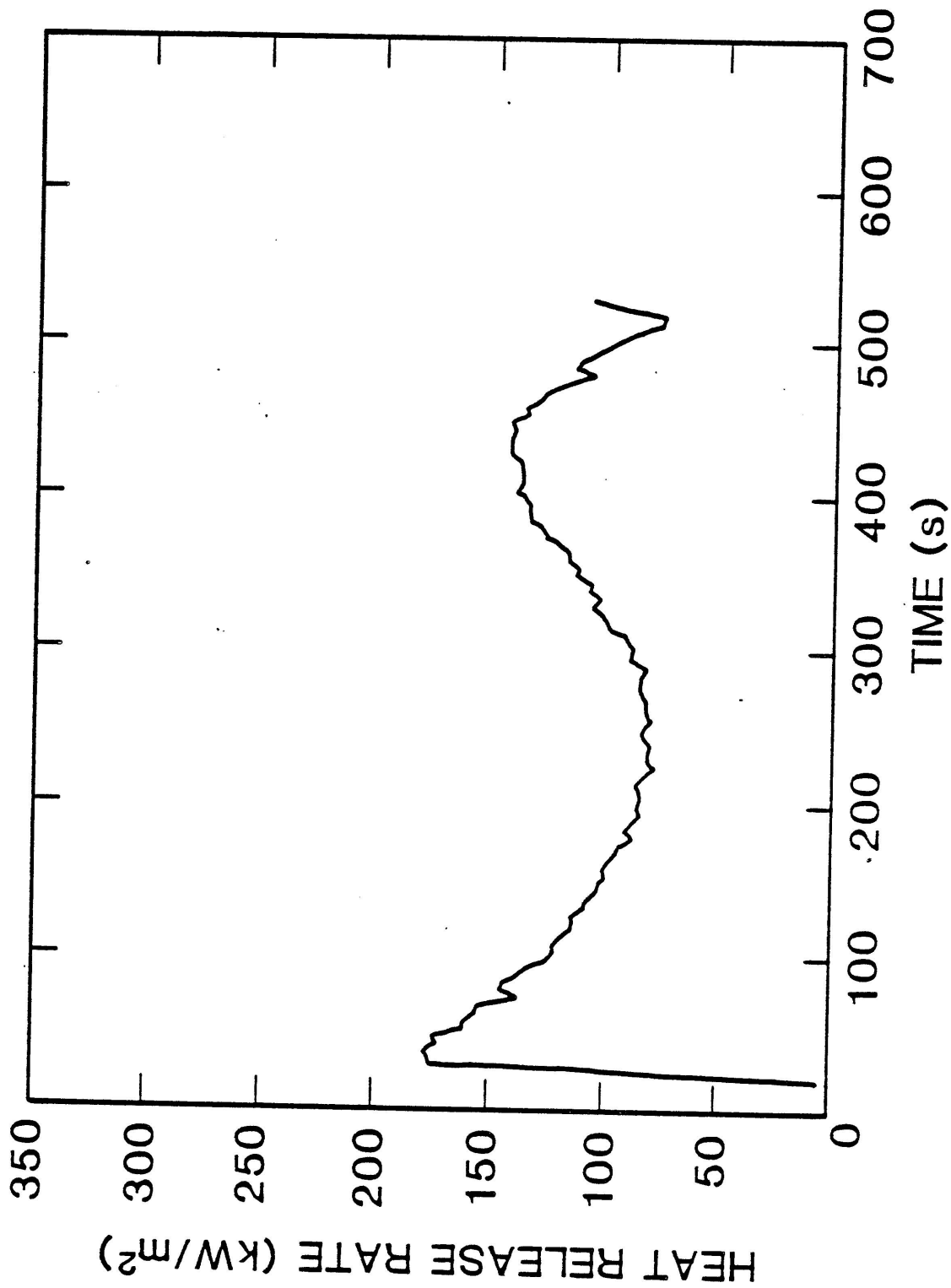
28. Measured Effective Heat of Combustion for Dry 12.7 mm Specimen of Douglas Fir Particle Board Exposed at an External Radiant Flux of 50 kW/m²



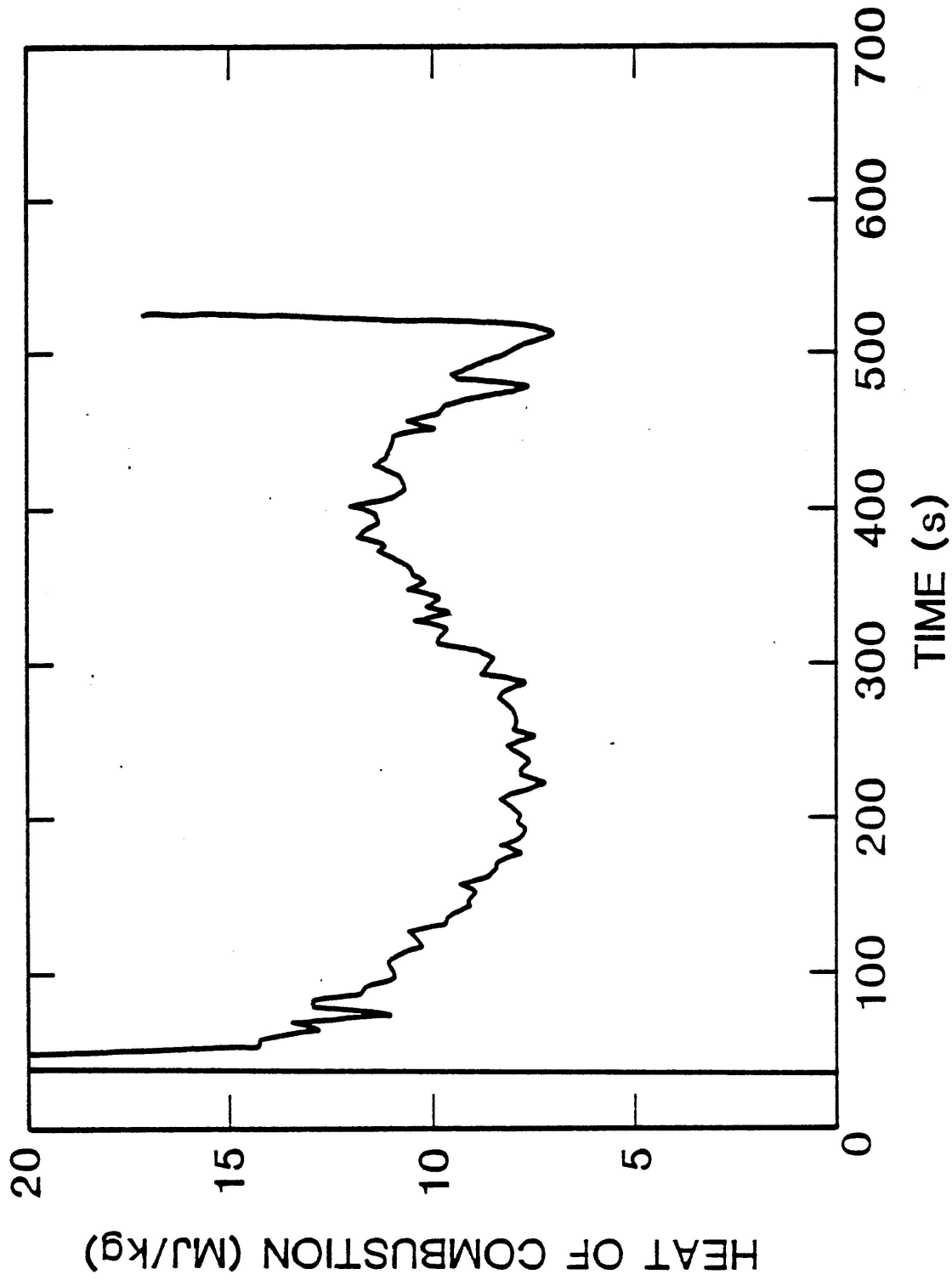
29. Measured Effective Heat of Combustion for Dry 12.7 mm Specimen of Douglas Fir Particle Board Exposed at an External Radiant Flux of 75 kW/m²



30. Measured Effective Heat of Combustion for Dry 12.7 mm Specimen of Douglas Fir Particle Board Exposed at External Radiant Flux of 100 kW/2



31. Measured Heat Release Rate Determined by the Three Analyzer Method for Dry 12.7 mm Specimen of Douglas Fir Particle Board Exposed at an External Radiant Flux of 50 kW/m²



32. Measured Effective Heat of Combustion Determined by the Three Analyzer Method for Dry 12.7 mm Specimen of Douglas Fir Particle Board Exposed at an External Radiant Flux of 50 kW/m²

U.S. DEPT. OF COMM. BIBLIOGRAPHIC DATA SHEET <i>(See instructions)</i>	1. PUBLICATION OR REPORT NO. NBSIR 85-3163	2. Performing Organ. Report No.	3. Publication Date JULY 1985
4. TITLE AND SUBTITLE Development of a Model For The Heat Release of Wood - A Status Report			
5. AUTHOR(S) William J. Parker			
6. PERFORMING ORGANIZATION <i>(If joint or other than NBS, see instructions)</i> NATIONAL BUREAU OF STANDARDS DEPARTMENT OF COMMERCE WASHINGTON, D.C. 20533 Gaithersburg, MD 20899		7. Contract/Grant No.	8. Type of Report & Period Covered
9. SPONSORING ORGANIZATION NAME AND COMPLETE ADDRESS <i>(Street, City, State, ZIP)</i>			
10. SUPPLEMENTARY NOTES <input type="checkbox"/> Document describes a computer program; SF-185, FIPS Software Summary, is attached.			
11. ABSTRACT <i>(A 200-word or less factual summary of most significant information. If document includes a significant bibliography or literature survey, mention it here)</i> This report describes the status of the development of a method for predicting the heat release rate of wood for different thicknesses, moisture contents, and exposure conditions. A computer model has been set up on a microcomputer. Experimental techniques have been devised to obtain the input data required by the model. These include (1) the thermal conductivity as a function of temperature and percent loss, (2) the kinetic constants needed to describe the mass loss rate, (3) the heat of combustion of the volatile pyrolysis products, and (4) the contraction factors due to charring. Sufficient data on these parameters were taken to exercise the model. Heat release rates and effective heats of combustion were measured as a function of external radiant flux on 12.5 mm thick dry vertical specimens of Douglas fir particle board. The calculated and measured peak heat release rate curves are similar in shape and amplitude but differ significantly in time scale. This may be due to the lack of thermal conductivity data on the char in the high temperature range. There is very good agreement between the calculated and measured effective heats of combustion. The initial results with the model are promising.			
12. KEY WORDS <i>(Six to twelve entries; alphabetical order; capitalize only proper names; and separate key words by semicolons)</i> heat release rate, wood, pyrolysis, heat of combustion, thermal conductivity, computer models			
13. AVAILABILITY <input checked="" type="checkbox"/> Unlimited <input type="checkbox"/> For Official Distribution. Do Not Release to NTIS <input type="checkbox"/> Order From Superintendent of Documents, U.S. Government Printing Office, Washington, D.C. 20402.		14. NO. OF PRINTED PAGES 108	
<input checked="" type="checkbox"/> Order From National Technical Information Service (NTIS), Springfield, VA. 22161		15. Price \$13.00	

